UNIVERSITÀ DEGLI STUDI DI TRIESTE

UNIVERSITÀ DEGLI STUDI DI TRIESTE

XXXV CICLO DEL DOTTORATO DI RICERCA IN

BIOMEDICINA MOLECOLARE

Identification of Deubiquitinases (DUBs) associated with TRIM18/MID1

Settore scientifico-disciplinare: BIO/18

DOTTORANDO / A
INÊS FERNANDES LAGES

COORDINATORE
PROF. GERMANA MERONI

SUPERVISORE DI TESI
PROF. GERMANA MERONI

ANNO ACCADEMICO 2021/2022

Table of Contents

List of Figures

List of Tables

Abbreviations

4E-BP1	Eukaryotic translation initiation factor 4E-Binding Protein 1
AD	Alzheimer's Disease
APP	Amyloid Precursor Protein
AR	Androgen Receptor
BACE1	β-Secretase 1
CC	Coiled-Coil
COS	C-terminal Subgroup One Signature
CP	20S Subunit Core Particle
DUB	Deubiquitinating Enzymes
DMSO	Dimethyl sulfoxide
E1	Ubiquitin-Activating Enzyme
E2	Ubiquitin-Conjugating Enzyme
E3	Ubiquitin-Ligase
EXOSC10	Exosome Component 10
FN3	Fibronectin Type III
HECT	Homologous to the E6–AP C-terminus
HTT	Huntingtin
IF	Immunofluorescence
IP	Immunoprecipitation
JAMM	JAB1/MPN/MOV34 Metalloenzymes
KO	Knock-Out
Lys	Lysine
MAP	Microtubule-Associated Proteins
MEF	Mouse Embryonic Fibroblasts
Met	Methionine
MID1/TRIM18	Midline1
MID2/TRIM1	Midline2
MINDY	MIU Containing Novel Deubiquitinating Enzymes Family
MIU	Motif Interacting with Ubiquitin
MJD	Josephin

mTOR	Mechanistic Targets of Rapamycin
mTORC1	Mechanistic Targets of Rapamycin Complex 1
OS	Opitz G/BBB Syndrome
OTUs	Ovarian Tumor Proteases
PBS	Phosphate saline buffer
PP2A	Protein Phosphatase 2A
PP2AC	Catalytic Subunit of Protein Phosphatase 2A
PPP	Phospho-Protein Phosphatases
PRY-SPRY	SPlA and RYanodine receptor
RBCC	RING, B-Box, Coiled-Coil
RBR/TRIAD	Ring-Between Ring-Ring
RING	Really Interesting New Genes
RNP	Ribonucleoprotein
RP	19S Regulatory Particle
S6K	40S Ribosomal S6 Kinase
SHH	Sonic Hedgehog
TBS	Tris-Buffered Saline
TRIM	TRIpartite Motif
UB	Ubiquitin
UBA	Ubiquitin-Associated Domain
UBC	Ubiquitin-Conjugating
UBDs	Ubiquitin-Binding Domains
UCHs	Ubiquitin C-terminal Hydrolases
UIM	Ubiquitin-Interacting Motif
UPS	Ubiquitin-Proteasome System
USP	Ubiquitin-Specific Proteases
WB	Western Blot
XLOS	X-linked form of Opitz G/BBB Syndrome
ZUFSP/ZUP1	Zinc Finger with UFM1-Specific Peptidase Domain Protein

Abstract

Ubiquitination is a post-translation modification process crucial to control protein degradation, localization, and activity. Tripartite Motif (TRIM) proteins participate in the ubiquitination process behaving as E3 ubiquitin ligases, responsible for the specific recognition of the substrate to be ubiquitinated. In the opposite process, Deubiquitinating enzymes (DUBs) can deconjugate the ubiquitin from the protein target. The antagonism of DUBs and E3s is essential to maintain protein homeostasis and signaling in cells.

In this project, we focused on TRIM18 (also named MID1) which when mutated causes the X-linked form of Opitz G/BBB Syndrome (XLOS). MID1 controls the ubiquitin-mediated proteasomal degradation of the catalytic subunit of PP2A (PP2AC), one of the major phosphatases in the cell. Although MID1 mutations lead to an increase in PP2AC levels, the exact mechanism remains unclear. The main objective of this project was to find DUBs that work in conjunction with MID1 rescuing the increase of PP2AC level observed upon its mutations.

We specifically silenced 24 DUBs and analyzed the protein abundance of PP2AC. A decrease in the protein target levels will be indicative of a suitable DUB candidate to further study. We also made the opposite assay, overexpressing the same 24 DUBs, in this case, the DUBs overexpression should increase the PP2AC protein. From both screenings, we found USP8 as a good candidate, which we confirmed in further assays, to modulate the PP2AC levels. Consistently with the regulation of PP2AC, USP8 overexpression alters 4E-BP1 phosphorylation levels, affecting the mTOR pathway. To conclude USP8/MID1 is a functional pair controlling the degradative fate of PP2AC.

Furthermore, we noticed that in Mouse Embryo Fibroblasts from *Mid1* KO, the Usp8 protein levels were up regulated. We found that USP8 levels are decreased in both the cytoplasmic and nuclear fractions when MID1 was overexpressed, recovering the USP8 levels when using the ΔRING form of MID1 (the non-catalytic form). Moreover, the nuclear fraction of PP2AC decreased when MID1 was overexpressed and increased when USP8 was overexpressed.

To conclude we discovered a new DUB/TRIM pair that works in a highly coordinated manner. MID1 controls the levels of USP8 in the cytoplasm and nucleus, and both MID1/USP8 control the levels of PP2AC, a mutual substrate, in the nucleus fraction. These findings will be relevant in basic knowledge and for the future investigation of potential therapeutic.

1. Introduction

1.1 Ubiquitination

Ubiquitination is a post-translation modification process that changes protein fate. On one hand, it can lead to a degradative outcome, controlling protein level and quality. On the other hand, it can regulate cellular signaling, for instance, the protein's activity or localization (Kliza and Husnjak 2020). The ubiquitin-proteasome pathway was first documented in 1980 by Ciechanover *et al,* describing a mechanism of intercellular protein degradation (Ciechanover et al., 1980).

The main player of ubiquitination is ubiquitin (Ub), a protein that is covalently attached to the target protein. Substrates can be modified with a single Ub or with a polyubiquitin chain in which one Ub is conjugated to the next. Ub is a stable and conserved protein, it has a flexible C-terminal tail, seven internal Lysin (Lys)-residues covering all Ub surfaces, and the N-terminal Methionine (Met). (Komander & Rape, 2012; Özkaynak et al., 1984).

1.1.1 Ubiquitination code

The extent and type of response of a targeted protein are achieved through a ubiquitination code (**Figure 1**). There are two types of ubiquitination: mono- or poly- ubiquitination. The monoubiquitin (mono-Ub) modification is formed by one Ub when it occurs on multiple residues of the substrate yield a modification referred to as multi-monoubiquitination. The polyubiquitin (poly-Ub) chain can be represented by several Ub links, which are characterized based on two variables: Ub chain topology and the type of Lys-residue of Ub used for linkage. Regarding the poly-Ub chain topology, there are two categories: homotypic chains (linked through one type of Lys-residues), and heterotypic/ branched chains (multiple types of Lys-residues and chains topologies (**Figure 1A**). Considering the Ub residue used for the binding of the following Ub in a chain, there are 8 different possible linkages: through Met^{1} to form a linear Ub chain, and via each of the seven internal Lys-residues (Lys^{6}-, Lys^{11}-, Lys^{27}-, Lys^{29}-, Lys^{33}-, Lys^{48}-, and Lys^{63}-linked Ub chains) (Gómez-Díaz & Ikeda, 2019; Kliza & Husnjak, 2020; Yau & Rape, 2016) (**Figure 1B**). The Lys^{48}-linked Ub chain was the first one to be identified, and it marks proteins for degradation through the 26S proteasome (Finley et al., 1994). The remaining homotypic chains are collectively called atypical, and their biological

significance is still under study. The Lys[11]-linked Ub chain is a quality control signal for the endoplasmic reticulum-associated degradation (ER-AD) pathway, in which misfolded or improperly assembled proteins on the ER are targeted for proteasomal degradation (Bosanac et al., 2011; Christianson & Ye, 2014). The Met[1]-, Lys[6]-, Lys[27]-, Lys[33]-, and Lys[63]-linked Ub chains are involved in non-degradative pathways, like autophagy, DNA damage repair, and innate immunity (**Figure 1B**) (Kulathu & Komander, 2012; Walczak et al., 2012).

The ubiquitination code is translated by proteins containing ubiquitin-binding domains (UBDs) that recognize chain topology and the linker regions connecting two Ub molecules. The majority of the UBDs fold into α-helical based structures, the ubiquitin-associated domain (UBA), ubiquitin-interacting motif (UIM), and coupling of ubiquitin conjugation to ER degradation (CUE). Non-helical UBDs are the ubiquitin-binding zinc fingers (ZnFn), the ubiquitin-conjugating (UBC) domain present in E2 enzymes, or the pleckstrin homology (PH) folds (Dikic et al., 2009; Grabbe & Dikic, 2009). The ubiquitination code is the result of the interaction between UBDs and different Ub chains present on the substrate.

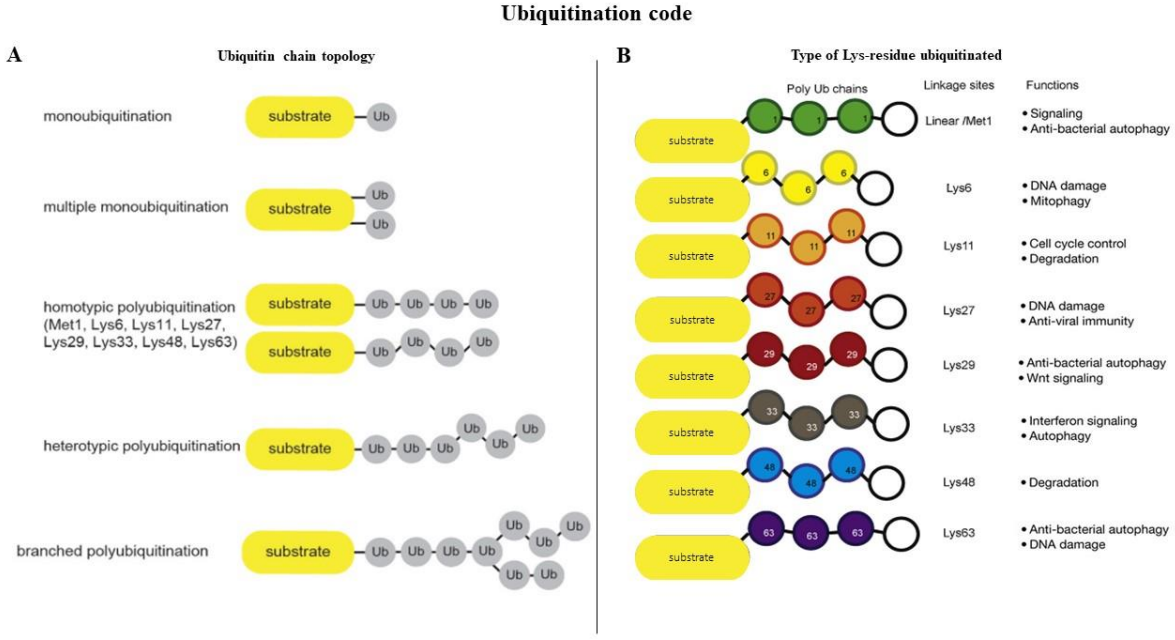

Figure 1. Ubiquitination code. A. Ubiquitin chain topology. Single Ub can modify proteins at one (monoubiquitination) or several (multiple monoubiquitinations) Lys-residues. Ub can form eight distinctive homotypic linkages, through either Met1 (linear Ub chain) or seven internal Lys-residues. Additional complexity is achieved through the formation of heterotypic Ub chains, which contain multiple Ub linkages and adopt mixed or branched topology. **B. Type of Lys-residue ubiquitination.** Substrate ubiquitination with eight possible linkage types (Met[1]/linear, Lys6, Lys[11], Lys[27], Lys[29], Lys[33], Lys[48], and Lys[63]) of Ub chains. Their major functions are indicated on the right. Abbreviations: Lys: Lysin, Met: Methionine, Ub: Ubiquitin. Adapted from Gómez-Díaz & Ikeda, 2019; Kliza & Husnjak, 2020.

1.1.2 Ubiquitination cascade

Ubiquitination is a highly coordinated process divided into three stages mediated by the following classes of enzymes (**Figure 2**): Ubiquitin-activating enzyme (E1), Ubiquitin-conjugating enzyme (E2), and Ubiquitin-ligase (E3). The Ub is activated by the enzyme E1 (E1∼Ub), which employs ATP to form a high-energy thioester bond between the Ub C-terminal and an E1 cysteine residue (active site). The activated Ub is transferred to an E2 enzyme cysteine residue through a thioester linkage (E2∼Ub). Finally, the E3 ligase places together the E2~Ub with the target substrate. The E3 ligase specifically transfers the Ub to the target substrate, producing a covalent bond between the Ub terminal glycine (Gly) residue with the substrate Lys-residue (Pickart & Eddins, 2004; Teyra et al., 2019; Zheng & Shabek, 2017). The activity of the ubiquitination machinery can be reversed by the deubiquitinating enzymes (DUBs), which can hydrolyze a peptide bond resulting in Ub deconjugation from the ubiquitinated protein (Komander et al., 2009; Pruneda & Komander, 2019).

The E1 family is composed of two members in mammals: the ubiquitin-activating enzyme (UBA1), the most abundant, and the ubiquitin-like modifier-activating enzyme-6 (UBA6), which is required during embryonic development. The conformational flexibility of the E1 ubiquitin fold domain (UFD) is decisive in binding and transferring the activated Ub to the E2s (Clague et al., 2015; Tokgöz et al., 2012).

The E2 family is composed of members containing a conserved ubiquitin-conjugating (UBC) catalytic fold responsible for the interactions with the other ubiquitination cascade components. The E2 family can be divided into four classes: Class I (UBC fold), Class II (UBC fold with N-terminal extension), Class III (UBC fold with C-terminal extension), and Class IV (UBC fold with N- and C-terminal extension). The E2 enzymes are in charge of the transfer of the Ub to the substrates and, in conjunction with some E3 classes, they determine the Ub chain topology. The different chain topologies can be achieved through two types of E2 catalytic activities: one type produces mono-ubiquitination or short Ub chain, and the second type is responsible for the extension of the Ub chain (Burroughs et al., 2008; Wijk & Timmers, 2010; Ye & Rape, 2009).

The E3 ligases are the critical components of the ubiquitination cascade due to their strict control of both reaction efficiency and substrate specificity. They are the most diverse components of the ubiquitination system, having hundreds of genes encoding them (Berndsen & Wolberger, 2014). The E3 family is divided into three classes, depending on their structural

and functional features (**Figure 2**): Homologous to the E6–AP C-terminus (HECTs), Really Interesting New Genes (RINGs), and RING-Between RING-RING (RBR or TRIAD). The HECT E3s (28 members) form a thioester-intermediate bond with the Ub on the active site before transferring it to the target protein (Huibregtse et al., 1995). The RING ligases (600 members) bind simultaneously with the E2~Ub and the target substrate. In this way, they facilitate the direct transfer of Ub from the E2 to the substrate, but without forming a direct bond with the Ub (Deshaies & Joazeiro, 2009). The RBR (14 members) employs both RING and HECT-like mechanisms. The Ub transfer is initiated by the interaction of an E2~Ub with the RBR (RING-like), followed by a thioester intermediate bond between Ub and RBR to further transfer the Ub to the substrate (HECT-like) (Wenzel et al., 2011).

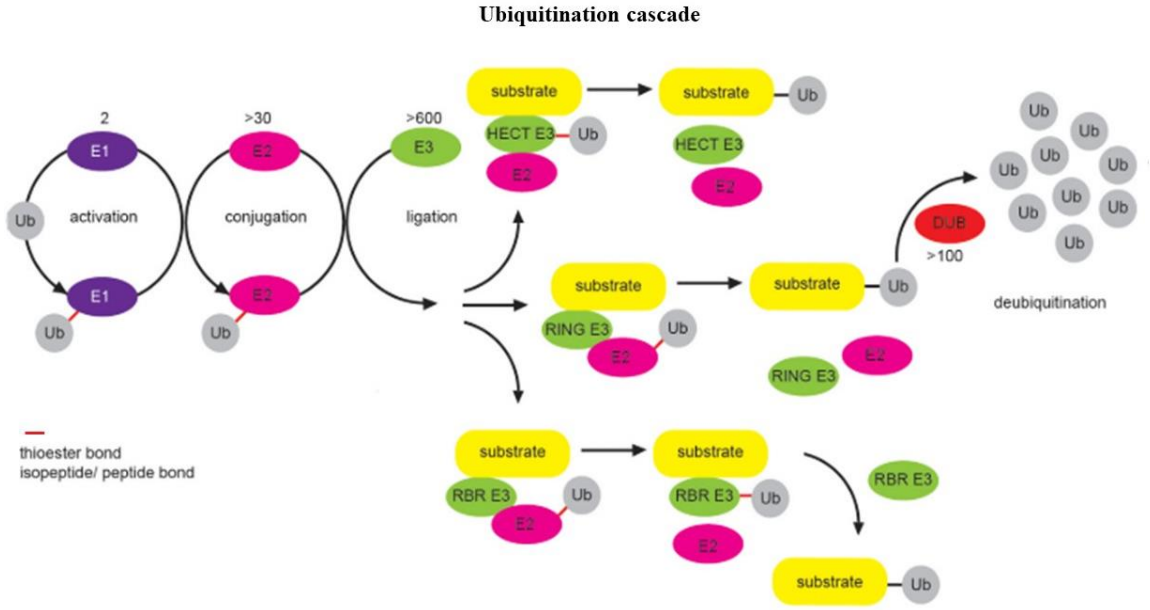

Figure 2. Ubiquitination cascade. Coordinated activity of Ub-activating (E1), Ub-conjugating (E2), and Ub-ligating enzyme (E3) are required for Ub attachment to a substrate protein. The action modes of the three main groups of E3 ligases (RING, HECT, and RBR) are also depicted. Abbreviations: HECT: Homologous to the E6–AP C-terminus, Ub: Ubiquitin, RBR: RING-BetweenRING-RING, RING: Really Interesting New Genes. Adapted from Kliza and Husnjak 2020

1.1.3 Proteasomal degradation

Three ubiquitin-dependent degradation pathways complement each other: ubiquitin-proteasome system (UPS), lysosomal degradation, and autophagy. Although the UPS was considered mainly the major route for Ub-driven degradation, it has been discovered that it is also connected to lysosomal degradation and autophagy. In this thesis, we will focus on proteasomal degradation (Weissman et al., 2011).

The Lys^{48}-linked polyubiquitination and the branched Lys^{48}-Lys^{11} chains are the most potent signals for degradation by the proteasome. The 26S proteasome is responsible for the proteolysis of ubiquitin-tagged substrates. It is an ATP-dependent protease containing two major assemblies: the 20S subunit core particle (CP) and a 19S regulatory particle (RP) subunit (**Figure 3**). The RP is composed of RPT (ATPase) and RPN (non-ATPase) subunits, which form a base and a lid, which will control the access of the ubiquitinated substrates to the proteasome core. The substrate is first bound, via its polyubiquitin chain(s), to the RPN (such as UIM, an α-helical UBD); secondly, it is unfolded by ATPases on the RPT ring, and then inserted via an open gate into the proteolytic chamber. The RP also contains DUBs (RPN11, UCHL5, and USP14) that recycle Ub and/or edit the polyubiquitin chain to enhance substrate binding to the RP. Proteolysis of the substrate is mediated in the CP which is composed of two β-rings flanked by two α-rings, each ring with seven subunits. Inside the proteolytic chamber, there are three β-subunits with catalytic activity responsible for the final proteasomal degradation (Clague & Urbé, 2010; Weissman et al., 2011).

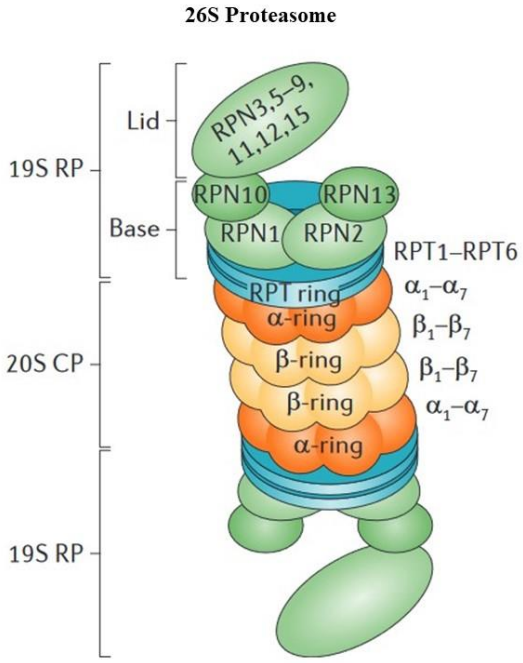

Figure 3. Structure of the 26S proteasome. The 26S proteasome is composed of a core 20S catalytic particle (CP) and the 19S regulatory particle (RP). The substrate is bound to specific subunits in the 19S RP, then unfolded by the ATPases in the RPT ring and inserted via an open gate in the α-ring of the 20S CP into the proteolytic chamber. The RP contains deubiquitinating enzymes that recycle ubiquitin. Abbreviation: CP: 20S Catalytic Particle; RP: Regulatory Particle; RPN: RP non-ATPase subunits; RPT: RP ATPase subunits. Adapted from Weissman et al, 2010.

Because of its complex structure, numerous targets, and the need for rapid adaptation to various physiological conditions, this multi-catalytic enzyme complex is stable and not regulated by degradation. Rather, it is primarily regulated by compositional variation. Some of the integral 20S proteolytic subunits can be switched in an inducible and tissue-specific way that alters proteolytic specificities and adapts them to changing needs. In addition to the 19S RP, other proteins and complexes bind to the end of the 20S cylinder and activate it by opening the gate: an example is proteasome-associated DUBs and E3s, which can remodel substrate-anchored polyubiquitin chains, modulating their susceptibility for degradation; and chaperones, which stabilize the association between different subcomplexes of the 26S proteasome (Clague & Urbé, 2010; Finley, 2009; Weissman et al., 2011). Consistent with its longevity, the proteasome appears to be degraded by the lysosome, probably through micro-autophagy (Cuervo et al., 1995).

1.2. RING E3 ligases

In the last decades, the ubiquitination process has received considerable attention in basic and applied research, allowing to successful develop pharmacological drugs that target some ubiquitination steps. Particularly, the RING ligases are the largest group of E3 ligases: they are involved in several cellular processes and their deregulation has been associated with multiple human diseases (C. Cai et al., 2022).

The RING domain is a type of zinc-finger domain that comprises 40–60 residues, and it is characterized by the presence of a Cys-X2-Cys-X (9-39)-Cys-X (1-3)-His-X (2-3)-Cys-X2-Cys-X (4-48)-Cys-X2-Cys motif (where X can be any amino acid; histidine (His) and cysteine (Cys) are sometimes interchangeable). The conserved Cys and His residues coordinate the two atoms of zinc to form a cross-brace 3D structure (Budhidarmo et al., 2012).

This E3s architecture is formed by RING homo- or hetero-dimers. In the case of heterodimers, one of the two RING proteins binds to the E2, possessing an E3 ligase activity, while the other has a structural role (Deshaies & Joazeiro, 2009). The binding of an E1 or an E3 to an E2 is mutually exclusive because the E3-binding site on E2s partially overlaps with the E1-binding site, thus the E2-RING E3 interaction is transient (Eletr et al., 2005). In many RING E3 ligases, the substrate-binding site is in the same polypeptide as the RING domain, while in others it is mediated by a separate subunit (for example the SCF complexes) (Zheng et al., 2002).

Considering the enzymatic activity mechanism, through crystal structures it was possible to observe that an arginine side chain on the RING subunit bridges the E2 and the Ub C-terminal tail (Dou et al., 2012). On one hand, the zinc-bound His interacts with Ub through a hydrogen bond, immobilizing its C-terminal tail; on the other hand, the RING domain interferes with E2 rearrangement, resulting in a thioester bond suitably positioned for attack by the substrate Lys-residue (Lima & Schulman, 2012). The first linkage of one Ub to the substrate is a slow and unspecific reaction. The chain elongation (polyubiquitin chains), that corresponds to the formation of the Ub-Ub isopeptide bond, is a faster and E2-specific reaction. The polyubiquitin chains can be built directly on the substrate or firstly on the E2 and then transferred to the substrate “en bloc” (W. Li et al., 2007).

1.2.1 Tripartite motif (TRIM) Family

Tripartite motif (TRIM) proteins constitute one of the largest subfamilies of RING E3 ligases, counting in humans more than 70 members. TRIM proteins have in common their N-terminal arrangement (named RBCC), which is composed of a RING finger, one or two B-box domain(s), and a Coiled-coil (CC) region. The RING domain is present in hundreds of other proteins, while the B-box domain is a signature of the TRIM family. The RBCC motif is present at the N-terminal of these proteins, while their C-terminal presents different combinations (Reymond et al., 2001).

The RING domain is defined by a (see above) arrangement of Cys and His residues that coordinate two atoms of zinc (Freemont, 1993). Some members do not have a RING domain, but they are still considered TRIMs because the rest of the motif (B-boxes and CC) is conserved in order and spacing. The RING domain is typically found within 10-20 amino acids of the first Met. The principal function of the RING finger domain is to recruit the E2~Ub for the subsequent transfer of the Ub to the substrate. Several TRIM E3 ligases require a RING dimerization as a prerequisite for their activity. This suggests a precise regulation level of TRIMs activity, where some are constitutively active, while others are selectively activated in time and space (Fiorentini et al., 2020).

The B-boxes, similarly to the RING domain, are zinc-binding domains. Many TRIMs only contain a B-box type 2, while those with two B-boxes always contain a tandem B-box1–B-box2 arrangement (Meroni & Diez-Roux, 2005). The role of the B-boxes is still unclear. It has been suggested that, due to similarities with the RING domain, they could enhance the E3 ligase activity and even confer E3 ligase activity to TRIMs without RING. It was also proposed that B-boxes may act as target recognition modules because they bind to proteins regulators, transcriptional regulators, protein localization modules, and protein-protein interaction domains (Tao et al., 2008). It is still to be elucidated if B-boxes have a unified function. Nevertheless, some mutations on the B-boxes domain have been found in severe genetic diseases, proving their importance in the overall function of the TRIM E3 ligase correct function (Fontanella et al., 2008).

The CC domain is responsible for TRIM homo- and hetero-interaction, a process required for the E3 ligase activity. The TRIM CC region adopts an antiparallel dimeric arrangement, placing the RING and B-box domains on opposite sides of the elongated central helical stem, limiting

the global protein architecture (Y. Li et al., 2014; Napolitano & Meroni, 2012; Sanchez et al., 2014).

Despite being united by their tripartite organization, TRIM members have different C-terminal domains that categorize them into 11 subtypes (**Figure 4**). The C-terminus mainly determines target specificity, allowing the involvement in different biological processes, and particular cellular localization. The most prevalent C-terminal is the PRY-SPRY domain (named from SPla and RYanodine Receptor), found in subfamilies C-I and C-IV. Other common C-terminal domains are the C-terminal subgroup one signature (COS) domain found in subfamilies C-I, C-II, and C-III, and the fibronectin type III (FN3) domain found in subfamilies C-I and C-III (Crawford et al., 2018).

TRIM proteins have been associated with diverse cellular processes, such as chromosomal translocations generating oncogenic fusions; developmental processes causing hereditary disorders; regulation of selective autophagy to name some (Watanabe & Hatakeyama, 2017).

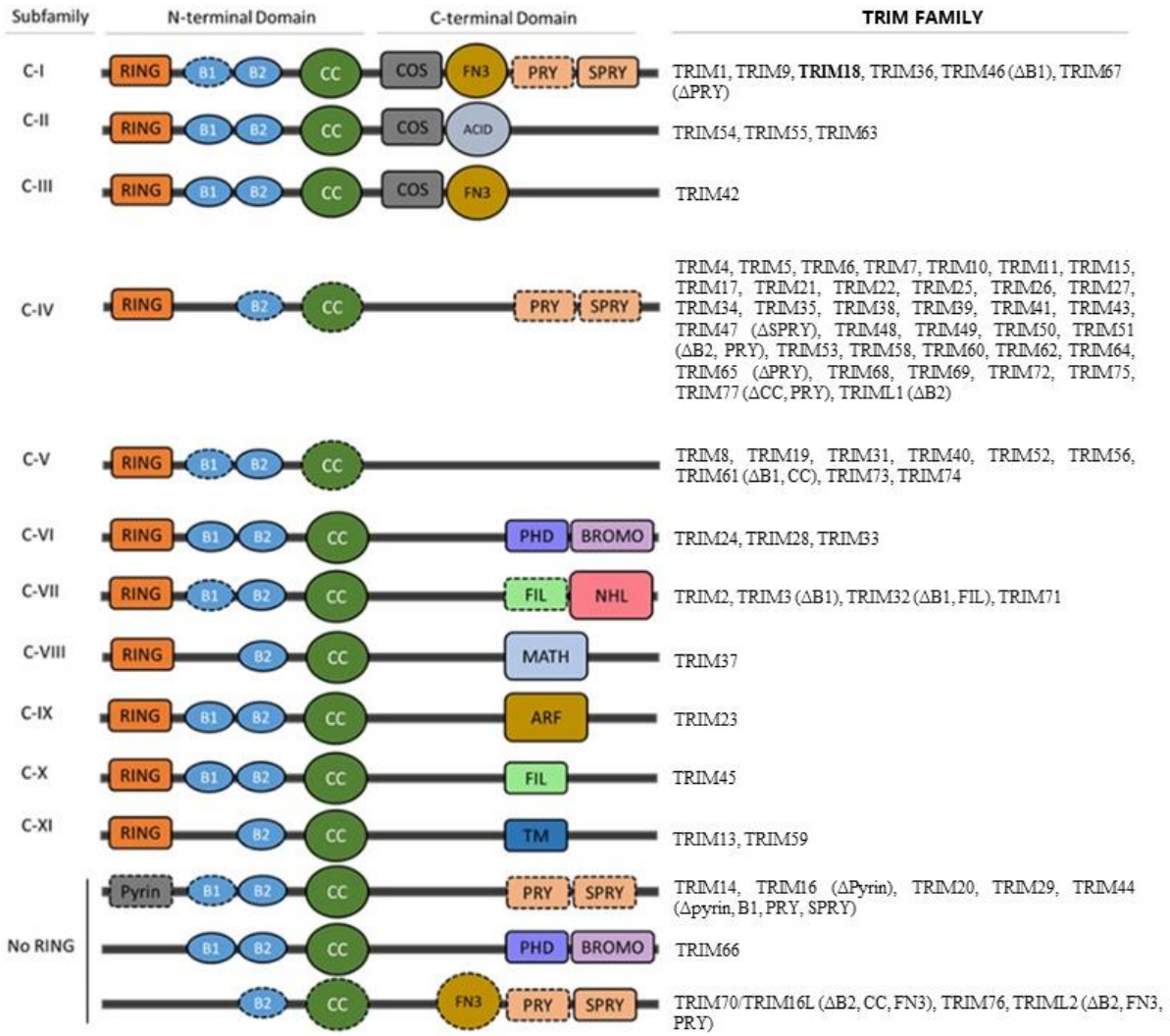

Figure 4. Classification of TRIM proteins. The TRIM proteins are classified into subgroups based on the C-terminal domain(s) associated with the tripartite motif. The name of the class is reported in the first column, followed by the domain composition, and in the right-most column the TRIM proteins that belong to each class. The domains shown as dashed may be absent in some members of the subgroup. Abbreviation: ACID: Acid Rich Region; ARF: ADP-Ribosylation Factor Family; B1/B2: B-box1–B-box2; BROMO: Bromodomain; CC: Coiled-coil; COS: C-terminal Subgroup one signature; FIL: Filamin-type I G; FN3: Fibronectin Type III; MATH: Meprin and TRAF homology; NHL: NCL1, HT2A, and LIN41 domain; PHD: Plant homeodomain; PRY-SPRY: SPla and RYanodine Receptor; RING: Really Interesting New Genes; TM: Transmembrane; TRIM: Tripartite motif. Adapted from Crawford, Johnston, and Irvine, 2017.

1.3 Midline1 (MID1)

This thesis will focus on a particular member of the TRIM family, TRIM18, also called Midline1 (MID1). MID1 is an E3 ligase that belongs to the subclass C-I, where the C-terminal is composed of COS, FN3, and PRY-SPRY domains (Reymond et al., 2001) (**Figure 4**).

1.3.1 *MID1* mutations in X-linked Opitz syndrome

The *MID1* gene is located on the short arm of the X chromosome (Xp22.2), and it consists of nine coding exons with several alternatively spliced exons, spanning approximately 400 kb of genomic sequence. The *MID1* gene encodes the 667 amino acid protein MID1 (Cainarca et al., 1999; Quaderi et al., 1997; Reymond et al., 2001).

Mutations in the *MID1* gene have been associated with the human X-linked Opitz G/BBB (XLOS) syndrome (**Figure 5**) (Quaderi et al., 1997). Analysis of isolated and familial cases of XLOS revealed the presence of more than 80 different mutations in the *MID1* gene. Pathogenetic mutations include nonsense, missense, indels, duplications, and splice-site changes, as well as partial or complete gene deletions. It has been reported that the predominant mutations are in the 3' region, and affect all protein domains, except for the RING domain (Fontanella et al., 2008). The presence of several types and the distribution of mutations along the entire length of the gene indicate the loss of function as the mechanism underlying the pathogenesis of XLOS (Cox et al., 2000). Importantly, the knowledge of both the type of mutation and the domain of the protein involved is not sufficient to predict the presence and/or the severity of specific clinical features (Migliore et al., 2013).

Opitz G/BBB Syndrome (OS) is a congenital disorder characterized by developmental defects of midline structures. OS is genetically heterogeneous, presenting an autosomal dominant form (ADOS) and an XLOS form that cannot be distinguished based on the clinical phenotype (Robin et al., 1995); in both cases, male patients exhibit a more complex and more severe phenotype than female patients (Robin et al., 1996). The autosomal dominant form is linked to a large region in chromosome 22 (22q11.2), and the *SPECC1L* gene on 22q11.2 has been reported as a candidate for ADOS, although this is still controversial (Kruszka et al., 2015; Migliore et al., 2022).

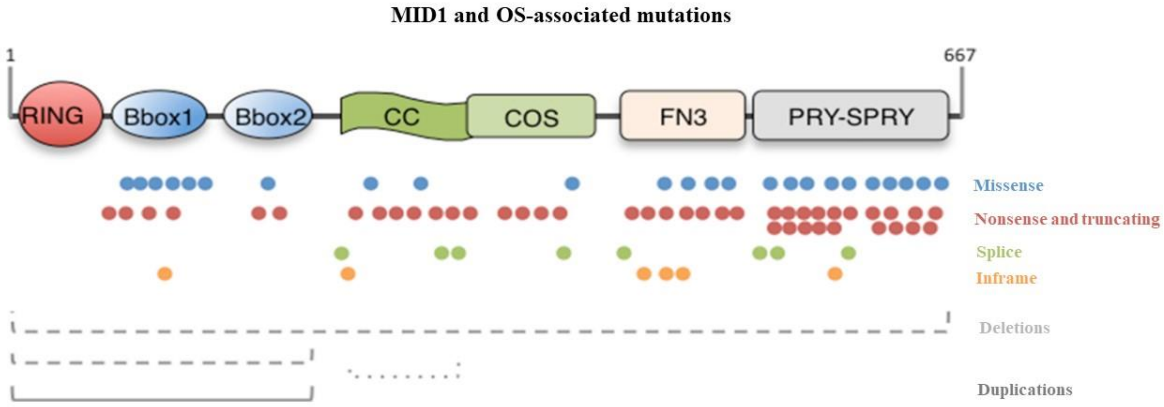

Figure 5. MID1 protein domain structure and OS-associated mutations. The domain composition of the MID1 protein: RING (10–59); B-Box (B1, 114–164; B2, 170–212); CC (219–319); COS (320–380); FN3 (382–472); PRY (483–528); SPRY (538–657). Below the scheme, color dots represent the different mutations reported on OS patients: blue dots, missense mutations; red dots, nonsense, and truncating mutations; green dots, splice site mutations; orange dots, in-frame indels. The dashed lines represent deletions and rearrangements; the continuous line represents duplications. Abbreviation: B1/B2: B-box1–B-box2; CC: Coiled-coil; COS: C-terminal Subgroup one signature; FN3: Fibronectin Type III; MID1: Midline1; PRY-SPRY: SPla and RYanodine Receptor; RING: Really Interesting New Genes. Adapted from Baldini, Mascaro, and Meroni 2020.

OS patients carrying mutations in the MID1 gene present a typical facial appearance, possibly as the result of incorrect morphogenetic processes during the formation, definition, and closure of the embryonic ventral midline. These patients are characterized by ocular hypertelorism, prominent forehead, broad nasal bridge, frontal bossing, anteverted nares, defects in the oral cavity (cleft lip/palate, bifid uvula, tooth abnormalities), and hypospadias. In severe cases, they can also present cardiac malformations, anal abnormalities (imperforate or anteriorly positioned anus), and other urogenital defects (Fontanella et al., 2008). Moreover, a high percentage of XLOS patients present cognitive disabilities and developmental delays associated with anatomical brain abnormalities. In XLOS, male hemizygous patients manifest variability of the clinical signs, while female carriers only show hypertelorism (Robin et al., 1995).

1.3.2. *Mid1* knock-out (KO) mouse line

The *Mid1*$^{-/Y}$ knock-out (*Mid1*$^{-/Y}$ KO) mouse line has been generated in our Lab (Lancioni et al., 2010). *Mid1*$^{-/Y}$ mouse line carries a nonfunctional ortholog of the human *MID1* gene, obtained by disruption of the first ATG-containing exon. *Mid1*$^{-/Y}$ mice are viable and fertile and do not show evident midline defects, but present anatomical brain abnormalities in the

dorsal midbrain and cerebellar regions. Whole mount and histological analyses of the *Mid1*$^{-/Y}$ brains show the presence of a malformed anterior cerebellum and, sagittal sections through the vermis, hypoplasia, and abnormalities of the most anterior lobes (I, II, and III): lobe I is missing, lobe II is not completely formed, and lobe III is in many cases abnormal in shape. These defects are occurring during embryonic development as abnormalities in the anterior development of the cerebellum are detectable since mid-gestation. Anterior cerebellar hypoplasia is also a brain anatomical abnormality observed in approximately 35% of OS patients. The *Mid1*$^{-/Y}$ mice also present impairments in motor coordination and non-associative and procedural learning. These behavioral defects can be correlated with intellectual disabilities and developmental delays observed in patients (Lancioni et al., 2010).

To conclude, the animal model recapitulates the neurological signs of the disease in humans. However, craniofacial, tracheoesophageal, cardiac, and urogenital abnormalities, that are shown by OS patients, are not present in *Mid1*$^{-/Y}$ mice (Lancioni et al., 2010). It may be that the human phenotype differs from the murine phenotype because of different genetic backgrounds or differences in evolutionary development between the two species. This may translate into different expressions of clinical symptoms.

1.3.3 MID1 protein

MID1 is a microtubule-associated protein due to the presence of the COS domain (**Figure 6**). The COS domain, constituted by two α-helices, together with the CC domain is essential for microtubular localization (J. Liu et al., 2001; Short & Cox, 2006; Wright et al., 2016). MID1 can also homodimerize and hetero-interacts with other members of the TRIM C-I subfamily, such as TRIM1/MID2, through its CC region (Cainarca et al., 1999; Sardiello et al., 2008; Short et al., 2002). Indeed, also MID2 has been localized to the microtubules, sharing some interactors with MID1 (Short et al., 2002). This chapter will focus on the role of MID1 as a microtubular protein.

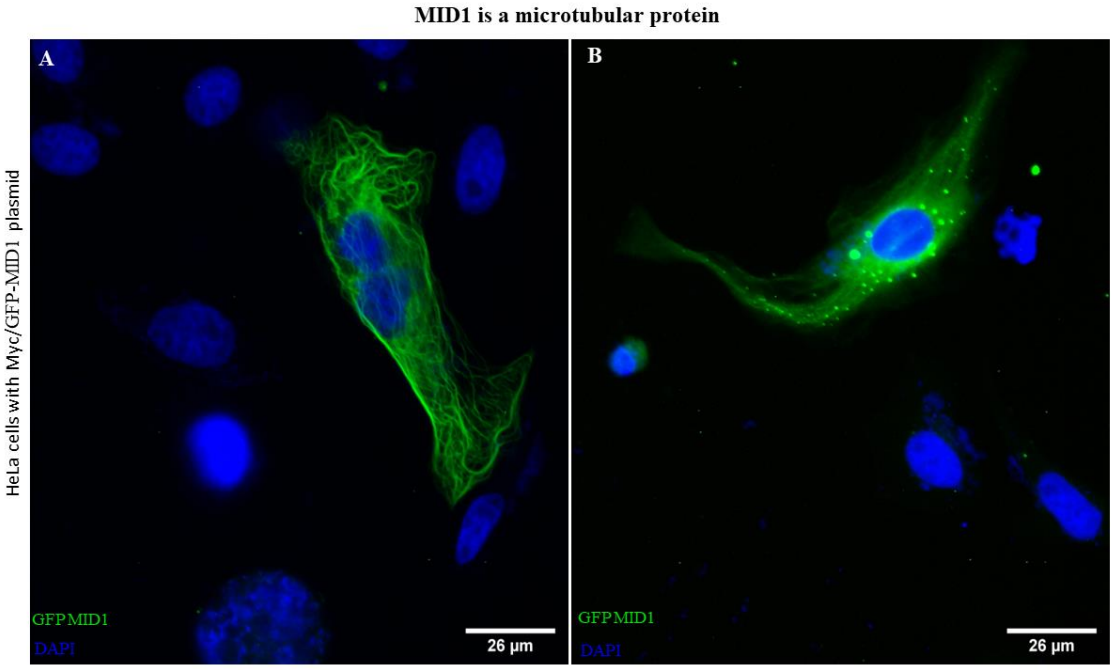

Figure 6. Microtubular localization of MID1 in HeLa cells. Immunofluorescence shows the distribution of MID1 (in green) in HeLa cells transfected for 48 hours with a Myc/GFP-MID1 plasmid. DAPI reagent was used as nuclear staining (in blue). MID1 is associated with microtubules dynamically either in a filamentous (A) or dots (B) form. Imagens were collected with an epifluorescent microscope (Leica DM2500) and analyzed with the Image J 1.53s program

The association of MID1 with microtubules occurs in different phases of the cell cycle: on the interphase microtubules, on the mitotic spindle, and on the midbodies during cytokinesis (Cainarca et al., 1999; Gholkar et al., 2016; Zanchetta et al., 2017). However, the mechanism through which MID1 is associated with microtubules is not clear. It was speculated that MID1 might act as a phosphoprotein: indeed, OS patients' fibroblasts presented a hypo-phosphorylated status of several microtubule-associated proteins (MAPs) (Trockenbacher et al., 2001). The hypothesis was that MID1 phosphorylation status could modulate microtubule binding. Liu et al in 2001 showed that MID1 phosphorylation promotes its association with microtubules (J. Liu et al., 2001). With contrasting results, Aranda-Orgillés et al in 2008, using the MID1 mutants in the serine residue (Ser^{96}) putative undergoing phosphorylation, showed a decrease in its association with microtubules (Aranda-Orgillés, Aigner, et al., 2008). This divergence is possibly explained by assuming that different microtubular proteins that bind to the MID1 (see discussion in the next chapter), together with the phosphorylation status, could produce different outcomes in terms of MID1 microtubular association. Moreover, in the same paper, Aranda-Orgillés et al showed that either phosphatase inhibition and simulation of

permanent phosphorylation of MID1 could block the transport of MID1 on microtubules in a kinesin- and dynein-dependent process (Aranda-Orgillés, Aigner, et al., 2008). In summary, MID1 phosphorylation status can regulate its bi-directional transport on microtubules, but the detailed mechanism requires more clarification.

Another debated topic is if and how MID1 affects microtubular dynamics and stability. In XLOS patients, MID1 association with microtubules is compromised and MID1 forms cytoplasmic foci or larger clumps; still, the microtubular distribution and dynamics are not affected in these patients (Cainarca et al., 1999). On the contrary, in *in vitro* assays, MID1 results in the protection of microtubules from depolymerizing drugs (Schweiger et al., 1999). Gholkar et al showed that cells in absence of MID1 display division defects, such as cytokinetic arrest and delayed or aborted abscission, which induce cell binucleation or death and may underlie microtubular dynamic changes (Gholkar et al., 2016). Zanchetta in her Ph.D. thesis showed that MID1 interacts with BRCA2-Associated Factor 35 (BRAF35) involved in cytokinesis and that both are localized at the midbody where stable microtubules are displayed (Zanchetta, 2015). Microtubule stabilization might occur transiently in specific phases of the cell cycle and under strict control. Another possibility is that the lack of MID1 in XLOS patients is only relevant for microtubular dynamics in the embryonic phase, where the cells are high proliferating and dividing with specific pathways activated, with this microtubular stabilization, becoming less in the adult phase.

1.3.4 MID1: E3 ligase activity

In MID1, like in the other TRIM family members, the RING domain is essential for E3 ligase activity. Instead, the role of B-boxes in the MID1 E3 Ub ligase activity is still debated. Moreover, MID1 has auto-E3 Ub ligase activity and can interact with several E2 conjugating enzymes, thus possibly promoting several types of Ub chains (Han et al., 2011; Napolitano et al., 2011). MID1 can control the stability and/or the activity of different substrates, such as Fu kinase, Pax6, and PP2AC. In the following chapters, the role of different substrates in embryogenesis (1.3.5 Involvement of MID1 in embryogenesis) and adulthood (1.3.6 MID1 in adulthood) will be described in more detail. The chapters below will focus on PP2AC, the main substrate studied in this thesis.

1.3.4.1 PP2AC

The E3 Ub ligase activity of MID1 was first described for the catalytic subunit of the protein phosphatase 2A (PP2AC). Trockenbacher and colleagues showed in XLOS patients' samples with loss of MID1 activity that PP2AC levels were increased due to reduced ubiquitin-mediated proteasomal degradation. Consistently, the PP2AC level decreases when MID1 is overexpressed in cells (Trockenbacher et al., 2001).

PP2Ac is part of the phospho-protein phosphatases (PPPs) family that belongs to the serine/threonine phosphatases (PSPs) superfamily (Haesen et al., 2014; Lechward et al., 2001). It is expressed in all mammalian cells, contributing to 0.3–1% of the total amount of protein in the cell (Ruediger et al., 1991). PP2AC regulates diverse physiological and cellular processes, such as neuronal stabilization, cardiac muscle function, transcription, translation, and cell cycle (Wlodarchak & Xing, 2016). It is implicated in many human diseases such as Alzheimer's disease (Martin et al., 2013), cardiac disease (Heijman et al., 2013; Kotlo et al., 2012), and cancer (Eichhorn et al., 2009); as such, it has been actively investigated as a therapeutic target. PP2A affects a variety of processes due to the formation of around 100 heterotrimeric holoenzymes (Lechward et al., 2001).

Structurally, PP2A is a multiform complex, and it exists in two distinct forms, namely heterodimeric and heterotrimeric forms (**Figure 7**). The dimeric form, also known as core enzyme, is composed of a scaffold subunit (PP2A-A, A subunit) and a catalytic subunit (PP2A-C, C subunit). The trimeric form in addition has the regulatory subunit (PP2A-B, B subunit), and this trimeric assembly is also called the holoenzyme complex. There are two isoforms, α, and β, for both A and C subunits, and they share high sequence homology. The two isoforms, of the C subunit each containing 309 amino acids with 97% sequence similarity, are encoded by two different genes (Haesen et al., 2014; Nematullah et al., 2018; Wlodarchak & Xing, 2016). The Cα isoform is abundantly localized in the plasma membrane, whereas the Cβ isoform is expressed in the cytoplasm and nucleus. Because of its stronger promoter activity and higher mRNA turnover, the Cα isoform is more abundantly expressed in cells, including the brain, than the Cβ isoform (Zhou et al., 2003). It is reported that PP2ACα is necessary for embryonic development, and PP2ACα knockout mice are not viable and die at 6.5 embryonic days (Götz et al., 1998).

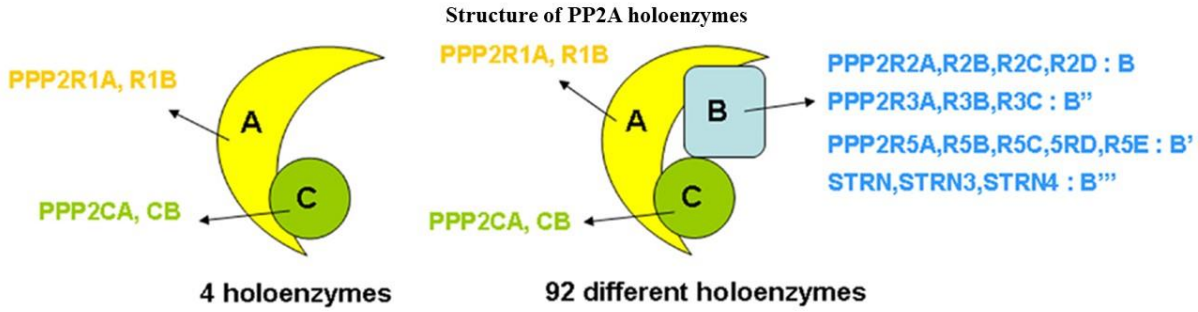

Figure 7. Structure of PP2A holoenzymes. The majority of PP2A enzymes have a heterotrimeric structure and consist of one catalytic C subunit, one scaffolding A subunit, and one regulatory B-type subunit. This is due to the existence of various isoforms of each of these subunits in human tissues, two C (encoded by *PPP2CA* and *PPP2CB*), two A (encoded by *PPP2R1A* and *PPP2R1B*), and 23 B-type isoforms (encoded by 15 different genes). The 92 different PP2A trimeric complexes can be assembled, and each one is characterized by its catalytic properties, substrate specificities, tissue or cell-specific expression, and subcellular localization. In addition, about one-third of PP2A occurs as a dimer of one A and one C subunit (four holoenzymes). Abbreviations: PP2Ac: catalytic subunit of the protein phosphatase 2A; *PPP2CA*: Protein Phosphatase 2 Catalytic Subunit Alpha; *PPP2CB*: Protein Phosphatase 2 Catalytic Subunit Beta; *PPP2R1A*: Protein Phosphatase 2 Scaffold Subunit A alpha; *PP2R1B*: Protein Phosphatase 2 Scaffold Subunit A beta. Adapted from Haesen et al., 2014.

The core of PP2AC contains two central β-sheets flanked by α-helices, with the loops connecting to the β-sheets forming the active site (J. Chen et al., 1992; Janssens & Goris, 2001). The active site of PP2AC has two catalytic metal ions coordinated by six conserved residues (two aspartate, one asparagine, and three His residues), and a catalytic water molecule. Phosphate binding is coordinated by one conserved His and two arginine residues (Shi, 2009; Wlodarchak & Xing, 2016). Several substrates have been attributed to PP2ACα: AK2 (Fuhrer & Yang, 1996), PKCδ (Boudreau et al., 2002), RAF-1 (Abraham et al., 2000), cdc6 (Yan et al., 2000), src (Yokoyama & Miller, 2001), STAT5 (Yokoyama et al., 2001), CIP2A (Junttila et al., 2007) and eRF1 (Andjelković et al., 1996) to name some. Regarding PP2ACβ, the NMDA receptor was reported as a substrate (Chan & Sucher, 2001)).

In addition to A and B subunits, PP2AC is also found associated with the α4 protein (Nakashima et al., 2013). The precise function of α4 on PP2AC is still not completely unraveled. The α4 stabilizes PP2AC protecting it from ubiquitination by MID1 and preventing its subsequent degradation (J. Liu et al., 2001; Short et al., 2002). In the next chapter, the MID1/PP2AC/α4 dynamics will be discussed in detail.

1.3.4.2 MID1/PP2Ac/α4 complex

The α4 is a highly conserved protein, first discovered as a phosphoprotein in B-cells, that interacts with and regulates the Type 2A family of serine/threonine phosphatases (J. Chen et al., 1998; Kloeker et al., 2003; Murata et al., 1997; Nanahoshi et al., 1999). Both α4 and PP2A are diffusely distributed in the nucleus and cytoplasm, and they can also assume a microtubular localization when MID1 is overexpressed. Numerous papers have studied the association between MID1, α4, and PP2AC on the microtubules, forming a MID1/PP2AC/α4 microtubular complex. A question has been raised as to whether the integrity of the complex is required for the various elements to be attached to microtubules. The α4 is a multidomain protein in which the N-terminus contains the residues responsible for binding to PP2AC, and the C-terminus has been shown to bind the B-box1 domain of MID1 (McConnell et al., 2010; Trockenbacher et al., 2001; Yang et al., 2007). Liu et al showed that high levels of α4 displace MID1 from microtubules, probably facilitating the dephosphorylation of MID1 and the consequent dissociation from the microtubules (Liu et al., 2001).

The α4 protein has been reported to protect the phosphatase catalytic subunit from degradation (Kong et al., 2009; LeNoue-Newton et al., 2011; McConnell et al., 2010). Structural studies suggest that it preferentially binds to the partially folded PP2AC and stabilizes it. In particular, the binding of α4 with PP2AC blocks access to the lysine residue in PP2AC, which is the target of polyubiquitination, thus leading to degradation (Jiang et al., 2013). No studies have shown that MID1 can change the protein levels of α4, or that it is directly ubiquitinating PP2AC; however, it is clear that the lack of MID1 increases the protein levels of PP2AC. This apparent contradiction can be explained by the following mechanism (**Figure 8**): MID1 mono-ubiquitinates α4, thus promoting its cleavage and the degradation of its C-terminal domain, which contains the MID1 binding region. Two papers from Han et al and Watkins et al proved that the RING domain of MID1 mono-ubiquitinates a 45-amino acid polypeptide of the C-terminus of α4 (Han et al., 2011; Watkins et al., 2012). The α4 cleavage is followed by a disruption of MID1/α4/PP2Ac complex in microtubules, with the result of releasing PP2AC to be redirected to other localizations, and this in turn permits PP2AC poly-ubiquitination by another E3 ubiquitin ligase (not discovered yet). In this way, only the microtubule pool of PP2AC is subjected to proteasomal degradation (Han et al., 2011; LeNoue-Newton et al., 2011; McConnell et al., 2010; Watkins et al., 2012). Overall, MID1 loss-of-function leads to a reduction of calpain-mediated cleavage of α4, resulting in the protection of PP2AC from

degradation (Watkins et al., 2012). The upregulation of PP2AC upon MID1 mutation could explain the hypo-phosphorylation of several MAPs as seen in OS fibroblasts (Trockenbacher et al., 2001).

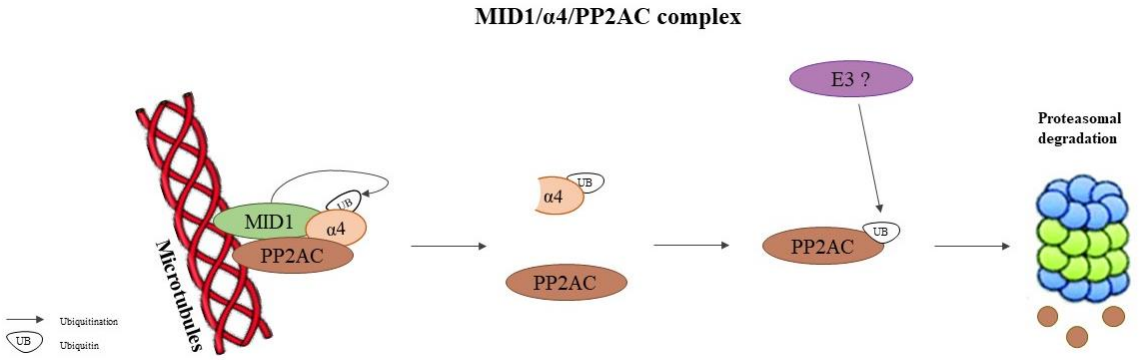

Figure 8. MID1, PP2AC, and α4 form a complex associated with microtubules. MID1 can interfere with the poly-ubiquitination and proteasomal degradation of PP2AC through the binding with α4, a regulatory subunit of PP2A. MID1 catalyzes a mono-ubiquitination on α4 which promotes calpain-mediated cleavage and degradation of its C-terminal domain that contains the MID1 binding region. The α4 cleavage is followed by a disruption of MID1/α4/PP2Ac complex in microtubules, with the result of releasing PP2AC to be redirected to other localizations, this in turn permits PP2AC poly-ubiquitination from another E3 ubiquitin ligase (not discovered yet). Abbreviations: MID1: Midline1; Ub: Ubiquitin; PP2AC: catalytic subunit of the protein phosphatase 2A.

1.3.4.3 MID1/PP2Ac and mTORC1 signaling

PP2A is involved in the regulation of several biological processes (discussed above), therefore the MID1/α4/PP2Ac complex participates in the modulation of these activities. Among others, PP2A regulates the mechanistic targets of rapamycin Complex 1 (mTORC1) signaling (**Figure 9**). The mTORC1 complex is composed of mTOR kinase, the target of rapamycin complex subunit LST8 (mLST8), and the regulatory-associated protein of mTOR (Raptor), with a role of recruiting substrates for phosphorylation. The mTOR is responsible for controlling translation initiation, through the phosphorylation of two substrates: eukaryotic translation initiation factor 4E-binding protein 1 (4E-BP1) and 40S ribosomal S6 kinase (S6K) (Ford et al., 1999; Nilsson et al., 2004; Sengupta et al., 2010; Winter et al., 2016). On one hand, PP2A dephosphorylates 4E-BP1 and S6K, and thereby downregulates the translation of several mRNAs (E. Liu et al., 2011). On the other hand, the MID1/α4 complex interacts, through the PRY-SPRY domain of MID1, with S6K and with the elongation factor-1α (EF-1α), forming a ribonucleoprotein (RNP) complex. The RNP is a large microtubule-bound multiprotein

complex, able to bind to RNA, and together with PP2A controls the activity of mTOR kinase (Aranda-Orgillés, Trockenbacher, et al., 2008).

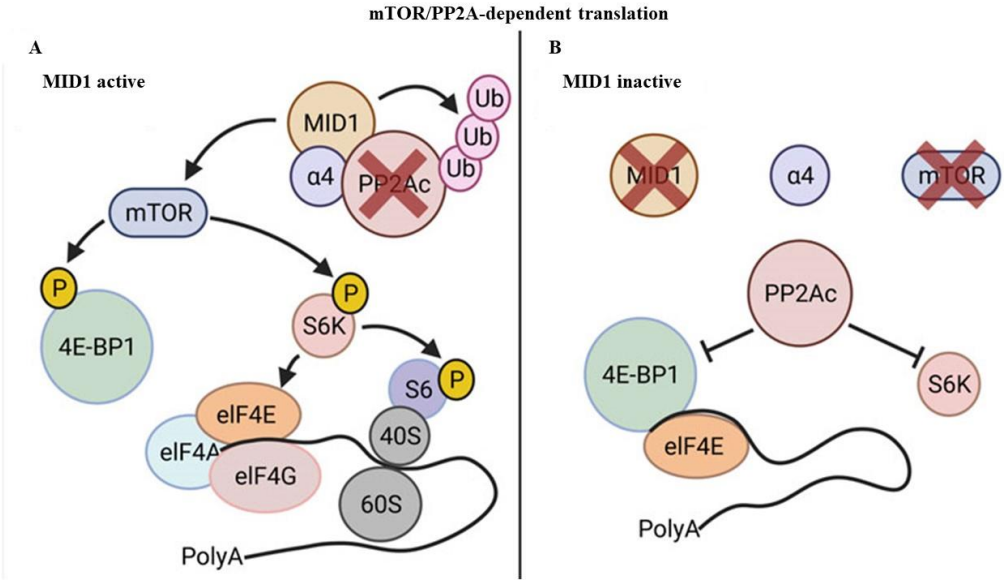

Figure 9. MID1 regulates mTOR/PP2A-dependent translation. MID1 is a positive regulator of mTOR and a negative regulator of PP2A, both controlling the phosphorylation status and the activity of their downstream targets S6K and 4E-BP1. By regulating the composition of the eIF complex (eIF4A, eIF4E, and eIF4G) and through the phosphorylation-dependent activation of eIF4B and ribosomal protein S6, 4E-BP1 and S6K mediate the unwinding and the linearizing of the 5'UTR of those mRNA that is associated with RNP complex, finally promoting the translation initiation. Abbreviations: 4E-BP1: 4E-binding protein 1; eIF complex: eukaryotic translation initiation factor complex; MID1: Midline1; PP2AC: catalytic subunit of the protein phosphatase 2A; S6K: 40S ribosomal S6 kinase. Adapted from Heinz et al., 2021.

The increased level of PP2AC, resulting from the depletion of MID1, also abolishes the interaction between mTOR and Raptor, thus downregulating mTORC1 signaling at another level. Indeed, cells derived from OS patients show decreased mTORC1 formation, S6K1 phosphorylation, and cap-dependent translation, all of which are rescued by the re-expression of wild-type *MID1* (E. Liu et al., 2011). The role of MID1 could also be extended to other pathways subjected to the mTORC1 feedback inhibition, such as PI3K/AKT and Ras/ ERK (Carracedo et al., 2008). Consequently, MID1 depletion affects a vast number of cellular processes such as cytoskeletal dynamics, intracellular transport, cell migration, autophagy, protein synthesis, cell metabolism, cell growth, and proliferation (Huang & Fingar, 2014; Jhanwar-Uniyal et al., 2019; E. Liu et al., 2011).

1.3.5 Involvement of MID1 in embryogenesis

MID1 is implicated in a congenital malformation disorder (XLOS), and it is highly expressed during embryonic development when its main function is carried out. The study of MID1's role during embryonic development has been conducted in mice (Dal Zotto et al., 1998), chicken (Richman et al., 2002), and humans (Pinson et al., 2004). Generally, the organogenesis stages are conserved among species. In human embryos, *MID1* is strongly expressed in the following progenitor cells: central nervous system, optic vesicle, pharyngeal arches, gastrointestinal tract, mesonephros, and heart interventricular septum (Pinson et al., 2004). In mouse and chicken embryos, *Mid1* expressions are partially comparable with the human one: is largely present in all embryonic tissues, in which the highest levels are observed in the undifferentiated progenitor cells of the central nervous system, developing branchial arches, gastrointestinal and urogenital systems (Dal Zotto et al., 1998). It is noticeable that the expression of *MID1* transcript during embryogenesis correlates with structures and organs whose development is affected in OS.

Mid1 exerts a pivotal role during the formation of the visual system, by regulating the temporal and spatial expression of Pax6 (**Figure 10**. **A**). During the development of the eye and the brain, Pax6 plays an important role; however, its role is time- and quantitative-dependent. (Shaham et al., 2012). In Xenopus, the expression of *Mid1* overlaps with *Pax6* in the optic vesicle during early embryogenesis. It was described that *Mid1* mediates Pax6 proteasomal degradation: when *Mid1* levels were reduced, Pax6 expression was expanded, and eyes enlarged (Pfirrmann et al., 2016). Through the modulation of Pax6, Mid1 regulates the optic stalk region, setting the border between the optic stalk and the retina.

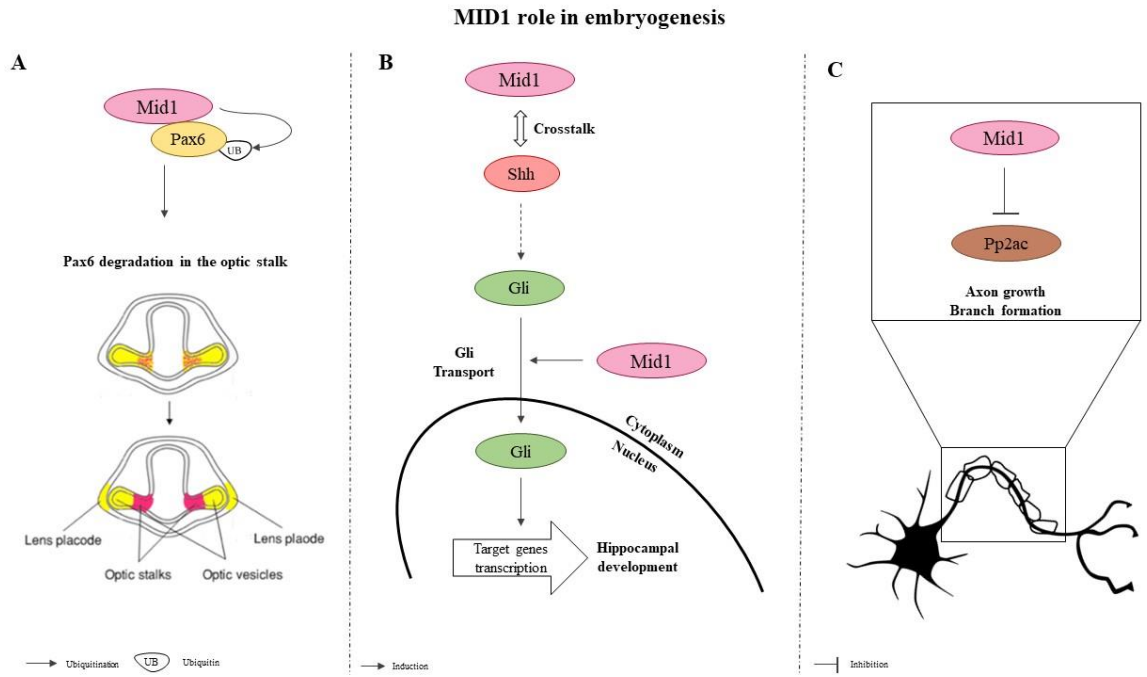

Figure 10. MID1 role in embryogenesis. A. In Xenopus, an overlapping expression of *Mid1* (in pink) and *Pax6* (in yellow) is observed in the optic stalk, in the early stages of the visual system development. *Mid1* regulates the ubiquitination and proteasomal degradation of Pax6 protein that is cleared from the optic stalk region, setting the border between the optic stalk and the retina. **B.** In chicken development, both Shh (dark red) and *Mid1* (pink) are initially expressed bilaterally in the Hensen's node. Shh can suppress *Mid1* expression and *Mid1* can act upstream of Shh. Simultaneously, MID1 can also regulate the GLI3 activity by affecting its transport to the nucleus. In turn, GLI3 is a mediator of Wnt/β-catenin signaling, an important pathway to form the axis during hippocampal development. **C.** Mid1 is highly expressed in the brain during development and enriched in the axon segment of developing neurons. By suppressing the Pp2ac levels, Mid1 act as a regulator of axon development and branch formation. Abbreviations: Mid1: Midline1; PP2AC: a catalytic subunit of the protein phosphatase 2A; Shh: 5; Wnt: wingless-related integration site. Adapted from: Baldini et al., 2020.

Another important pathway that MID1 has been associated with is the Sonic hedgehog (Shh) (**Figure 10**. **B**). The Shh pathway has strong implications for ventral midline definition during development, which is the main process compromised in OS patients (Ingham & McMahon, 2001). In detail, Shh binds to the membrane protein Patched (Ptch), releasing the repression effect of Ptch on Smoothened (Smo), another membrane protein. The activation of Smo culminates in the release of Gli, a family of transcription factors, into the nucleus (Sasai et al., 2019). MID1 is associated with the Shh pathway in two moments. The first one is that MID1 can regulate the activity of GLI3, by affecting its transport to the nucleus. In turn, GLI3 is a mediator of wingless-related integration site (Wnt)/β-catenin signaling, an important pathway to form the axis during brain development (Hasenpusch-Theil et al., 2012). The second association is a possible feedback loop between *Mid1* and Shh. During development in

Xenopus, ectopic *Shh* induces *Mid1* expression in the developing optic vesicle, and the prospective forebrain (Pfirrmann et al., 2016). Moreover, in the chicken Hensen's node, Shh can suppress *Mid1* expression and *Mid1* can act upstream of Shh (Granata & Quaderi, 2003).

Some studies have reported a Mid1 role in neural development (Alexander et al., 2010; Suzuki et al., 2010), contributing to the development of the cerebellum, a structure commonly found altered in OS patients (Dierssen et al., 2012; Lancioni et al., 2010; T. Nakamura et al., 2017). Downregulation of *Mid1* has been reported in the cerebellum and hippocampus of transgenic mice expressing a dominant active downstream regulatory element antagonist modulator (DREAM) mutant. At the same time, those mice exhibit a significant shortening of the rostro caudal axis of the cerebellum, and a severe delay in neuromotor development early after birth (Dierssen et al., 2012). The migration of immature neurons from germinal zones toward their final destination is an essential process during cerebellar development and might be dependent on MID1. Tangential and radial migrations are mediated by Rac proteins, which belong to the Rho family of small GTPases (Govek et al., 2005). Indeed axonogenesis, dendritogenesis, tangential, and radial migrations are impaired in transgenic mice depleted for *Rac1* and *Rac3*. Interestingly, *Rac*-KO mice exhibited higher levels of *Mid1* transcripts, suggesting that the upregulation of *Mid1* might be responsible for the defective processes observed in these mice (T. Nakamura et al., 2017). Another study reported that Mid1 is highly expressed in the brain during development and enriched in the axon segment of developing neurons (**Figure 10**. **C**). Lu and colleagues showed that depletion of *Mid1* in cultured neurons results in Pp2ac accumulation in the axons, which originates abnormal axonal growth and branch formation. Moreover, the Pp2ac upregulation results in accelerated axonal growth and altered projection pattern in the corpus callosum of the mouse embryos (Lu et al., 2013). Therefore, Mid1 is required for proper axon development acting as an inhibitory factor to regulate axon growth. This ensures precise structural and functional patterning, which is crucial for proper circuit formation.

1.3.6 MID1 in adulthood

MID1 is implicated in a wide variety of cellular mechanisms, via the selective regulation of proteins involved in several pathways. As a consequence, alterations in MID1 are associated with pathological conditions like cancer (Demir et al., 2014), Huntington's disease (Krauß et

al., 2013), and Alzheimer's disease (Hettich et al., 2014; Matthes et al., 2018). The next chapters will deal with the involvement of MID1 in immunity, neurology, and cancer (**Figure 11**).

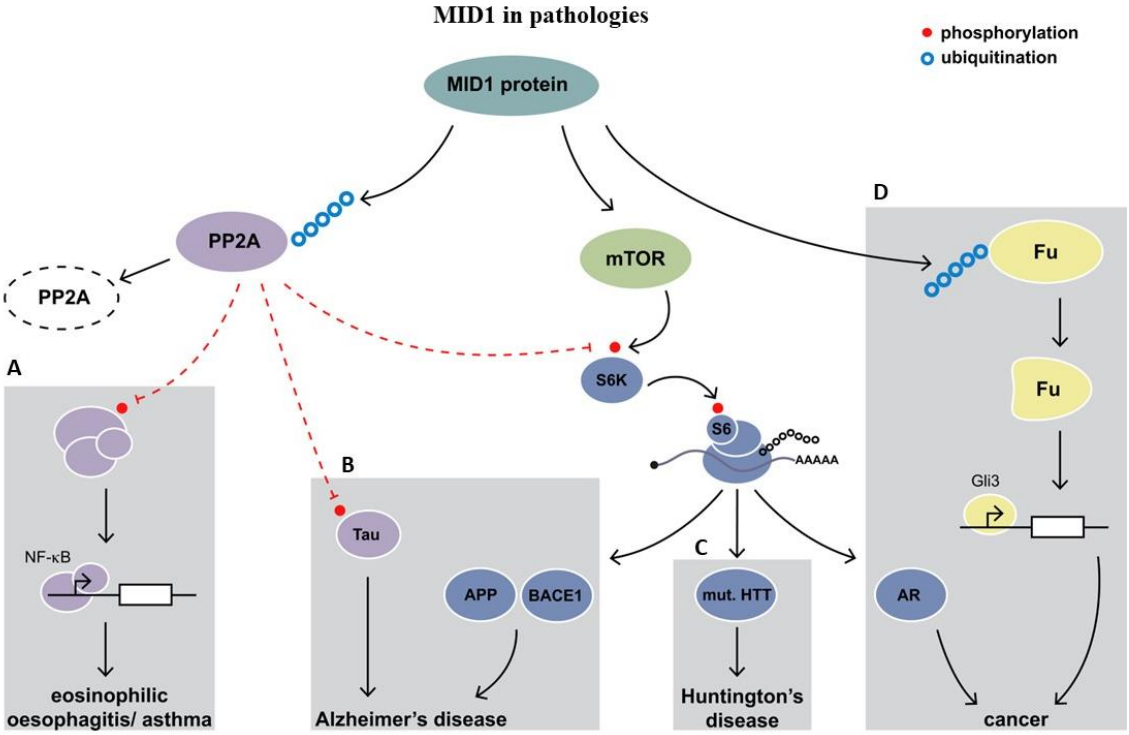

Figure 11. MID1 functions in different pathological conditions. **A**. The MID1, by limiting PP2A activity, can be a regulator of inflammatory genes via NF-κB signaling. This pathway is involved in asthma, eosinophilic esophagitis, and rhinovirus-induced exacerbations. **B.** MID1 regulates the pathological hallmarks of Alzheimer's disease by influencing the translation and the activity of the β-Secretase 1 (BACE1) secretase and by mediating the hyperphosphorylation of Tau protein. **C.** MID1 is involved in Huntington's disease, through the binding and the further stimulation of mutant HTT mRNA translation. **D.** MID1 has a role in cancer. On one hand, MID1 regulates the activity of an effector of the mammalian Sonic Hedgehog (SHH) pathway, the GLI3 transcription factor, by ubiquitinating Fu. On the other hand, MID1 binds to and induces the translation of the Androgen Receptor (AR) mRNA, which is involved in prostate tumor progression. Abbreviations: APP: Amyloid Precursor Protein; AR: Androgen Receptor; BACE1: Beta-Secretase 1; HTT: Huntingtin; MID1: Midline1; NF-κB: Nuclear factor kappa-light-chain-enhancer of activated B cells; PP2AC: a catalytic subunit of the protein phosphatase 2A; S6K: 40S ribosomal S6 kinase; Shh: Sonic Hedgehog. Adapted from Unterbruner et al. 2018.

1.3.6.1 MID1 in immunity

The Ub system, particularly the TRIM family, has been vastly associated with immunity. MID1 was identified as a regulator of allergic airway inflammation in the bronchial epithelium with asthma and rhinovirus (**Figure 11. A**) (Collison et al., 2013). Mice sensitized with rhinovirus infection and displaying pathological signs of allergic asthma, showed upregulated Mid1 in

bronchial cells at both mRNA and protein levels (Collison et al., 2013). This upregulation is associated with decreased PP2A activity and PP2AC protein level while, conversely, silencing of Mid1 attenuates asthma signs. Hence, Mid1 can promote allergic airway disease by controlling the PP2A-mediated deactivation of NF-κB among other pathways (Collison et al., 2013; Foster et al., 2017). These results were confirmed by the observation that MID1 activates proinflammatory signaling in bronchial epithelial cells from human patients (Collison et al., 2015, 2019).

1.3.6.2 MID1 in neurodegenerative disease

Several studies have reported the implication of MID1 in different neurological diseases, one of them being Alzheimer's disease (AD) (**Figure 11. B**). The two pathological hallmarks of this type of dementia are extracellular amyloid plaques, which contain A-β, and intracellular neurofibrillary tangles, which are composed of hyperphosphorylated Tau (Stelzmann et al., 1995). The A-β peptides are generated by two sequential cleavages of the amyloid precursor protein (APP), the first of them being performed by the β-site APP-cleaving enzyme β-Secretase 1 (BACE1) (Zhang et al., 2011). Three different levels of regulation connect MID1 to AD. First, the phosphorylation status of both Tau and BACE1 is crucially important for determining the physiological and pathological role of these proteins. MID1, by reducing the activity of PP2A, can indirectly increase BACE1 translation and Tau phosphorylation. It was shown that the disassembly of the MID1-PP2A complex by specific drugs may target both pathological hallmarks of AD (Hettich et al., 2014; Schweiger et al., 2017). Second, the protein synthesis of APP is controlled by MID1 through the modulation of mTOR-eIF signaling (Matthes et al., 2018). Lastly, APP mRNA was identified as a binding partner of MID1, indicating that the MID1 complex can also induce its translation (Matthes et al., 2018).

MID1 has also a role in Huntington's disease, by stimulating the translation of the mutant Huntingtin (HTT) protein (**Figure 11**. **C**). Some genes, such as HTT, present nucleotide expansions in their sequence, leading to the formation of stable double-stranded RNA structures that are predisposed to bound proteins in the RNP complex. Expanded CAG repeats in HTT are described to trigger translation in a MID1/PP2A/mTOR-dependent manner, thus enhancing the translation of mutant HTT mRNA (Krauß et al., 2013).

1.3.6.3 MID1 and neoplasia

The MID1 complex interacts with and regulates diverse signaling pathways that are associated with carcinogenesis. In this section we will discuss how the MID1 protein complex promotes tumor growth by interacting with two different tumorigenic pathways: SHH, and AR, signaling.

SHH pathway not only plays an active role during embryogenesis but is also implicated in oncogenesis. Together with mTOR, the MID1/α4/PP2Ac complex controls the subcellular localization and the activity of the zinc finger protein GLI3 transcription factor. An increase in PP2A activity mediated by a downregulation of MID1 results in cytosolic retention of GLI3 and its reduced transcriptional activity. Conversely, inhibition of PP2A mediates its nuclear localization (Krauß et al., 2008). MID1/α4/PP2Ac complex does not affect GLI3 directly, but rather through the protein Fu. MID1 promotes Lys^{6}, Lys^{48}, and Lys^{63}-linked ubiquitination of Fu, leading to its proteasome-dependent cleavage. As a result, the kinase domain of Fu is cleaved-off, permitting nuclear translocation of GLI3 and transcriptional activation (Schweiger et al., 2014).

The involvement of MID1 in prostate cancer has been reported. It was demonstrated that the androgen receptor (*AR*) mRNA bounds MID1 (**Figure 11**. **D**). AR is a ligand-activated transcription factor able to trigger several intracellular processes upon androgen binding. The binding of MID1 to *AR* mRNA induces its translation; in turn, AR also regulates MID1 transcription in response to androgen stimulation, suppressing it. AR transcription factor physiologically regulates androgen-dependent gene expression, but it is aberrantly activated in prostate cancer. Additionally, the most aggressive cases of prostate cancer show a high level of MID1 protein, delineating a possible role of MID1 as a factor for tumor progress and metastasis-promoting (Demir et al., 2014).

1.4 Deubiquitinating enzymes (DUBs)

In the cell, the activity of degraded proteins is carefully controlled. This tight control is essential since an unsettled activation can be tragic for the cell. The regulation of protein levels and activity are achieved thanks to the balance between ubiquitination and deubiquitination. DUBs can reverse the ubiquitination process by hydrolyzing the peptide bond from the ubiquitinated protein, resulting in free Ub (**Figure 2**). DUBs maintain cellular Ub levels by processing newly synthesized Ub precursors and by reclaiming Ub from proteins destined for degradation (Clague et al., 2019; Sahtoe & Sixma, 2015).

In humans there exist 99 DUB members, 11 of which are considered to be pseudo enzymes due to the loss of critical residues for their activity, although they can perform vital functions (Walden et al., 2018). DUBs can be subdivided into seven families (**Figure 12**): ubiquitin C-terminal hydrolases (UCHs); ubiquitin-specific proteases (USPs), ovarian tumor proteases (OTUs); Josephins (MJDs); JAB1/MPN/MOV34 metalloenzymes (JAMMs; also known as MPN+ or JAMM/MPN+), and the most recently discovered, i.e., the motif interacting with ubiquitin (MIU)-containing novel DUB family (MINDY); and zinc finger with UFM1-specific peptidase domain protein (ZUFSP/ZUP1). All of these families are cysteine isopeptidases except for the JAMM family members, which are zinc-dependent metalloproteinases (Clague et al., 2019; Sahtoe & Sixma, 2015). Cysteine proteases DUBs generally contain catalytic dyads or triads (either two or three amino acids) to catalyze the hydrolysis of the amide bonds between Ub and the substrate. In contrast, metalloproteases coordinate zinc ions with histidine, aspartate, and serine residues, which activate water molecules and enable them to attack the isopeptide bond (Zong et al., 2021).

DUBs are frequently inactive or autoinhibited, remaining in this state until they are recruited to their place of activity and/or bind to the correct substrates. To achieve proper localization and specificity, DUBs are modular, thus requiring domains outside the catalytic core to associate with scaffolds, substrate adapters, or the substrates themselves (Eletr & Wilkinson, 2013). These additional domains include the zinc finger (ZnF) domain, ubiquitin-like domain (UBL), coiled-coil (CC) domain, and MIU domain (**Figure 12**).

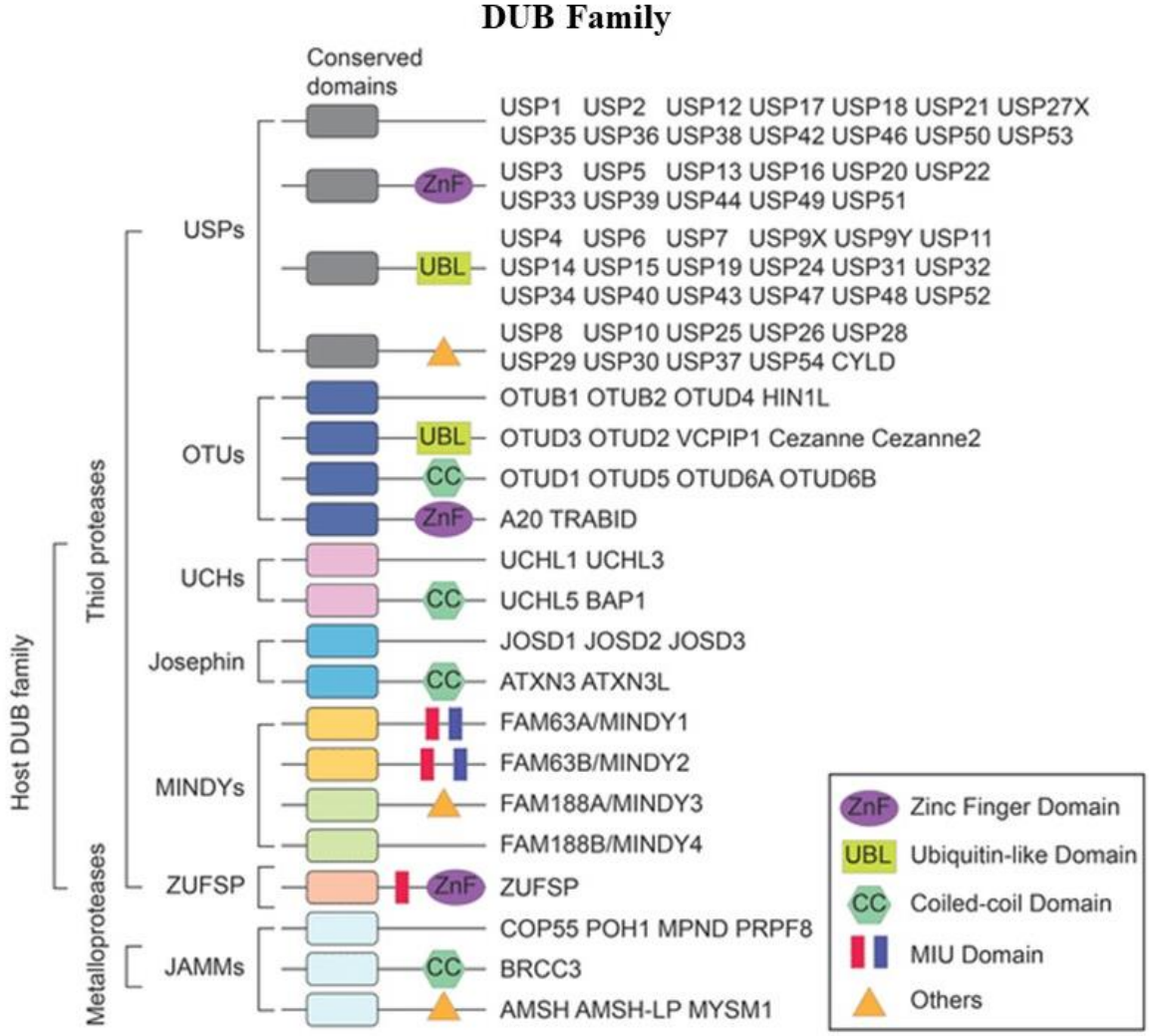

Figure 12. Classification and domain architecture of the DUB family. The host DUB family can be divided into six families of cysteine proteases, namely ubiquitin-specific proteases (USPs), ovarian tumor proteases (OTUs), ubiquitin C-terminal hydrolases (UCHs), the Josephin family, the motif interacting with ubiquitin (MIU)-containing novel DUB family (MINDYs), zinc finger with UFM1-specific peptidase domain protein (ZUFSP), and one family of metalloprotease group, namely the JAB1/MPN/MOV34 metalloenzyme family (JAMMs). The conserved and specific domains are indicated by different shapes and colors. Abbreviations: CC: coiled-coil domain; DUB: Deubiquitinating enzymes; JAMMs: JAB1/MPN/MOV34 metalloenzymes; MINDYs: MIU-containing novel DUB family; MIU: Motif interacting with ubiquitin; OTUs: ovarian tumor proteases; Ub: Ubiquitin; UBL: Ubiquitin-like domain; UCHs: ubiquitin C-terminal hydrolases; USPs: ubiquitin-specific proteases; ZnF: Zinc Finger Domain; ZUFSP: zinc finger with UFM1-specific peptidase domain protein. Adapted from: Zong et al., 2021.

1.4.1 Cleavage and binding of DUBs

DUBs are proteases that cleave peptide or isopeptide bonds between conjoined Ub molecules or between Ub and a modified protein. Most DUBs catalyze a proteolytic reaction between a Lys ε-amino group and a carboxyl group corresponding to the C-terminus of Ub (Komander & Barford, 2008).

The complexity of Ub chain architectures dictates the wide variety of distinct DUB activities and preferences (**Figure 13**) (Clague et al., 2019; Mevissen & Komander, 2017). The OTU family shows remarkable specificity for different Ub chain linkages and may recognize substrates based on those linkages (Eletr & Wilkinson, 2013; Mevissen et al., 2013). Aside from discriminating chain linkage type (**Figure 13. A**), DUBs may choose between processing from the distal end, gradually chewing down the chain (exo-DUB activity), or cleaving within chains (endo- DUB activity) (**Figure 13. B**). Endo-DUBs must accommodate Ub molecules on either side of the cleavage site, whereas exo-DUBs only need to bind to a single Ub (Mevissen et al., 2013; Walden et al., 2018; Winborn et al., 2008). JAMM family cleavages are based on the chain, between proximal Ub and substrate, and/or they are highly specific for Lys^{63} poly-Ub linkages. Ub chain length provides another variable, with the Josephin family specializing in distinguishing between poly-Ub chains of different lengths (Cooper et al., 2009; Eletr & Wilkinson, 2013; McCullough et al., 2006).

Many DUBs are directed towards specific substrates via protein interaction domains distinct from the catalytic domain (**Figure 13. C**). The USP class recognizes substrates by the interaction of variable regions of sequence with the substrate protein directly. This interaction can also occur with scaffolds or substrate adapters in multiprotein complexes. The USP family thanks to its substrate recognition can, selectively, regulate cellular processes. Notably, most USPs remove Ub regardless of linkage type (Eletr & Wilkinson, 2013; Faesen et al., 2011; Ritorto et al., 2014). These substrate-specific DUBs can lead to a single-step chain amputation, whereas the promiscuous DUBs might remove Ub completely from substrates (**Figure 13. C-left**). Alternatively, they may leave the substrate monoubiquitylated, especially if the DUB is linkage-specific (**Figure 13. C-right**). Monoubiquitin could then be extended again with a different linkage (Ub chain editing). Some DUBs specialized in mono-deubiquitinating, sometimes combined with substrate recognition (particularly associated with histones) (**Figure 13. D**).

An important group is the recycling DUBs, such as the UCH family that removes small disordered sequences from the C-terminus of Ub, such as peptide remnants after proteasomal degradation, and can disassemble poly-Ub chains (**Figure 13. E-left)** (Eletr & Wilkinson, 2013). Other DUBs are responsible for the recycling of free Ub from unattached Ub chains, like USP5 which especially recognizes the free C-terminus of Ub (**Figure 13. E-right**) (Komander et al., 2009).

Regarding the new family MINDY, little is known about the cellular function of this family, but each member tested to date shows specificity for Lys^{48}-linked Ub chains, strongly indicating roles in protein homeostasis (Kristariyanto et al., 2017; Rehman et al., 2016). Another recently discovered DUB family is the ZUP1, with just one representative: it has specificity for Lys^{63}-linked chains with multiple Ub- binding domains and has been linked to genome maintenance pathways (Kwasna et al., 2018).

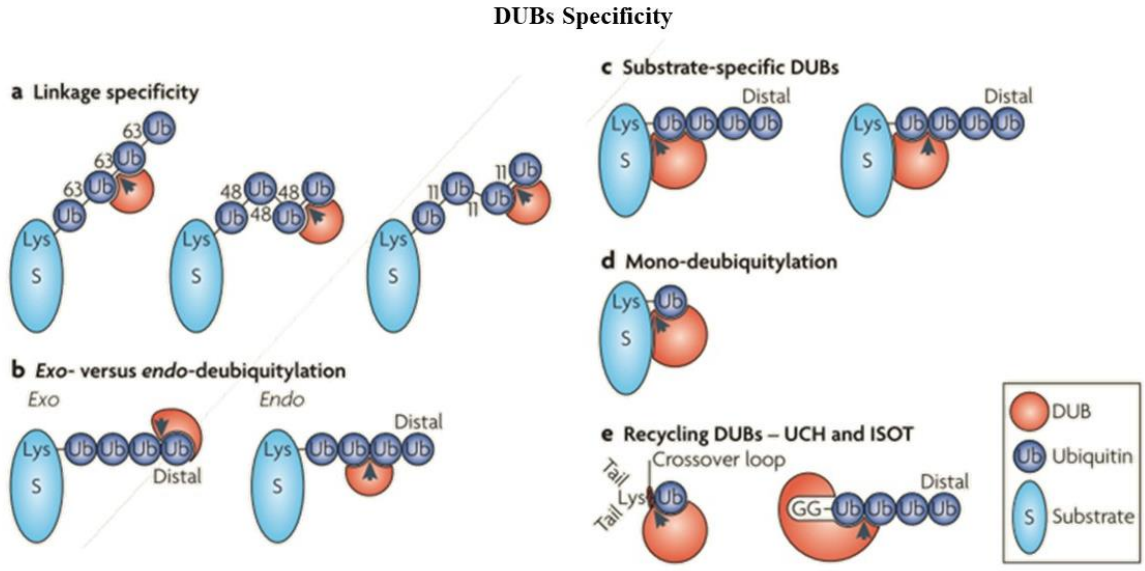

Figure 13. Layers of DUB specificity. Different ways to hydrolyze Ub have been reported. **A. DUBs chain type specific.** The existence of eight topologically different Ub chains allows for differential recognition by the DUBs. **B. Exo- and Endo- DUBs.** In Ub chains, cleavage (shown by the arrows) can occur from the ends (Exo) or within a chain (endo). **C. DUB directly substrate specific.** DUBs are directed towards specific substrates, removing Ub completely from the substrate (**C – left**), or might leave the substrate monoubiquitylated, especially if the DUB is also linkage-specific (**C - right**). **D. DUBs specialized in de-monoubiquitinating.** DUBs specifically recognize their cognate protein substrate to remove monoubiquitin. **E. Recycling DUBs.** UCH family members are designed to effectively remove small disordered sequences from the C terminus of Ub, such as peptide remnants after proteasomal degradation and C-terminal extensions of polyubiquitin precursors. (**E - left**). DUBs are also responsible for the recycling of free Ub from unattached Ub chains (**E - right**). Abbreviations: DUB: Deubiquitinating enzymes; Lys: Lysine; Ub: Ubiquitin; UCHs: ubiquitin C-terminal hydrolases. Adapted from Komander et al., 2009.

1.4.2 Roles of DUBs

DUB activities fall into three major functional categories (**Figure 14**). First, Ub can be transcribed from several genes as a linear fusion of multiple Ub molecules or with ribosomal proteins, such that the generation of free Ub requires DUB activity (**Figure 14**. **A**). Second, DUBs can remove Ub chains from post-translationally modified proteins, leading to the reversal of Ub signaling or to protein stabilization by rescue from either proteasomal (for example, cytosolic proteins) (**Figure 14**. **B**) or lysosomal (for example, internalized receptors) (**Figure 14**. **C**) degradation. However, once a protein is committed to these degradative machines, DUBs maintain the free Ub levels by directly removing the Ub from the target's proteins (**Figure 14**. **D**) and by processing en bloc Ub chain removal (**Figure 14**. **E**). Third, DUBs can be used to edit the form of Ub modification by trimming Ub chains (**Figure 14**. **F**) (Amerik & Hochstrasser, 2004; Clague et al., 2019; Komander et al., 2009).

All Ub genes encode C-terminally extended forms of Ub. The Ub precursors are either fusions with certain ribosomal proteins or head-to-tail-linked Ub multimers that also have an additional amino acid following the last Ub monomer (Amerik & Hochstrasser, 2004). Proper processing of these precursors is essential for the generation of competent Ub. Many of the DUBs can cleave the peptide bond by linking Ub to various C-terminal peptide extensions (Amerik et al., 2000). This processing is extremely rapid in vivo and can occur co-translationally (Turner & Varshavsky, 2000). The reason why all Ub proteins are synthesized in precursor form might be to provide a quality control step. If a DUB cannot bind and cleave an aberrantly synthesized or folded version of the Ub precursor, then the Ub will not be able to enter the active cellular pool (Amerik & Hochstrasser, 2004).

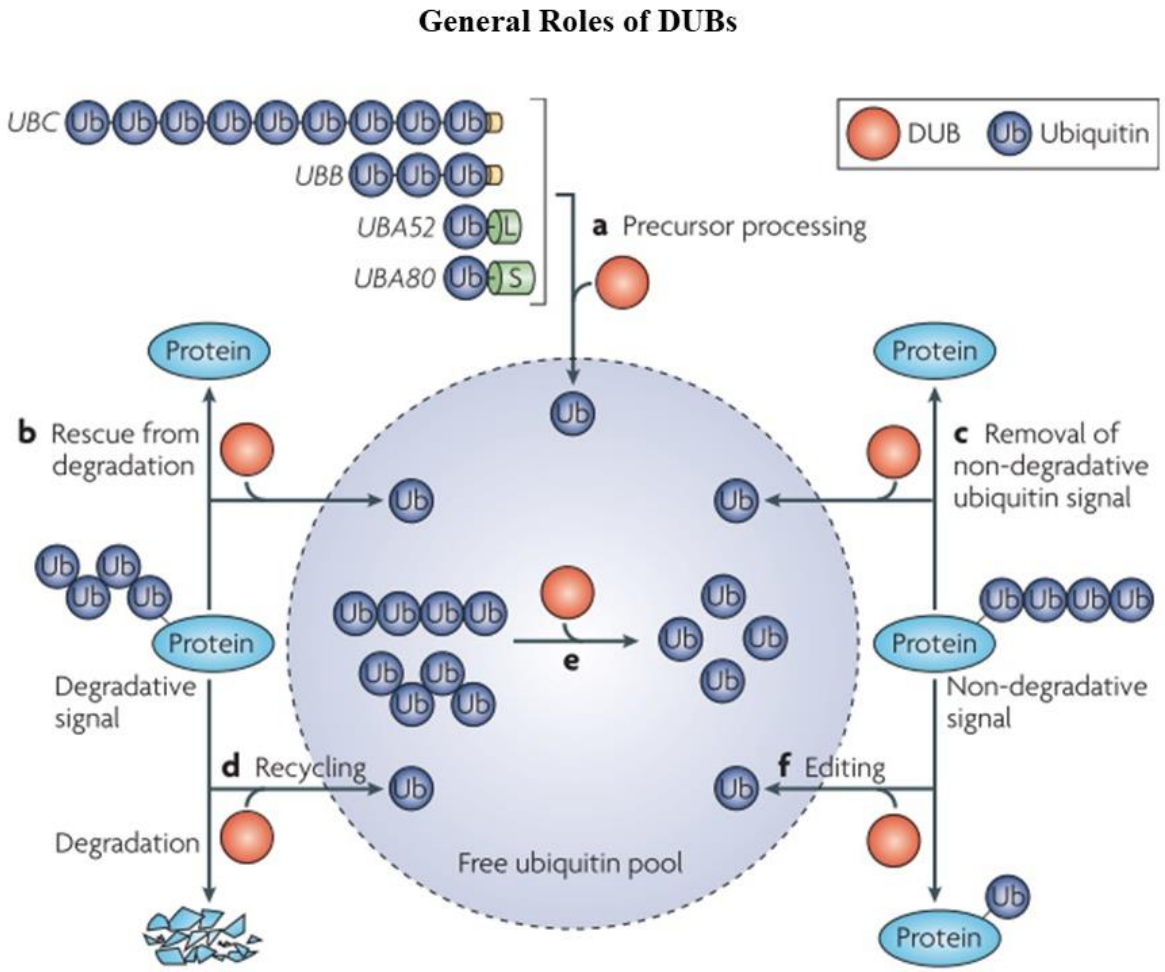

Figure 14. Major roles of DUBs. DUBs are involved in the generation of newly synthesized Ub by releasing monomeric Ub from multimeric precursor proteins encoded by four genes (**A**). *UBB* and *UBC* encode multiple copies of Ub that are transcribed and translated as linear fusion proteins with a carboxy-terminal extension of one or two amino acids (shown in yellow). *UBA52* and *UBA80* yield Ub fused to the amino terminus of two ribosomal subunits, 40S ribosomal protein L40 (L) and 60S ribosomal protein S27a (S) (shown in green). DUBs have key roles in maintaining protein homeostasis and signaling in cells. By removing Ub signals DUBs can regulate protein function directly or through multiprotein signaling complexes and rescue proteins from either proteasomal (**B**) or lysosomal degradation (**C**). DUBs also maintain Ub levels by recycling Ub from proteins that are committed to degradation (**D**) and by chain processing following en bloc Ub chain removal (**E**) to maintain free Ub levels. Finally, DUBs might function to edit Ub chains and thereby help to exchange one type of Ub signal for another (**F**). Abbreviations: DUB: Deubiquitinating enzymes; Ub: Ubiquitin; UBA52: Ubiquitin A-fused to ribosomal protein L40; UBA80: Ubiquitin A-fused to ribosomal protein S27; UBB: Ubiquitin B; UBC: Ubiquitin C. Adapted from Clague et al., 2019.

DUBs contribute in two known ways to rescue proteins from ubiquitination. First, some ubiquitinated proteins can be selectively deubiquitinated by certain DUBs, especially the USP family, as previously discussed. The second mechanism is a more general editing role reversing the modification of a wide range of proteins. This situation occurs particularly on the proteasome. The efficient binding of polyubiquitinated proteins to the proteasome generally requires polymers of at least four Ub. If a DUB preferred to remove single Ub moieties from the end of the chain most distal to the substrate, it could act as an editing or proofreading enzyme for proteasome targeting. Specifically, substrates with longer Ub chains could maintain proteasome-binding competence longer than those with only short chains (near the limit of four Ub). Hence Ub substrates, which may generally have shorter chains, could erroneously be rescued from proteolysis (Amerik & Hochstrasser, 2004; Clague et al., 2019). A DUB identified by Lam et al. doing editing work on proteasome is UCHL5, with distal-to-proximal Ub chain disassembly activity (Lam et al., 1997).

Another important function of deubiquitination is to release Ub chains from Ub–protein conjugates once they have been targeted to the proteasome and are committed to degradation. Failure to detach polyubiquitin could lead to inappropriate degradation of the Ub tag along with the substrate. Additionally, it could interfere with the entry of the substrate into the narrow opening leading to the central proteolytic chamber of the proteasome. Together with UCHL5, also USP14 and PSMD14 (JAMM family) are regulatory members of the 19S lid, coordinating critical proteasomal substrate pre-processing (Amerik & Hochstrasser, 2004; Clague et al., 2019; de Poot et al., 2017).

DUBs provide many important cellular functions, and several are essential for cell viability. DUB functions are often associated with the specificity for chain architectures and the generation of cleavage products that have defined cellular roles, such as DNA repair, cell cycle, and innate immune signaling pathways. Recently Clague, Urbé, and Komander reviewed the most recent advances in understanding the physiological functions of DUBs (Clague et al., 2019).

1.4.3 DUB subcellular localization

The impact of DUBs on cellular processes needs to take into consideration both the individual protein levels and their intracellular locations. For DUBs, the estimated range of copy numbers is large, from the low hundreds (limit of detection) to hundreds of thousands per cell (Clague et al., 2015, 2019). It is suggested that high-level DUB perform broad maintenance functions (for example, proteasomal DUBs), while the DUBs with lower amounts have more specialistic roles (Damgaard et al., 2016).

The localization is a key factor in explaining how a relatively limited number of DUBs can exert a large range of specific functions (Wing & Coyne, 2016). The specific effect of DUBs can be achieved thanks to their precise expression in tissue(s)/cell type (Clague et al., 2013) and/or upon activation with stimuli (Y. Zhu et al., 1997). DUB localization is a regulatory mechanism that allows the DUB action on substrates, which otherwise might not occur at significant rates if both enzyme and substrate are diluted in the cytoplasm (Wing & Coyne, 2016). The DUBs localization is predominantly cytosolic, however, approximately 25% of the enzymes are found in specific subcellular structures (Urbé et al., 2012). **Table 1** is a resume of the cellular localization of DUBs. Several DUBs have multiple splice variants, each one can localize in different compartments and have a different half-life depending on the splice variant (Clague et al., 2019). Not surprisingly USP family, that is the family with substrate specificity, is also the family with more members confined to a particular cellular compartment.

Table 1. DUBs localization. A summary of the DUBs-specific subcellular localization. Table based on Wing & Coyne, 2016 with the required updates considering the recent literature. Abbreviations: DUB: Deubiquitinating enzymes; JAMMs: JAB1/MPN/MOV34 metalloenzymes; UCHs: ubiquitin C-terminal hydrolases; USPs: ubiquitin-specific proteases.

Localization	Family	DUB	Reference
Nucleus	USP	USP1	(Nijman et al., 2005)
		USP3	(Nicassio et al., 2007)
		USP4	(Song et al., 2010)
		USP7	(vanLoosdregt et al., 2013)
		USP16	(Joo et al., 2007)
		USP21	(García-Santisteban et al., 2012)
		USP22	(Xiong et al., 2014)
		USP26	(Dirac & Bernards, 2010)v
		USP28	(Popov et al., 2007)
		USP36	(X. X. Sun et al., 2015)
		USP39	(Makarova et al., 2001)
		USP44	(Suresh et al., 2010)
	UCH	UCHL5	(Yao et al., 2008)
		BAP1	(Mashtalir et al., 2014)
	MJD	ATXN3	(Tait et al., 1998)
	JAMM	BRCC3	(Feng et al., 2010)
		MYSM1	(P. Zhu et al., 2007)
Mitochondria	USP	USP8	(Durcan et al., 2014)
		USP15	(Cornelissen et al., 2014)
		USP30	(N. Nakamura & Hirose, 2008)
		USP35	(Bingol et al., 2014)
Endoplasmic reticulum	USP	USP19	(Hassink et al., 2009)
		USP20	(Curcio-Morelli et al., 2003)
		USP25	(Blount et al., 2012)
		USP33	(Curcio-Morelli et al., 2003)
		USP35	(Leznicki et al., 2018)
	UCH	UCHL1	(Z. Liu et al., 2009)
Golgi	USP	USP32	(Akhavantabasi et al., 2010)
		USP33	(Thorne et al., 2011)
Endosome	USP	USP8	(Kato et al., 2000)
	JAMM	AMSH	(Tanaka et al., 1999)
Microtubules	USP	USP8	(Berruti et al., 2010)
		USP21	(Urbé et al., 2012)
Centrosome	USP	USP9X	(X. Li et al., 2017)
		USP21	(Heride et al., 2016)
		USP33	(J. Li et al., 2013)
Peroxisomes	USP	USP30	(Marcassa et al., 2018)

1.5 DUBs and E3 ligases pairs

The biochemistry of the ubiquitination reactions has been studied for decades and their roles in regulating diverse cellular processes are well appreciated. As our understanding of the complexity of the Ub code continues to grow, more emphasis must be placed on investigating how cells manage the complexity of the Ub code and how conjugation and deconjugation activities manage cellular Ub dynamics (Nielsen & MacGurn, 2020).

The number of E3 ligases encoded in the human genome (~700) is considerably larger than the number of DUBs (~100), even though new DUBs are still being discovered. The balance of Ub activities often involves the coupling of DUB-E3 ligase pairs. Evidence is being reported of DUB-E3 ligase machinery that contributes to the regulation of shared substrates and mutual circuits, providing many layers of regulation within the Ub network. A full characterization, functional and biochemical, of these pairs is still an open challenge. However, the research on DUB-E3 ligase pairs is rapidly increasing (Nielsen & MacGurn, 2020). In the next chapter, we will focus on the documented pairs of DUBs with the TRIM family members of E3 ligases.

1.5.1 DUBs and TRIMs pairs

The interaction of DUB members with the TRIM family is a recent research topic that started in the last decade. **Table 2** summarizes the papers that describe a DUB-TRIM pair relationship.

The regulatory logic of the TRIM-DUB pairs can be divided into four types, schematically shown in **Figure 15**. The first is the switch-like antagonism (**Figure 15. A**), where DUB-TRIM complexes can operate on a shared substrate, resulting in the regulation of the substrate fate. The activity of the DUB-TRIM pair with the substrate can either be a direct (de)ubiquitination on the target (**Figure 15. A-left**), or an indirect one, resulting in a functional interface (**Figure 15. A-right**). There are many examples of switch-like antagonist pairs (**Table 2**). A representative one was shown by Luo et al in which TRIM32 and USP11 play roles in controlling ARID1A stability. They proved by coimmunoprecipitation (co-IP) assay that TRIM32 and USP11 could interact with each other and that the presence of TRIM32 significantly reduced the association between USP11 and ARID1A, and vice versa (Luo et al., 2020).

The second type is mutual regulation (**Figure 15. B**). In particular, the DUB can protect the TRIM from degradation resulting from auto-ubiquitination, while the TRIM can ubiquitinate the DUB and thereby alter its activity or promote its degradation. In **Table 2**, four pairs with a mutual regulation are described: TRIM11/USP14, TRIM25/USP15, TRIM27/USP7, and TRIM47/CYLD. An example is presented by Ji and colleagues, where CYLD is progressively degraded upon interaction with TRIM47. Moreover, they also identified by co-IP assay the domains responsible for this interaction: the SPRY/B30.2 (C-terminal SplA/ryanodine receptor) domain from TRIM47 with the CAP (cysteine-rich secretory proteins, antigen 5, and pathogenesis-related 1 proteins) domain of CYLD (Ji et al., 2018).

The third type is the rheostat-like antagonism (**Figure 15. C**)**.** The regulatory logic of DUB–TRIM becomes even more complex when one considers that the scenarios outlined earlier include an operation on a shared substrate. Indeed, Hao and colleagues showed that the Wiskott–Aldrich syndrome protein and SCAR homolog (WASH) are controlled through Lys^{63}-linked ubiquitination by the melanoma antigen gene (MAGE)-L2-TRIM27 ligase (**Table 2**). Simultaneously, USP7 is an integral component of the MAGE-L2-TRIM27 ligase by controlling the auto-ubiquitination of TRIM27. Mechanistically, USP7 acts as a precise fine-tuning of WASH by counteracting TRIM27 auto-ubiquitination/degradation and through directly deubiquitinating WASH (Hao et al., 2015).

The last type is polyubiquitin chain editing (**Figure 15. D**)**.** This occurs when the DUB–E3 complex conducts a sequential modification on the polyubiquitin chain of the substrate. In detail, the DUB activity removes the extant polyubiquitin chain, and the TRIM activity adds a polyubiquitin chain of a different linkage type. This type of chain remodeling can result in changing the substrate fate. No examples have yet been found of DUB-TRIM pairs with the ubiquitination chain editing role.

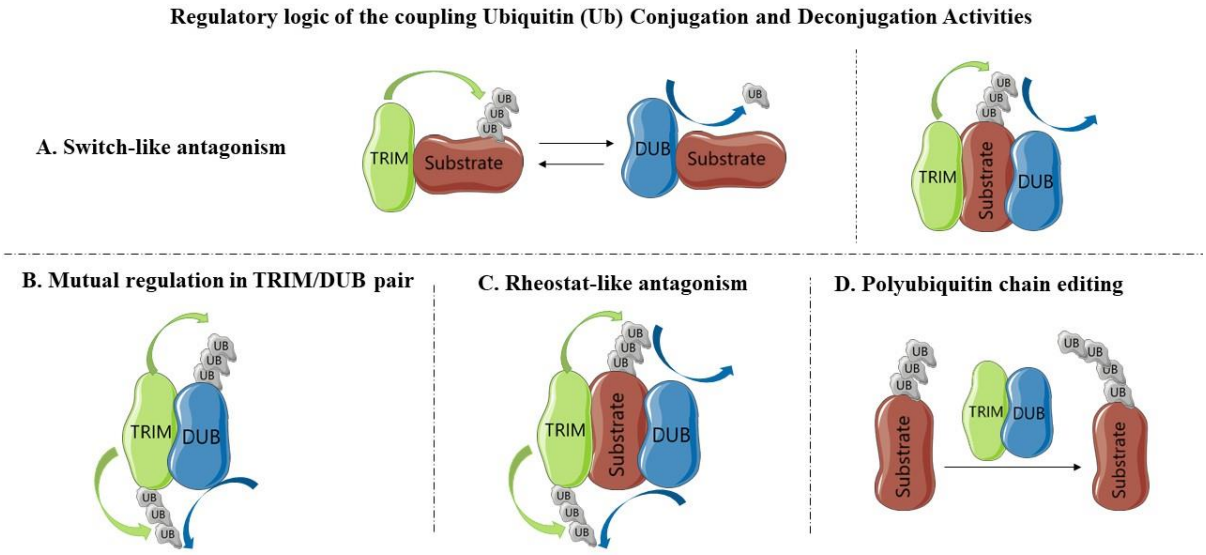

Figure 15. The hypothetical regulatory logic of coupling Ubiquitin (Ub) conjugation and deconjugation activities. A. Switch-like antagonism. DUB- TRIM complexes can operate on a shared substrate, resulting in the regulation of substrate protein fate. The activity of the DUB-TRIM pair with the substrate can either be a direct (de)ubiquitination on the target (A - left) or an indirect one, resulting in functional interface (A - right) **B. Mutual regulation.** DUB–E3 complexes can also lead to mutual regulation of DUB and TRIM stability. Specifically, DUBs can protect an interacting TRIM from the potential degradation resulting from auto-ubiquitination, while the TRIM can ubiquitinate an interacting DUB and thereby alter its activity or promote its degradation. **C. Rheostat-like antagonism.** Rheostat-like behavior can also result from a mutual regulation on a DUB–TRIM pair associated with a common substrate. **D. Polyubiquitin chain editing.** This occurs when the DUB–TRIM complex operates sequentially on a polyubiquitylated substrate, with the DUB activity removing the extant polyubiquitin chain and the TRIM activity adding a polyubiquitin chain of a different linkage type. Abbreviations: DUB: Deubiquitinating enzymes; TRIM: Tripartite motif; Ub: Ubiquitin.

These TRIM-DUB interactions suggest an important role in tuning the dynamics of cellular ubiquitination, but the regulatory logic underlying these complexes has not been fully elucidated. Considering that many different DUBs and TRIMs are currently being investigated as potential therapeutic targets for various diseases, further investigation of DUB–TRIMs complexes and their regulatory function in cells is expected to have important implications for drug development (Nielsen & MacGurn, 2020).

Table 2. DUB–E3 pair reported in the TRIM family. A summary of the literature showing a DUB-TRIM pair interaction. The table specifies the substrate involved; the type of interaction, if functional (switch-like antagonism) and/or physical, proved by coimmunoprecipitation (when known has also reported the domains involved); the cellular compartment where the interaction occurs; and the cell types used in the study. Abbreviations: A549: Adenocarcinoma human alveolar basal epithelial; DUB: Deubiquitinating enzymes; HCT116: Human colon cancer; Hek293T: Human embryonic kidney; HeLa: Human cervical cancer; hTERT: immortalized retinal pigment epithelial; L02: Hepatic cell line; NSCs: stem cells of the nervous system; NHLF: Normal human lung fibroblasts; TRIM: Tripartite motif; U2OS: Human bone osteosarcoma; VCaP: Human prostate cancer.

TRIM	DUB	Substrate	Type of interaction	Cellular compartment	Cell Type	Reference
11	USP14	Itself	TRIM RING + DUB UBL	Proteasome	HCT116	(L. Chen et al., 2018)
25	USP9X	ERG	Functional	Cytoplasm	HeLa; VCaP	(Wang et al., 2016)
	USP10	PCNA	Functional	Nucleoplasm	HeLa	(Park et al., 2014)
	USP15	TRIM itself	TRIM B-boxes + DUB C-terminal (His-box)	Cytoplasm	HeLa; HEK293T; NHFL	(Pauli et al., 2011; Teyra et al., 2019; Torre et al., 2017)
	A20	RIG-I	Functional	-	Hek293T	(Fan et al., 2014; Oshiumi et al., 2012)
	USP3					
	USP21					
	CYLD					
27	USP7	WASH	TRIM C-terminal + DUB Catalytic domain	Cytoplasm puncta	HCT116; HeLa; U2OS	(Hao et al., 2015; Tacer & Potts, 2017)
		MAGE-L2				
		TBK1; TRIM itself				(J. Cai et al., 2018)
32	USP9X	NPHP5	Functional	Centrosome	HEK293T; hTERT-RPE-1	(Das et al., 2017)
	USP7	C-Myc	Functional	Nucleus	NSCs E12.5-E14.5; HEK293T	(Nicklas et al., 2019)
	USP11	ARID1A	Physical	Nucleus	HEK293T	(Luo et al., 2020)
	OTULIN	NF-kB	C-terminal (NHL repeats)	Nucleus	HEK293T; A549	(Zhao et al., 2019)
33	USP9X	SMAD4	Functional	Separated compartments	Xenopus embryos and HEK293T	(Dupont et al., 2009)
47	CYLD	DUB itself	TRIM C-terminal (SYPRY/B30.2) + DUB CAP	-	L02	(Ji et al., 2018)

2. Aim of the work

MID1 is an E3 ligase that ubiquitinates specific substrates leading to their degradation or change in the signaling pathway. When MID1 is mutated causes the X-linked form of Opitz G/BBB Syndrome (XLOS). MID1 loss leads to developmental problems but causes no detrimental effects on adult-life. Because XLOS is a genetic disease caused by a loss-of-function mechanism, it is not easy to target or to design therapies, a new strategy could be to interfere with specific ubiquitination activity by targeting the relative deubiquitinating enzymes (DUBs) responsible for the reverse process on the same substrates.

The principal goal of this project was to discover DUBs that work in a highly coordinated manner with the E3 ubiquitin ligase MID1, addressing three specific aims:

1. Screening for MID1-relevant DUB candidates. The first aim was to discover suitable DUBs candidates that functionally interact with MID1. For that, 24 selected DUBs were silenced and the main MID1 target was investigated. Additionally, the opposite assay overexpressing the 24 DUBs was performed.

2. Characterization of the MID1/DUB pair. Once the relevant DUB has been selected, a characterization of the MID1/DUB interaction and subcellular localization was performed.

3. Study the complex MID1/DUB/Substrate. Once identified, the effect of the selected DUB was investigated in the pathways regulated by the MID1 substrates, and an analysis of cellular distribution was performed.

3. Materials and Methods

3.1 Cell lines and cell culture

HEK293T (CRL-3216) and HeLa (CCL-2) are adherent epithelial cells derived, obtained from the American Type Culture Collection (ATCC, MD, USA). HEK293T is from embryonic kidney tissue and Hela is from a cervix adenocarcinoma. Particularly the HEK293T is a competent cell line able to replicate vectors carrying the SV40 region of replication.

All the cell lines were maintained in Dulbecco's Modified Eagle's Medium (DMEM, High Glucose with Pyruvate, Euroclone, ECB7501L) supplemented with 10% of Fetal Bovine Serum (FBS, GIBCO, Invitrogen), 2% L-Glutamine 200nM (GIBCO, Invitrogen), and 1% of Penicillin/Streptomycin (P/S, GIBCO, Invitrogen). Cells were grown in a humidified atmosphere at 37ºC and 5% of CO_2 and the entire procedures involving cell lines' manipulation were performed under sterile conditions, operating in a cell culture hood.

3.2 *Mid1* Knock-out Mouse line (*Mid1* KO)

Mid1 Knock-out (KO, *Mid1*$^{-/Y}$) mouse line was previously generated in the laboratory by targeted recombination. The wild-type *Mid1* locus was replaced with a non-functional Mid1 allele by disruption of the first ATG-containing exon (Lancioni et al., 2010). The *Mid1*$^{-/Y}$ and *Mid1* wild type (WT, *Mid*1$^{+/Y}$) embryos used in this thesis were males from the same litter obtained by mating heterozygous females (*Mid1*$^{+/-}$) with WT males (*Mid1*$^{-/Y}$). All mice were housed and handled according to the institutional guidelines in compliance with the European Council Directive 86/609 and Italian law (Dl. 26/2014).

3.2.1 Mouse embryonic fibroblasts (MEFs)

Mouse Embryonic Fibroblasts (MEFs) were prepared from *Mid1*$^{+/Y}$ and *Mid*1$^{-/Y}$ embryos obtained from a heterozygous pregnant female (*Mid1*$^{+/-}$). Embryos from E13.5 pregnant mice were harvested, and the head of the embryos was removed. The embryos were placed in a 10 cm cell culture dish and minced with a sterile razor blade. After 10 minutes of trypsin digestion at 37°C, a complete growth medium (DMEM with 10% FBS, 2% L-Glutamine, and 1% P/S)

was added, and the suspension was pipetted 10-20 times to further break up tissues. The cellular suspension was then transferred to a 10-cm plate and regularly cultured.

3.2.2 Genotyping

The animals' genotypes were assessed by extracting genomic DNA from the tail. The kit KAPA Mouse Genotyping Kit (KAPA Biosystems) was used for DNA extraction and amplification.

For the DNA extraction (60µl volume) each piece of tissue was mixed with 6 µL of KAPA Express Extract Buffer with 1.2 µL U/µl KAPA Express Extract Enzyme and completed with PCR water to reach the final volume. To lyse the cells and release the DNA, the reactions were incubated at 75°C for 10 min. Followed by incubation for 5 minutes at 95°C to ensure the heat-inactivation of the thermostable KAPA Express Extract protease.

For the PCR we performed three reactions for each sample: one with the primers for *Mid1*, the other with the primers for *Sry* (Y chromosome for sex identification), and a negative control without DNA. The master mix (15 µL) is constituted of: 1µL of cDNA, 7.5µL of KAPA2G Fast Genotyping Mix with dye, 200ng/µl of each primer (**Table 3**), and complete with PCR water to reach the final volume. PCR tubes were placed in a thermocycler with a program established as denaturation of DNA at 95°C for 3 minutes, followed by 30 cycles of 15 seconds at 95ºC (denaturation), 15 seconds at 58°C for *Mid1* or 54°C for *Sry* (annealing of primers) and 15 seconds at 72°C (extension of DNA), after the cycles the sample was maintained 3 minutes at 72ºC and then analyzed.

Table 3 Primers used in genotyping. *Mid1* Null F (Forward) and *Mid1* Null R (Reverse) to identify the wild-type (WT) allele (400bp). *Mid1* Null F and *Neo1* R to identify the knock-out (KO) allele (320 bp). *Sry* F and R to identify male embryos.

Primer	Sequence	Size	Identification
Mid1 Null R	5'-GAGCCCGTCTAGACCTCGC-3'	400bp	*Mid1* WT
Mid1 Null F	5'-GCTCCCAGTAAAGACAGAG-3'		
Neo1 R	5'-CCAGAGGCCACTTGTGTAG-3'	320bp	*Mid1* KO
Sry F	5'-GAGAGCATGGAGGGCCAT-3'	250bp	Male
Sry R	5'-CCACTCCTCTGTGACACT-3'		

The PCR products (**Figure 16**) were analyzed in a 1.2% agarose gel in Tris-Acetate-EDTA (TAE, 40 mM Tris base, 20 mM acetic acid, 1 mM EDTA, pH 8.0) with 3µl of GelRed Nucleic Acid Gel Stain (Biotium). Electrophoresis was performed at 100 volts and examined at the ChemiDoc MP Imaging System (Bio-Rad, 12003154).

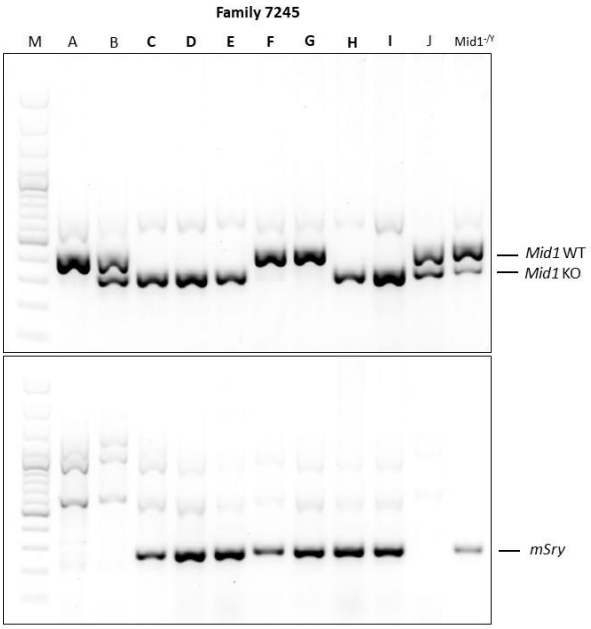

Figure 16. Mouse Embryonic Fibroblasts (MEFs) Genotype. Top gel, *Mid1* WT, and KO amplified fragments; bottom gel, *Sry* amplification for sex determination. Letters indicate different embryos of the family 7245. M: 100 bp molecular weight marker (Gene Ruler 100bp DNA ladder SM0322 (Thermo Scientific); Lane A: homozygous female (*Mid1*$^{+/+}$); Lane B and J: heterozygote females (*Mid1*$^{-/+}$); Lane F and G: WT males (*Mid1*$^{+/Y}$); Lane C, D, E, H, and I: KO males (*Mid1* $^{-/Y}$).

3.3 *In vitro* silencing with siRNA

Gene silencing was carried out in HeLa cells with a specific small interfering RNA (siRNA) library targeting 24 DUB genes. From Horizon Discovery, we purchased the Human ON-TARGET*plus* SMARTpool siRNA library, which consists of four siRNAs targeting one DUB gene (**Table 4**). The pooled siRNAs were designed to guarantee a silence target gene expression at the mRNA level by at least 75%.

Table 4. Sequence information of each DUB siRNA pool. Description of the Human ON-TARGET*plus* SMARTpool siRNA of 24 DUB genes (Horizon Discovery) used on the silencing screen. Information about each gene (ID, accession, and GI numbers) and the four specific siRNA sequences. Abbreviation: DUB: Deubiquitinating enzymes; siRNA: specific small interfering RNA.

Gene Symbol	Gene ID	Gene Accession	GI Number	Sequence
USP2	9099	NM_171997	28565284	ACACCAACCAUGCUGUUUA
				GCGCUUUGUUGGCUAUAAU
				GUGUACAGAUUGUGGUUAC
				GACCUAAGUCCAACCCUGA
USP4	7375	NM_199443	40795666	CCAAAUGGAUGAAGGUUUA
				AAACUCAACUCUCGAUCUA
				GGGAUAAGCUCGACACAGU
				AAUCACAGGUUGAGGAAUG
USP6	9098	NM_004505	4758563	GAGAAUGGGAGACAUAUAA
				GCGGAGAGGUUCACAACAA
				CGGAACCAAUUCUUCGAUA
				CAGCUAAGAUCUCAAGUCA
USP7	7874	NM_003470	4507856	AAGCGUCCCUUUAGCAUUA
				GCAUAGUGAUAAACCUGUA
				UAAGGACCCUGCAAAUUAU
				GUAAAGAAGUAGACUAUCG
USP8	9101	NM_005154	41281375	GGCAAGCCAUUUAAGAUUA
				CCACUAGCAUCCACAAGUA
				CUUCGUAACUUAGGAAAUA
				CAGAUUAGAUCGUGAUGAG
USP9X	8239	NM_021906	74315357	AGAAAUCGCUGGUAUAAAU
				ACACGAUGCUUUAGAAUUU
				GUACGACGAUGUAUUCUCA
				GAAAUAACUUCCUACCGAA
USP11	8237	NM_004651	75992939	GCGCACAGCUGCAUGUCAU
				GAGAAGCACUGGUAUAAGC
				GGACCGUGAUGAUAUCUUC
				GAAGAAGCGUUACUAUGAC
USP15	9958	NM_006313	14149626	GAUGAUACCAGGCAUAUAA
				GGUAUUGUCCGAAUUGUAA
				CCAAACCUAUGCAGUACAA
				GAGUAUUUCCUCAAUGAUA
USP20	10868	NM_001008563	56682956	GGACAAUGAUGCUCACCUA
				GCGAGUGGCUCAACAAGUU
				GAACGCCGAGGGCUACGUA
				GCCAGAACGUGAUCAAUGG
USP25	29761	NM_013396	50312665	ACAAGUUCCUUAUCGAUUA
				UGAAAGGUGUCACAACAUA
				UAAGGAUGCUUUCAAAUCA
				GAAGACAACCAACGAUUUG
USP28	57646	NM_020886	40217782	GAAGGUGGCUCAAGCGAAA
				GAGGAUAACUGGCGGUUUG
				ACUAAACGCUCAAAGAGAA
				UCCCGGACAUGCUGAAAUA
USP32	84669	NM_032582	44889413	GGAGAUAUCCUGUGGGUUA

				GAGAAACGCUAUUGGUUAU
				GGACACAGCAGUCUAACAU
				GGAACUAUGUUAUACGGGA
USP33	23032	NM_201626	42516560	GUAGUAACCUUGCAAGAUU
				GGGCAUGUCUGGAGAAUAG
				CAGCUCAAAUUGUGACAUA
				CGAAAUCAUUGUCCACAUU
USP34	9736	NM_014709	41056186	GCAGGGAAGUUCUGACGAA
				CAACAGAUCAGUAGUAAUU
				GCAGCUAUCCAGUAUAUUA
				CCAUGUGACUGGAGAUUUA
CYLD	1540	NM_015247	14165257	GGACAUGGAUAACCCUAUU
				AGAGAUAUCUACAGACUUU
				GGAGAGUACUUGAAGAUGU
				GAAGGUUGGAGAAACAAUA
UCHL1	7345	NM_004181	34147658	GCCAAUGUCGGGUAGAUGA
				CCGAGAUGCUGAACAAAGU
				GCUGAAGGGACAAGAAGUU
				CAAGGUGAAUUUCCAUUUU
UCHL3	7347	NM_006002	37059734	CAGCAUAGCUUGUCAAUAA
				GCAAUUCGUUGAUGUAUAU
				GAACAAUUGGACUGAUUCA
				GGGCAUCUCUAUGAAUUAG
OTUD3	23252	XM_375697	51459100	UCGCAAAGGUCACAAACAA
				GAAAUCAGGGCUUAAAUGA
				GGCCAGCCCUAGUGAAGAA
				GCGCUGAACUGUACUAGUA
OTUD5	55593	NM_017602	40353201	CAACAGUGAGGACGAGUAU
				CAACACAUUCCAUGGGAUA
				GAAAGCAUUGCAUGGACUA
				GGAUGGCGCCUGUCUCUUC
OTUD6A	139562	NM_207320	46409281	CAUUGAAUCUGUCGUCGAA
				GCACUACAACUCCGUGACA
				ACGACGACUUCAUGAUCUA
				GAGAAAGAAUGGAGUCCGA
OTUD6B	51633	NM_016023	40254878	GGAGCGAGAAGAACGGAUA
				GCUAGACAGUUAGAAAUUA
				CAUUAUAGUUGGUGAAGAA
				UGACUACUAAGGAGAAUAA
TNFAIP3	7128	NM_006290	26051241	CUGCAGUACUUGCUUCAAA
				CAACUCAUCUCAUCAAUGC
				UCUGGUAGAUGAUUACUUU
				CAACGAAUGCUUUCAGUUC
OTUD7B	56957	NM_020205	9910155	CCGAUUGGCCAGUGUAAUU
				CCGAGUGGCUGAUUCCUAU
				GCAUCUAGGUACCAAUGGA
				UAACGGAGGGAGCAAGUAU
VCPIP1	80124	NM_025054	38569451	GAGAAGCUCUGGUGAUUAU
				GGGACAGACUUUAGUAAUA
				GGAGAUGGGUCUAUUGUGU
				CGACAGAAUUACAAUAGAA

Hela cells were seeded into 96-well-plates or 24-well-plates at 80% of confluency in complete medium and allowed overnight to attach. On the next day, transfection was performed according to the manufacturer's protocols (**Table 5**): DharmaFECT reagent (Dharmacon- Horizon Discovery) and the siRNA were diluted in Serum-Free Media (DMEM) and incubated at Room Temperature (RT) for 5 minutes. Then the siRNA was mixed with the reagent and incubated at RT for 20 minutes, later added to the growth medium without antibiotics. The control was transfected with non-Targeted siRNA. After 24 hours, the medium was changed, and cells were collected by scraping at 72 hours after transfection.

Table 5. Volumes to silencing with DharmaFECT reagent.

Plate	Growth medium (mL)	Dilution DharmaFECT		Dilution siRNA	
		Serum-Free Media (µL)	DharmaFECT (µL)	Serum-Free Media (µL)	siRNA 5 µM (µL)
24-well	0.5	49.75	0.25	47.5	2.5
96-well	0.1	9.95	0.5	9.5	0.5

To optimize the concentration of siRNA, one DUB for which an antibody was available was tested. HeLa cells were transfected in duplicate with two different concentrations of USP33 siRNA (25nM and 35nM) for 72 hours, while the control was transfected with non-Targeted siRNA (25nM and 35nM). According to **Figure 17**, USP33 silencing results in a protein reduction of 70-80% for siRNA concentrations of 25nM and 85% for siRNA concentrations of 35nM. SiRNA concentrations of 25nM were determined to be sufficient for the effective silencing of DUB proteins.

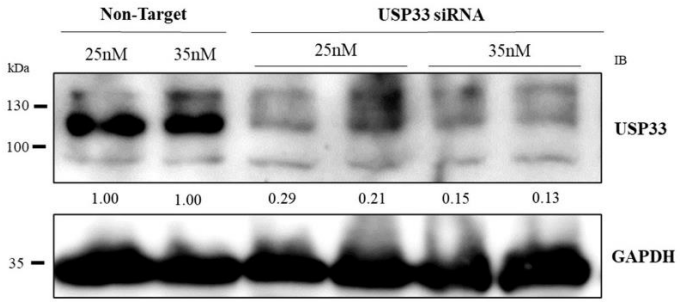

Figure 17. Optimization of the siRNA concentration. HeLa cells were transfected in duplicate with 25nM or 35nM of USP33 siRNA for 72 hours. The control was treated with non-Target (NT) siRNA (25nM and 35nM). Quantification of the assay was made with densitometry analysis with the Image Lab software. Expression is shown as the ratio between USP33 and GAPDH referenced to the respective NT concentration. Antibodies: GAPDH (53 kDa) from Sigma (1:2500); USP33 (107 kDa) from Abcam (1:2000).

3.4 Plasmid Transient Transfections

3.4.1 Lipofectamine 3000 reagent

Hela cells were seeded into 6-well-plates or 12-well-plates at 80% confluency per well in complete medium and allowed overnight to attach. On the next day, transfection was performed according to the manufacturer's protocols (**Table 6**): Lipofectamine 3000 reagent (Invitrogen) was mixed with the plasmid and P3000 (Invitrogen) and diluted in Reduced Serum Media (Opti-MEM, GIBCO, Invitrogen, Thermo-Fisher). The complex was incubated at RT for 10 minutes and later added to the growth medium in the well. After 24 hours, the medium was changed, and cells were collected by scraping at different time points of 24 hours, 48 hours, and 72 hours after transfection.

Table 6. Volumes to transfect with Lipofectamine 3000 reagent.

Plate	Growth medium (mL)	Reduced Serum Media (µL)	Lipofectamine 3000 (µL)	DNA (µg)	P3000 (µL)
6-well	2	125	3.75	2.5	5
12-well	1	50	1.5	1	2

3.4.2 X-tremeGENE HP DNA reagent

The HEK293T cells were seeded into 10 cm plates or 12-well-plates at a density of 80% in complete medium and allowed overnight to attach. On the next day, transfection was performed according to the manufacturer's protocols (**Table 7**): X-tremeGENE HP DNA reagent (Roche) was mixed with the plasmid and diluted in Reduced Serum Media. The complex was incubated at RT for 15 minutes and later added to the growth medium in the well. After 24 hours, the medium was changed, and cells were collected by scraping at different time points of 24 hours and 48 hours of transfection.

Table 7. Volumes to transfect with X-tremeGENE HP DNA reagent.

Plate	Growth medium (mL)	Reduced Serum Media (µL)	X-tremeGENE HP DNA (µL)	DNA (µg)
10 cm	10	950	20	10
12-well	1	100	2.5	1

3.4.3 Calcium phosphate method

HEK293T cells were seeded in 10 cm plates at a density of 80% in complete medium and allowed overnight to attach. On the next day, transfection was performed according to the standard calcium phosphate method (Graham & van der Eb, 1973):

-Solution A was prepared with 490µL of 2X HBS (Hepes 10g/L, NaCl 16g/L, pH 7.1) and 10µL of 100X 1:1 mix of 70mM disodium phosphate (Na_2HPO_4) with 70mM sodium mono-basic phosphate (NaH_2PO_4).

- Solution B was prepared with 60µL of 2M calcium chloride ($CaCl_2$, final concentration of 125mM), DNA (10µg), and distilled H_2O until the final volume (500µL).

Solution B was added dropwise to solution A while aerating the mix. The complex was incubated at RT for 20 minutes and later added to the growth medium on the plate. After 24 hours, the medium was changed, and cells were collected by scraping at different time points after 24 and 48 hours.

3.4.4 Plasmids

In this work, the plasmids, described in **Table 8**, were used and purified with the QIAGEN Midi kit. Our thanks go to Michael Clague, Claudio Brancolini, Giovanna Mantovani, and Pascual Sanz for kindly providing the plasmids. In **Figure 18**, HEK293T cells were transfected with the corresponding plasmids at the optimal time point (24 hours, 48 hours, or 72 hours) for each protein expression.

Table 8. Description of the plasmids. Expression System Mammalian. Abbreviation: Amp: Ampicillin; FL: Full Length; Kan: Kanamycin.

Gene	Specie	Vector	TAG	Resistance	Lab Source
CYLD	FL Human	pcDNA	HA	Amp	P. Sanz
MID1	FL Human	pcDNA 3.2-DEST	MYC/ GFP	Amp	G. Meroni
ΔRING MID1	FL Human	pcDNA 3.2-DEST	MYC/ GFP	Amp	G. Meroni
OTUD3	FL Human	pEGFP-GW-JJ-JJ	GFP	Kan	M. Clague
OTUD6A	FL Human	pEGFP-GW-JJ	GFP	Kan	M. Clague
OTUD6B	FL Human	pEGFP-GW-JJ	GFP	Kan	M. Clague
OTUD7B	FL Human	pEGFP-GW-JJ	GFP	Kan	M. Clague
OTUD7B	FL Human	pcDNA 5/FRT/TO	HA	Amp	P. Sanz
TNFAIP3	FL Human	pEGFP-C1	GFP	Kan	P. Sanz
TRIM32	FL Human	pcDNA 3.2-DEST	MYC/ GFP	Amp	G. Meroni
UCHL1	FL Human	pEGFP-GW-JJ	GFP	Kan	M. Clague
UCHL3	FL Human	pEGFP-GW-JJ	GFP	Kan	M. Clague
UCHL5	FL Human	pEGFP-GW-JJ	GFP	Kan	M. Clague
USP2	FL Human	pEGFP-GW-JJ	GFP	Kan	M. Clague
USP6	FL Human	pEGFP-GW-JJ	GFP	Kan	M. Clague
USP7	FL Human	pcDNA 3.1	MYC	Amp	P. Sanz
USP8	FL Human	pME-FLAG	FLAG	Amp	G. Mantovani
USP11	FL Human	pEGFP-GW-JJ	GFP	Kan	M. Clague
USP15	FL Human	p5953 pcDNA -4C	HIS	Amp	P. Sanz
USP18	FL Human	pFLAG-CMV5α	FLAG	Amp	C. Brancolini
USP20	FL Human	pEGFP-GW-JJ	GFP	Kan	M. Clague
USP21	FL Human	pEGFP-C1	GFP	Kan	M. Clague
USP25	FL Human	pEGFP-GW-JJ	GFP	Kan	M. Clague
USP28	FL Human	pDZ	FLAG	Amp	P. Sanz
USP32	FL Human	pEGFP-GW-JJ	GFP	Kan	M. Clague
USP33	FL Human	pEGFP-C1	GFP	Kan	C. Brancolini
VCPIP1	FL Human	pEGFP-C1	GFP	Kan	P. Sanz

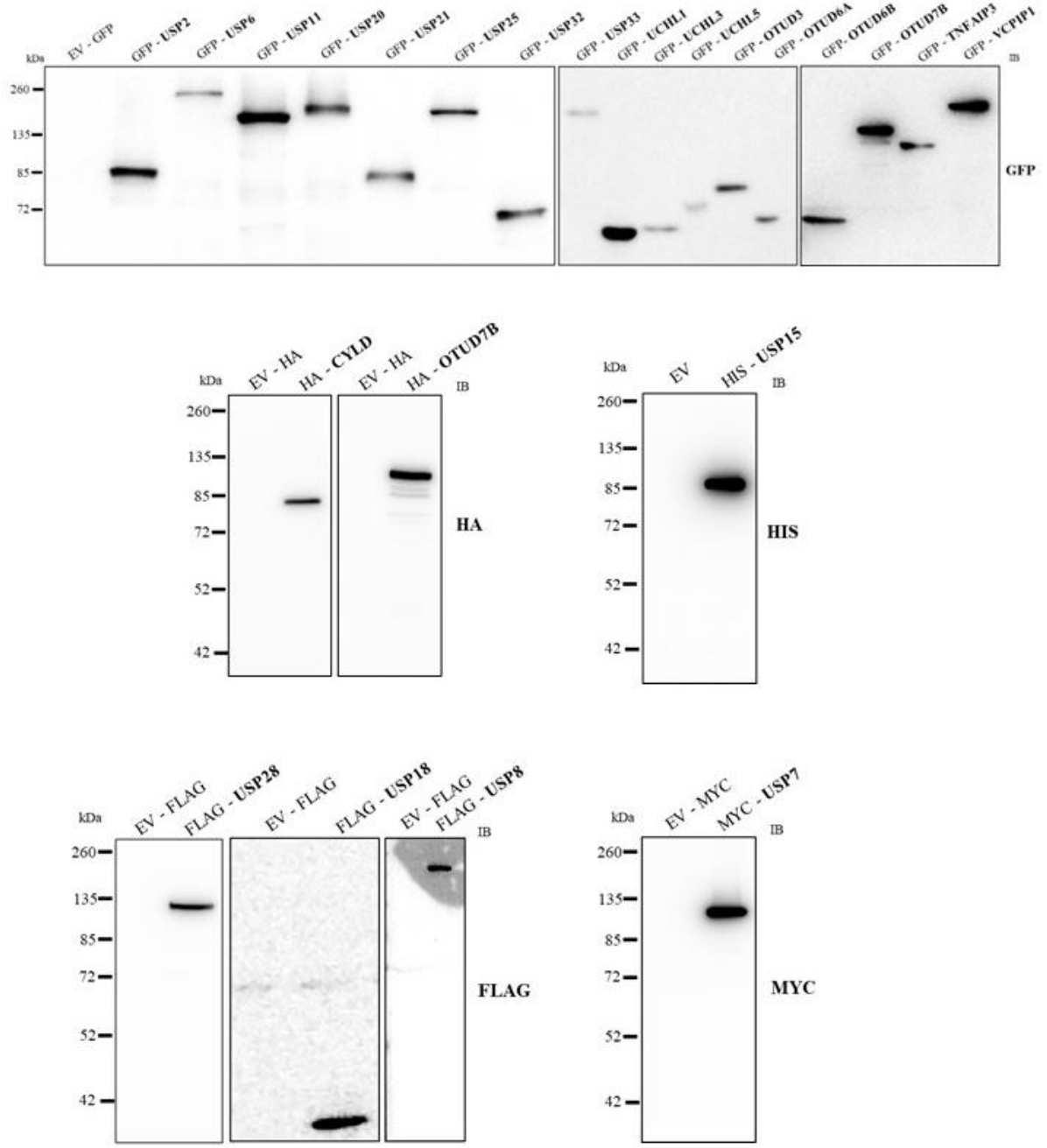

Figure 18. Protein expression of DUB plasmids in HEK293T cells. The HEK293T cells were transfected with X-tremeGENE HP DNA reagent and 1µg of each plasmid in a 12 well-plate. The cells were collected in RIPA buffer at 24h (HA-CYLD, GFP-OTUD3, GFP-OTUD6A, GFP-OTUD6B, HA-/GFP-OTUD7B, GFP-UCHL1, GFP-UCHL3, GFP-UCHL5, GFP-USP2, GFP-USP6, GFP-USP11, GFP-USP20, GFP-USP21, GFP-USP25, FLAG-USP28, GFP-USP32), 48h (GFP-TNFAIP3, MYC-USP7, HIS-USP15, FLAG-USP18, GFP-USP33, GFP-VCPIP1), and 72h (FLAG-USP8). Molecular weight of each protein: A20 (90kDa), CYLD (107kDa), OTUD3 (45kDa), OTUD6A (33kDa), OTUD6B (34kDa), OTUD7B (93kDa), UCHL1 (25kDa), UCHL3 (26kDa), UCHL5 (38kDa), USP2 (68kDa), USP6 (159kDa), USP7 (128kDa), USP8 (130kDa), USP11 (110kDa), USP15 (112kDa), USP18 (43kDa), USP20 (102kDa), USP21 (63kDa), USP25 (122kDa), USP28 (122kDa), USP32 (182kDa), USP33 (140kDa). Antibodies: FLAG from Sigma F3165 (1:1000), GFP from Invitrogen (1:5000), HA from SIGMA (1:1000), HIS from Healthcare (1:1000), MYC from SIGMA (1:1000).

3.5 *In vitro* treatments with drugs

The drugs used in this project were: Cycloheximide (CHX, Sigma 1810) and MG132 (Sigma C2211) prepared as stock solutions in Dimethyl Sulfoxide (DMSO, Invitrogen) and stored at -20ºC and Chloroquine (CQ, InvivoGen) diluted in H_2O and stored at 4 ºC, as recommended by the manufacturer. For the experimental conditions, drugs were diluted in complete medium at a final concentration of 10µM (MG132 and Chloroquine) or 50µg/mL (Cycloheximide), using the respective vehicle (DMSO or H_2O) as a control.

3.6 Protein extracts

3.6.1 Total fraction

Cells, after treatment and/or transfection (previously described), were scraped at different time points in RIPA buffer (50mM Tris-HCl pH 8, 0.1% Sodium Dodecyl Sulfate (SDS), 150mM NaCl, 0.5% Sodium deoxycholate (NaDOC), 1% NP40, 5µL/mL protease inhibitors cocktail (P8340 Sigma)). When protein was extracted to analyze protein phosphorylation, the following anti-phosphatases are added: 10mM tetrasodium pyrophosphate ($Na_4P_2O_7$), 20mM sodium fluoride (NaF), 1mM Sodium orthovanadate (Na_3VP_4), and 30mM β-glycerophosphate. These procedures were performed at a low temperature, maintaining all solutions on ice. Cell lysates were sonicated and centrifuged at 4ºC, 13000 rpm for 15 minutes, and the supernatant was kept. Proteins were quantified with Bradford reagent (Thermo-Fisher 1856208) through spectroscopy. Each sample was added Loading Buffer (0.25 M Tris-HCl pH 6.8, 8% Glycerol, 4% SDS, 200nM Dithiothreitol (DTT), 0.02% w/v bromophenol blue), denatured by boiling at 95ºC for 5 minutes before electrophoresis.

3.6.2 Subcellular fractionation

For the subcellular fraction, the NE-PER™ Nuclear and Cytoplasmic Extraction kit (Thermo-Fisher) was used to allow the separation of cytoplasmic and nuclear extracts. Hela cells were collected in PBS, 10% of the pellet was lysed in RIPA buffer (Whole Cell Lysate - WCL), and the remaining 90% in cold Cytoplasmic Extraction Reagent I (CER I). The tube was vortexed for 15 seconds to fully suspend the cell pellet and incubated on ice for 10 minutes. After,

Cytoplasmic Extraction Reagent II (CER II) was added, vortexed for 5 seconds, and incubated on ice for 1 minute. The extract was vortexed for 5 seconds and centrifuged at 16000*g* for 5 minutes at 4°C. The supernatant was transferred (Cytoplasmic extract - CYT) to a clean tube. The pellet was resuspended in a cold Nuclear Extraction Reagent (NER), then vortexed for 15 seconds, placed on ice, and vortex for 15 seconds each 10 minutes, for a total of 40 minutes. The extract was centrifuged at 16000g for 10 minutes at 4°C. The supernatant (Nuclear extract - NUC) fraction was transferred to a new tube. The final volume ratio of CER I: CER II: NER reagents was 200:11:100μL, respectively. The WCL and the fractions were added Loading Buffer, denatured at 95ºC for 5 minutes, and subjected to electrophoresis.

3.7 Western Blot (WB)

The analytical technique used to separate and detect proteins was western blot (WB). Protein extracts were analyzed on SDS–Polyacrylamide Gel Electrophoresis (SDS-PAGE) composed of a 5% acrylamide stacking gel (Acrylamide/bis 40% 29:1, 0.5M Tris–HCl pH 6.8, 10% SDS, N, N, N′, N′ tetramethyl ethylene diamine (TEMED), 10% Ammonium persulfate (APS)) and a 10% or 7.5% acrylamide running gel (Acrylamide/bis 40% 29:1, 1.5M Tris–HCl pH 8.8, 10% SDS, TEMED, 10% APS). Proteins were separated electrophoretically at 100V and afterward transferred on to a polyvinylidene difluoride membrane (PVDF - Millipore) previously activated in methanol. The transfer was performed in Transfer buffer (25mM Tris, 192mM Glycine, 20% v/v methanol) at 30 V, 90 mA for 16 hours at 4 ºC (for high molecular weight proteins) or 100 V, 350 mA for 90 minutes at room temperature (RT).

Membranes were blocked with 5% non-fat milk (Cell Signaling) in Tris-Buffered Saline-Tween (TBS-T, pH 8, 20mM Tris, 150mM NaCl, 0.1% Tween Twenty) for 1 hour at RT and incubated overnight at 4°C or 1-3 hours at RT with primary antibody. The primary antibodies, described in **Table 9**, were prepared in 5% milk in TBS-T. Membranes were then washed with TBS-T and incubated for 1 hour at RT with the secondary antibody coupled to horseradish peroxidase (anti-rabbit (Bethyl A120-208P) and anti-mouse (Millipore AP308P)), previously diluted at 1:2500 with 5% skimmed milk in TBS-T. Detection was performed with Enhanced Chemiluminescent Substrate (ECL-Western Blotting Detection Reagents, Bio-Rad) in the ChemiDoc MP Imaging System. Protein expression was analyzed by Image Lab 6.1 (Bio-Rad) and β-Tubulin was used as a control.

3.8 Immunoprecipitation assay (IP)

Immunoprecipitation (IP) is the small-scale affinity purification of antigens using a specific antibody that is immobilized on a support resin, resulting in the isolation of proteins. HEK293T cells were seeded into 10 cm plates at 80% confluency in complete medium. Depending on the assay, cells were transfected with the calcium phosphate method or X-tremeGENE HP DNA reagent, as previously described. Cells were collected with a non-denaturing lysis buffer (50mM Tris-HCl pH 7.4, 300mM NaCl, 5mM EDTA pH 8.0, 1% Triton X-100, 5µL/mL protease inhibitors cocktail (P8340 Sigma)). Cell lysates were incubated with 1µg of the desired antibody, overnight or for 3 hours at 4°C. Subsequently, the lysate was incubated with protein G beads (Millipore) for 2 hours at 4°C or protein A agarose beads (Sigma) for 3 hours at 4°C. The correct selection of the beads type depends on the antibody used for the precipitation. The immunocomplexes were collected by centrifugation at 500g for 90 seconds at 4°C and the beads were washed three times with the wash buffer (50mM Tris-HCl pH 7.4, 300mM NaCl, 5mM EDTA pH 8.0, 0,1% Triton X-100). Immunoprecipitated proteins were resuspended in Loading Buffer and denatured at 95ºC for 5 minutes for further analysis by WB.

3.9 Immunofluorescence (IF)

Immunofluorescence (IF) is an immunochemical technique that allows the detection and localization of proteins in cell preparations. Hela cells were seeded on a glass coverslip to 80% confluence. After treatment and/or transfection, cells were washed in Phosphate-buffered saline (PBS) and fixed with 4% Paraformaldehyde (PFA) in PBS for 10 minutes at RT. Cells were washed three times in PBS and permeabilized with 0.25% Triton X-100 in PBS for 5 minutes at RT. Afterward, cells were washed three times in PBS and blocked in 10% Bovine Serum Albumin (BSA, VWR 0332) in PBS for 30 minutes at 37 ºC. The coverslips were then incubated with primary antibodies in 3% BSA/PBS for 2 hours at 37 ºC. Finally, the coverslips were washed three times in PBS and incubated with anti-mouse conjugated with tetramethyl rhodamine (TRITC, 1:1000, Jackson Immunoresearch) for 45 minutes at 37 ºC. The coverslips were washed two times in PBS followed by a wash in distilled water and then mounted with an anti-fading mounting medium with DAPI (Vectashield H-1200 for epifluorescent microscope and H-1800 for confocal microscope) for nuclei staining. Cells were observed at the

epifluorescent (Leica DM2500) and confocal (Nikon Eclipse TE2000-U, D-Eclipse C1) microscopes, and images were analyzed with Image J 1.53s and Fiji 2.5.0 (GitHub).

3.10 Statistical analysis

Statistical analysis was performed using the GraphPad Prism 8 software. Graph representations were presented as mean (M) ± standard deviation (SD).

Data were tested for normality/homogeneity through the Shapiro-Wilk test; when normality was not verified an equivalent non-parametric test was applied. Subsequently, a T-test two-tailed was applied for comparisons of two independent groups (MEFs experiments). For data normalized, and the groups were only compared to a control, a One sample T-test was performed setting 0 or 1 as the reference value. For experiments with more than two groups compared among them (Subcellular fraction experiments), a One-way Analysis of Variance (ANOVA) and Tukey's tests were applied for multiple comparisons. For experiments with two variables (MG132 treatment with MID1 overexpression), a Two-way ANOVA and Bonferroni's tests were applied for multiple comparisons. Differences were considered statistically significant for p-values below 0.05.

The half-life ($t_{1/2}$) value on the cycloheximide assay was calculated as a Nonlinear regression (Exponential Decay) considering the formula $N(t)=N_0^{-\lambda t}$, where N_0 is the initial quantity of protein (100%), N_t is the remaining quantity after the time (t), and λ is the decay constant.

3.11 Antibodies

Table 9. Description of the antibodies used in this work. Abbreviation: H: Human; IF: Immunofluorescence; IP: Immunoprecipitation. WB: Western Blot. M: Mouse.

Antibodies	Reference	Description	Dilution WB	Dilution IF	Amount IP
4E-BP1	GeneTex GTX32323	Rabbit Polyclonal (H)	1:500		
4E-BP1 (Phospho Thr^{46})	GeneTex GTX109162	Rabbit Polyclonal (H, M)	1:500		
ACTIN	Cytoskeleton AAN01	Rabbit Polyclonal (H, M)	1:2000		
α-TUBULIN	Sigma T16199	Mouse Monoclonal (H, M)	1:2000		
β-TUBULIN	Sigma T4026	Mouse Monoclonal (H, M)	1:2500		
EXOSC8	Proteintech 11979	Rabbit Polyclonal (H, M)	1:2000		
EXOSC10	Bethyl A303-987A	Rabbit Polyclonal (H, M)	1:2500		
FLAG	Sigma F1804	Mouse Monoclonal (H, M)	1:2000	1:500	1µg
	Sigma F3165	Mouse Monoclonal (H, M)	1:1000		
GAPDH	Sigma G8795	Mouse Monoclonal (H, M)	1:2500		
GFP	Invitrogen GF28R	Mouse Monoclonal (H, M)	1:2500		1µg
HA	Sigma HA-7	Mouse Monoclonal (H, M)	1:1000		
HIS	Healthcare 27-4710-01	Mouse Monoclonal (H, M)	1:1000		
MIDLINE-1 (MID1)	GeneTex GTX34076	Rabbit Polyclonal (H)	1:2000		
MYC	Sigma M5546	Mouse Monoclonal (H)	1:1000		
USP8	Proteintech 27791	Rabbit (H, M)	1:2000	1:200	1µg
USP33	Abcam 71716	Rabbit Polyclonal (H)	1:2000		
P84	Abcam 5E10 ab487	Mouse Monoclonal (H, M)	1:5000		
PP2AC	Cell Signaling 2038	Rabbit Polyclonal (H, M)	1:1000		

4. Results and Discussion

4.1. MID1 substrates

The main objective of this thesis is to select DUB candidates that work in a highly coordinated manner with MID1 to regulate its substrates. To begin, we selected and characterized the MID1 substrates to be used in the following experiments.

The main target of MID1 is PP2AC, the catalytic subunit of protein phosphatase 2A, which has been shown to increase in the absence of MID1 or in presence of non-functional MID1 (see section 1.3.4.1 PP2AC). Furthermore, our lab group previously discovered new putative targets of MID1: Exosome Component 10 (EXOSC10) and Exosome Component 8 (EXOSC8), both subunits of the RNA exosome complex (Kalluri & LeBleu, 2020). Rossella Baldini in her Ph.D. thesis describes that in *Mid1*$^{-/Y}$ embryonic brains differential proteomic analysis, Exosc8 and Exosc10 proteins levels were increased. Furthermore, this result was confirmed in HEK293T cells with MID1 overexpression. The exosome components modulation is presumably driven through an indirect or transient interaction, as neither EXOSC10 nor EXOSC8 directly binds MID1. Moreover, the nuclear distribution of EXOSC8 was found affected in hTERT-RPE cells upon MID1 overexpression and in MEFs *Mid1*$^{-/Y}$ (Baldini, et al, unpublished data; Baldini, 2018).

To confirm Pp2ac, Exosc8, and Exosc10 as substrates of Mid1, we used MEFs obtained from littermate embryos: three *Mid1*$^{+/Y}$ (WT) and three *Mid*1$^{-/Y}$ (KO) (see section 3.2.1 Mouse embryonic fibroblasts (MEFs)). MEFs were collected at passage 2 in RIPA buffer and a WB was performed to analyze the protein amount of Pp2ac, Exosc10, and Exosc8 (**Figure 19**). The data passed the Shapiro-Wilk test for normality, and Student's t-test two-tailed was performed to compare *Mid1* WT and KO samples in WB for the amount of each protein normalized against a loading control. Pp2ac levels (**Figure 19**. **A -** WT: *M*=0.49, SD=0.46; *Mid1* KO: *M*=1.44, SD=0.34) are significantly increased in the absence of *Mid1* KO compared with the WT **(***t* (4) =2.90, *p*=0.044, *d*=2.90). This result is expected considering the consolidate results of Pp2ac reduction when Mid1 is overexpressed. For Exosc10 levels (**Figure 19**. **B** – WT: *M*=0.31, SD=0.030; *Mid1* KO: *M*=0.40, SD=0.34) there was no statistically significant difference but a trend (0.50<d<0.80) of increase in the *Mid1* KO (Welch corrected t (2) =0.45, *p*=0.70, *d*=0.45). Regarding Exosc8 protein levels (**Figure 19**. **C -** WT: *M*=0.084, SD=0.065; *Mid1* KO: *M*=0.10, SD=0.12), there was no statistical difference but a small tendency effect (0.20<d<0.50) of

increase in the *Mid1* KO (t (4) =0.24, p=0.82, d=0.24). For both RNA exosome components, it was not possible to observe a statistically significant increase of these proteins in the *Mid1* KO. This is possible since Baldini studied the cerebella of embryonic brains, whereas here we used MEFs, thus reducing an effect that could be specific to defined structures.

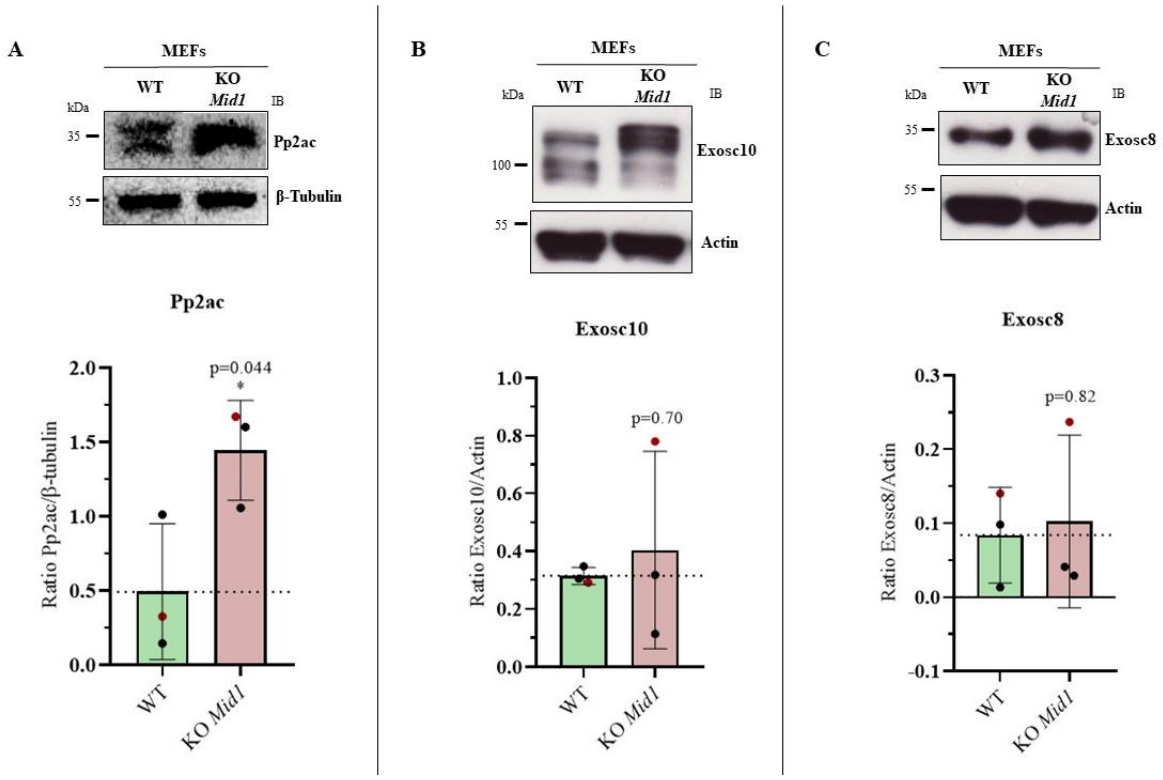

Figure 19. Protein targets of Mid1. The protein levels of Pp2ac (**A**), Exosc8 (**B**), and Exosc10 (**C**) are increased in Mouse Embryonic Fibroblasts (MEFs) from *Mid1* knockout (KO) compared with the wildtype (WT). Quantification of the three *Mid1* KO and WT (n=3) using densitometry analysis with the Image Lab software was performed. Relative abundance results are presented as the ratio between Pp2ac and β-tubulin and Exosc8 or Exosc10 and Actin. **A.** (Pp2ac) - WT: M=0.49, SD=0.46; *Mid1* KO: M=1.44, SD=0.34. **B.** (Exosc10) - WT: M=0.31, SD=0.030; *Mid1* KO: M=0.40, SD=0.34. **C.** (Exsoc8) - WT: M=0.084, SD=0.065; *Mid1* KO: M=0.10, SD=0.12. Statistical analysis was performed by a student's t-test two-tailed *p≤0.05. Antibodies: Exosc8 (35kDa) from Proteintech (1:2000); Exosc10 (100kDa) from Bethyl (1:5000); β-tubulin (55kDa) from Sigma (1:5000); Actin (45kDa) from Cytoskeleton (1:5000) and Pp2ac (35kDa) from Cell Signaling (1:1000).

To validate the effects observed on Pp2ac protein in the *Mid1* KO, we performed the opposite assay overexpressing MID1 which should decrease the PP2AC total protein. HeLa cells were transfected with a GFP-MID1 plasmid and proteins were collected at two-time points: 24 and 48 hours. According to **Figure 20**, MID1 overexpression decreases PP2AC protein levels along the time (24h=0.54; 48h=0.49), as expected. The exogenous MID1 protein tends to decrease

over time likely by the effect of degradation summed to the loss of the plasmid; however, the effects on PP2AC levels are maintained. To conclude, the best time point to overexpress MID1 is 24 hours, which will be used in future experiments.

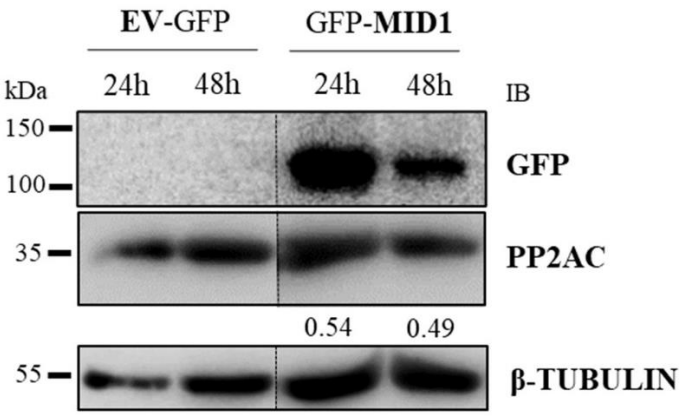

Figure 20. MID1 overexpression downregulates PP2AC levels over time. In HeLa cells, we re-confirmed the effect of MID1 on the PP2AC total protein amount. HeLa cells were transfected with 1µg GFP-MID1 plasmid in a 12-well-plate and protein was collected in RIPA buffer at two-time points: 24 and 48 hours. The control was transfected with Empty Vector - GFP (EV-GFP). Quantification of the assay was made with densitometry analysis with the Image Lab software. Expression is shown as the ratio between PP2AC, and β-TUBULIN normalized at each time point with the corresponding EV-GFP. Antibodies: β-TUBULIN (55 kDa) from Sigma (1:2500); GFP (100 kDa) from Sigma (1:2500), PP2AC (35 kDa) from Cell Signaling (1:1000).

Among the three substrates analyzed, Pp2ac and Exosc10 were the ones showing a more consistent increase in the *Mid1* KO. For this reason, we selected these two proteins as the principal substrates to be studied in this thesis. To better optimize the following experiments, we analyzed the half-life ($t_{1/2}$) of PP2AC and EXOSC10 proteins. To this end, we treated HeLa cells with 50µg/mL of cycloheximide (protein synthesis inhibitor) for 24 hours (time points: 4, 8, 16, and 24 hours). **Figure 21** shows that both proteins are stable, with a $t_{1/2}$= 14.2 hours for PP2AC (τ (mean lifetime) =20.5; λ (decay constant) =0.049) and $t_{1/2}$=34.8 hours for EXOSC10 (τ=50.2; λ =0.020).

WB of **Figure 21** shows two PP2AC bands that are very similar in molecular weight and are both disappearing over time. The two PP2AC bands can also be seen in the assay of **Figure 19** where mouse protein was used. When the double band of PP2AC is present it displays the same pattern. Thus, to obtain the total level of PP2AC, the two bands were quantified together and summed. The presence of a double band of PP2AC appeared to be dependent on the total protein amount loaded, on the run of the gel, and the percentage of acrylamide used. Moreover,

the antibody datasheet (Cell Signaling 2038) shows two bands of PP2AC protein for several cell lines. It would be interesting to study in the future if these bands represent αand β isoforms or are instead related to PP2AC methylation (Leucine^{309}) and/or phosphorylation (Threonine^{304}) status.

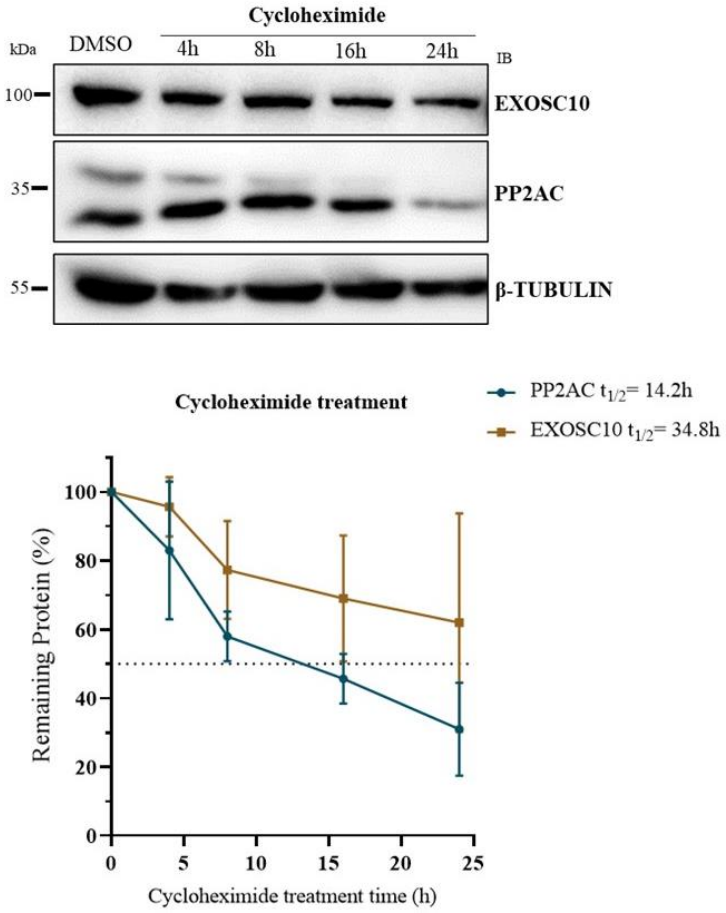

Figure 21. The half-life of PP2AC and EXOSC10. HeLa cells were treated with 50µg/mL of cycloheximide for as long as 24 hours (h) and the control was treated with the vehicle DMSO. The protein levels of PP2AC and EXOSC10 were collected in RIPA buffer and analyzed at different time points: 4h, 8h, 16h, and 24h. Quantification of three independent assays (n=3) using densitometry analysis with the Image Lab software. For relative expression results are presented as the ratio between PP2AC or EXOSC10 and β-TUBULIN and referred to the DMSO-treated sample as 1. PP2AC: 4h (*M*= 83.0%; SD=20.0%), 8h (*M*=58.0%; SD=7.20%), 16h (*M*=45.7%; SD=7.30%), 24h (*M*=31.0%; SD=13.5%). EXOSC10: 4h (*M*=95.7%; SD=8.60%), 8h (*M*=77.3% SD=14.2%), 16h (*M*=69.0%; SD=18.3%), 24h (*M*=62.0%; SD=31.8%). The half-life ($t_{1/2}$) value was calculated as a Nonlinear regression Exponential Decay ($N(t)=N0^{-\lambda t}$). PP2AC: τ (mean lifetime) =20.5; λ (decay constant) =0.049; $t_{1/2}$=14.2h. EXOSC10: τ=50.2; λ=0.020; $t_{1/2}$=34.8h. Antibodies: EXOSC10 (100kDa) from Bethyl (1:5000); β-TUBULIN (55kDa) from Sigma (1:5000); and PP2AC (35kDa) from Cell Signaling (1:1000).

4.2 Screening for DUBs modulating MID1 substrates

Considering that around 100 DUBs exist in humans, we decided to select 24 DUBs for the first screen set. In selecting the 24 DUBs, a review of the literature was conducted concerning the reported interactions between members of the TRIM family and DUBs (**Table 2**). This was done with the rationale that common mechanisms of TRIM/DUB functional interaction can be conserved. Additionally, this selection integrated other DUB candidates based on the type of regulation (preference for the degradative ones), substrates, and subcellular localization (**Table 1**). The DUBs selected for the first screening belong to different DUB subfamilies and are listed in the next figures.

4.2.1 Screening upon DUBs silencing

The first aim of this work was to discover suitable DUB candidates with an effect on PP2AC and/or EXOSC10 levels, and we decided to silence the selected DUBs via siRNAs and check for the substrates by WB. A decrease in the protein target level would be indicative of a suitable DUB candidate to further study.

As a first step, we selected the cell line in which to perform the screening, among four different human cell lines tested (HEK293T, ARPE, hTERT-RPE, and HeLa), HeLa cells show the best detection conditions. We opted for a siRNA concentration of 25nM since it is the minimal siRNA concentration for effective DUB protein silencing (**Figure 17**). Moreover, considering the results of the cycloheximide assay, where PP2AC and EXOSC10 showed high stability, we opted for a long time of silencing (72 hours) for the screen.

Hence, HeLa cells were transfected with 25nM siRNA (pool of four siRNAs targeting one gene - **Table 4**) for each of the 24 DUBs in a 96-well-plate for 72 hours. Afterward, a WB was performed to analyze the abundance of PP2AC and EXOSC10. For each DUB silencing, a minimum of three (n=3) and a maximum of eight (n=8) assays were quantified. PP2AC and EXOSC10 levels were normalized with the loading control (β-TUBULIN) and a control condition (transfected with non-targeting siRNA). In the quantification, the control is set to zero as the reference value: positive values indicate an increase in protein level and negative values indicate a decrease in protein level.

For PP2AC all conditions passed the Shapiro-Wilk test for normality, so One sample t-test was performed setting zero as the reference value. **Figure 22** shows the results of the DUBs silencing screening for PP2AC levels. Two DUBs emerged as candidates for future validation: USP8 (*M*=-0.19; SD=0.18; *t* (7) =2.90; *p*=0.023; *d*=1.02) and USP25 (*M*=-0.30; SD=0.31; *t* (7)=2.73; *p*=0.029; *d*=0.96). Both DUBs significantly decrease the levels of PP2AC when silenced.

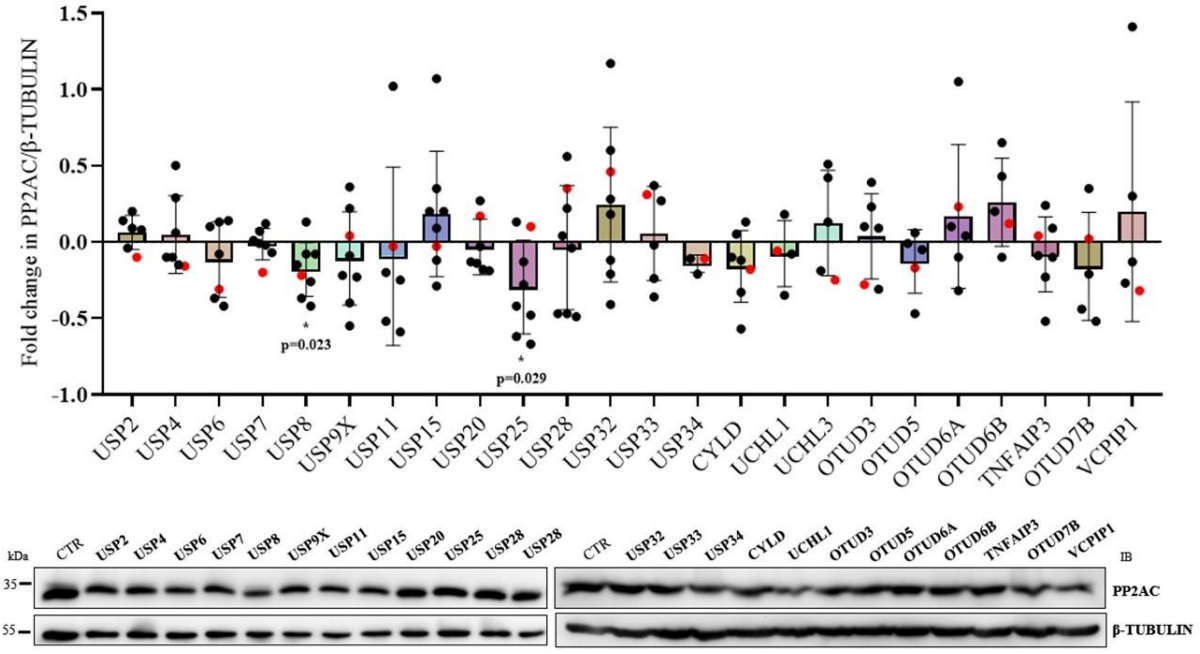

Figure 22. DUBs silencing screening for PP2AC. HeLa cells were transfected with 25nM of the indicated DUBs siRNA and collected in RIPA buffer after 72 hours. The control (CTR) was treated with non-Target siRNA. Representative Western Blot assay of the PP2AC levels upon each DUB silencing. Quantification of at least three assays for each condition (n=3) using densitometry analysis with the Image Lab software. Abundance is shown in the fold change of the ratio between PP2AC and β-TUBULIN with reference to the CTR. The graph is presented as mean ± standard deviation and the PP2AC level of the WB shown is highlighted in red. USP2 (*M*=0.062; SD=0.11); USP4 (*M*=0.049; SD=0.25); USP6 (*M*=-0.12; SD=0.25); USP7 (*M*=-0.014; SD=0.10); USP8 (*M*=-0.18; SD=0.18); USP9X (*M*=-0.11; SD=0.31); USP11 (*M*=-0.095; SD=0.58); USP15 (*M*=0.18; SD=0.41); USP20 (*M*=-0.033; SD=0.18); USP25 (*M*=-0.30; SD=0.31); USP28 (*M* -0.038; SD=0.41); USP32 (*M*=0.24; SD=0.51); USP33 (*M*=0.055; SD=0.31); USP34 (*M*=-0.14; SD=0.058); CYLD (*M*=-0.16; SD=0.23); UCHL1(*M*=-0.078; SD=0.22); UCHL3 (*M*=0.12; SD=0.35); OTUD3 (*M*=0.037; SD=0.28); OTUD5 (*M*=-0.13; SD=0.21); OTUD6A (*M*=0.17; SD=0.47); OTUD6B (*M*=0.26; SD=0.29); TNFAIP3 (*M*=-0.081; SD=0.25); OTUD7B (*M*=-0.16; SD=0.35); VCPIP1 (*M*=0.20; SD=0.72). For statistical analysis a One sample t-test was performed setting zero as the reference value, *p≤0.05. Antibodies: β-TUBULIN (55 kDa) from Sigma (1:2500); PP2Ac (35 kDa) from Cell Signaling (1:1000).

For EXOSC10 data, not all conditions passed the Shapiro-Wilk test for normality (OTUD5: W=0.75; p=0.027), and consequently, One sample Wilcoxon (non-parametric) test was

performed setting zero as the reference value. **Figure 23** shows the results of the DUBs silencing screening for EXOSC10 protein levels. In this case, the variability is significantly higher when compared with the PP2AC results. This irreproducibility may be caused by the long half-life of EXOSC10 or by the fact that EXOSC10 is a large protein, and this may lead to increased technical variability, especially during the transfer step in the WB experiment. Although we expected to see a decrease in EXOSC10 levels, OTUD6B silencing (Median (*Mdn)*=0.11; Z=21.0; *p*=0.031; *r*=2.45) displays the exact opposite effect. This can be interesting to explore in the future since OTUD6B also plays a role in the mTORC1 pathway as MID1 (Sobol et al., 2017).

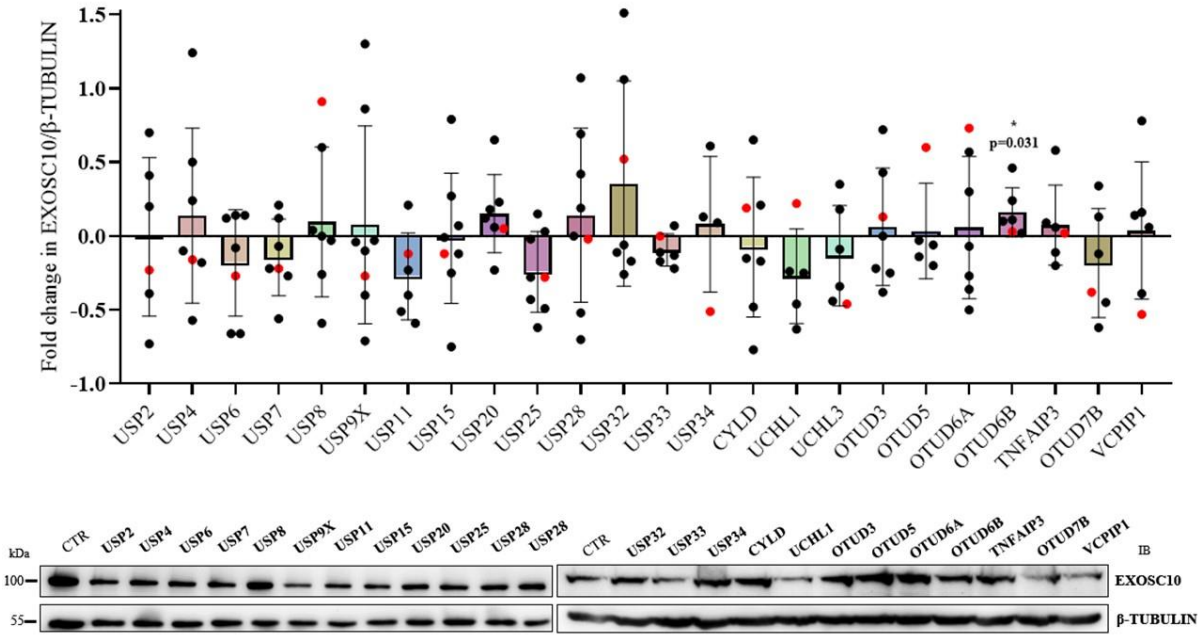

Figure 23. DUBs silencing screening for EXOSC10. HeLa cells were transfected with 25nM of the indicated DUBs siRNA and collected in RIPA buffer after 72 hours. The control (CTR) was treated with non-Target siRNA. Representative Western Blot assay of the EXOSC10 levels upon each DUB silencing. Quantification of at least four assays for each condition (n=4) using densitometry analysis with the Image Lab software. Abundance is shown in the fold change of the ratio between EXOSC10 and β-TUBULIN with reference to the CTR. The graph is presented as mean ± standard deviation and the EXOSC10 level of the WB shown is highlighted in red. USP2 (*Mdn*=-0.015); USP4 (*Mdn*=-0.10); USP6 (*Mdn*=-0.080); USP7 (*Mdn*=-0.22); USP8 (*Mdn*=0.0); USP9X (*Mdn*=-0.070); USP11 (*Mdn*=-0.32), USP15 (*Mdn*=-0.065); USP20 (*Mdn*=0.12); USP25 (*Mdn*=0.28); USP28 (*Mdn*=0.095); USP32 (*Mdn*=-0.060); USP33 (*Mdn*=-0.12); USP34 (*Mdn*=0.11); CYLD (*Mdn*=-0.15); UCHL1 (*Mdn*=-0.25); UCHL3 (*Mdn*=-0.22); OTUD3 (*Mdn*=0.0); OTUD5 (*Mdn*=-0.060); OTUD6A (*Mdn*=-0.070); OTUD6B (*Mdn*=0.11); TNFAIP3 (*Mdn*=0.040); OTUD7B (*Mdn*=-0.25), VCPIP1 (*Mdn*=0.10). For statistical analysis a One sample Wilcoxon test was performed setting zero as the reference value, *p≤0.05. Antibodies: β-TUBULIN (55 kDa) from Sigma (1:2500); EXOSC10 (100 kDa) from Bethyl (1:2500).

From the screening with DUBs siRNA, we selected the most promising candidates, and we repeated the silencing on a larger scale to check for both PP2AC and EXOSC10. HeLa cells were transfected with 25nM of each DUBs siRNA in a 24-well-plate for 72 hours. From this experiment (data not shown) we could confirm that the best candidate to decrease the PP2AC levels was USP8, excluding the potential candidate USP25. Nevertheless, there were no conclusive DUB candidates that significantly decrease EXOSC10 protein levels. For this reason, we decided to focus on PP2AC as the main protein target of MID1 under study.

4.2.2 Screening of PP2AC level upon DUBs overexpression

For validation of the results of the screening with DUBs siRNA, an opposite assay overexpressing the 24 DUB was performed in Pascual Sanz's lab at the CSIC, Institute of Biomedicine (Valencia, Spain). Herein, the purpose was to confirm the results obtained by doing the complementary experiment, i.e., DUBs overexpression should increase PP2AC total protein.

Through a collaboration between both Labs (Meroni and Sanz), we collected 24 DUB plasmids and confirmed the correct expression in HEK293 cells (**Figure 18**). Afterward, transient transfection of each DUB plasmid was performed in a 12-well-plate and by WB we quantified PP2AC protein levels. To better evaluate the PP2AC and DUB behavior along the time, this assay was performed at three-time points 24, 48, and 72 hours. **Figure 24** represents a WB at the best time point of expression for each DUB. Analyzing the PP2AC quantification, we have four DUB candidates that at least double the protein amount: USP2 (2.05), USP6 (2.01), USP11 (1.90), and USP8 (2.49).

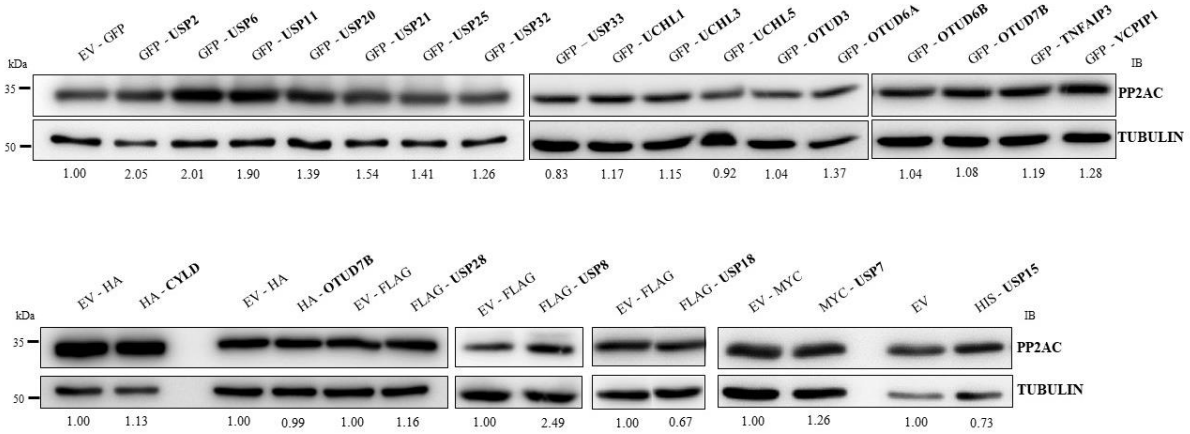

Figure 24. DUBs overexpression screening for PP2AC. HEK293 cells were transfected with 1µg of each DUB plasmid in a 12-well -plate and the control were transfected with the respective Empty Vector (EV). The cells were collected in RIPA buffer at 24h (HA-CYLD, GFP-OTUD3, GFP-OTUD6A, GFP-OTUD6B, HA-/GFP-OTUD7B, GFP-UCHL1, GFP-UCHL3, GFP-UCHL5, GFP-USP2, GFP-USP6, GFP-USP11, GFP-USP20, GFP-USP21, GFP-USP25, FLAG-USP28, GFP-USP32), 48h (GFP-TNFAIP3, MYC-USP7, HIS-USP15, FLAG-USP18, GFP-USP33, GFP-VCPIP1), and 72h (FLAG-USP8). Quantification of the assay was made with densitometry analysis with the Image Lab software. Expression is shown as the ratio between PP2AC, and TUBULIN normalized with the respective EV control. Antibodies: α-/β-TUBULIN (55 kDa) from Sigma (1:2500); PP2AC (35 kDa) from Cell Signaling (1:1000).

Thus, from both screenings (overexpression and silencing), we could confirm that the best candidate is USP8, which when silenced decreases PP2AC levels and shows the opposite effect when overexpressed, increasing PP2AC levels. The next chapters will be focused on characterizing the USP8 relationship with the PP2AC protein.

4.2.3 Validation of the DUBs screenings result: USP8 regulates PP2AC levels

From the screening with the DUBs siRNA (**Figure 22**), we could observe that the USP8 silencing significantly decreases the PP2AC levels. However, the silencing efficiency of the USP8 protein was not verified. Hence, HeLa cells were transfected with 25nM of USP8 siRNA in a 24-well-plate for 72 hours. According to **Figure 25**, USP8 siRNA, as previously described and confirmed once again, decreases PP2AC protein levels (0.43). Moreover, silencing of USP8 results in a reduction of 70% of the protein.

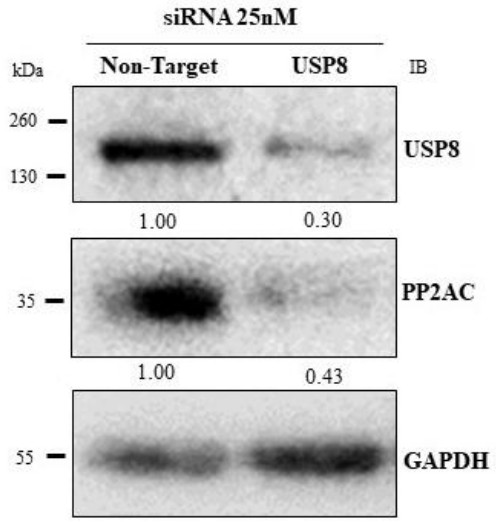

Figure 25. Silencing of USP8 decreases PP2AC levels. HeLa cells were transfected with 25nM of USP8 siRNA for 72 hours. The control was treated with non-Target (NT) siRNA. Quantification of the assay was made with densitometry analysis with the Image Lab software. Expression is shown as the ratio between PP2AC and GAPDH referenced to the NT. Antibodies: GAPDH (53 kDa) from Sigma (1:2500); PP2AC (35 kDa) from Cell Signaling (1:1000); USP8 (200kDa) from Proteintech (1:2000).

Secondly, we aim to confirm the result obtained in the DUBs overexpression screening suggesting that USP8 can increase PP2AC total protein (**Figure 24**). Moreover, we also studied the EXOSC10 and EXOSC8 protein levels as additional information. Hence, HeLa cells were transfected with 2.5µg FLAG-USP8 plasmid in a 6-well-plate for 72 hours (the optimal time point for FLAG-USP8 plasmid expression). Afterward, a WB was performed to analyze the protein abundance of PP2AC, EXOSC10, and EXOSC8. For each protein analyzed, we performed and quantified at least three (n=3) assays. Protein levels were normalized with the loading control (β-TUBULIN) and a control condition (transfected with Empty-Vector (EV)) as follows: zero is the reference value, positive values indicate an increase in protein levels, and negative values indicate a decrease in protein levels. All conditions passed the Shapiro-Wilk test for normality, so a One sample t-test was performed setting zero as the reference value.

Figure 26 shows the results for PP2AC (M=1.67; SD=0.34), EXOSC10 (M=0.72; SD=0.74) and EXOSC8 (*M*=0.16; SD=0.33) levels upon USP8 overexpression. The PP2AC increment is statistically significant when USP8 is overexpressed (t (3) =9.92; p=0.002; d=4.96), as expected from the DUB overexpression screening (**Figure 24**). For EXOSC10 protein levels, there is no statistical difference but a strong tendency (d<0.80) to be increased when USP8 is

overexpressed (*t* (3) =1.96; *p*=0.15; *d*=0.98). Regarding EXOSC8 protein levels, there is no significant statistical difference and a medium tendency (0.50<d<0.80) to be increased when USP8 is overexpressed (*t* (2) =0.82; *p*=0.50; *d*=0.47). To conclude USP8 overexpression leads to the accumulation of PP2AC protein levels in a significant manner (**Figure 26**).

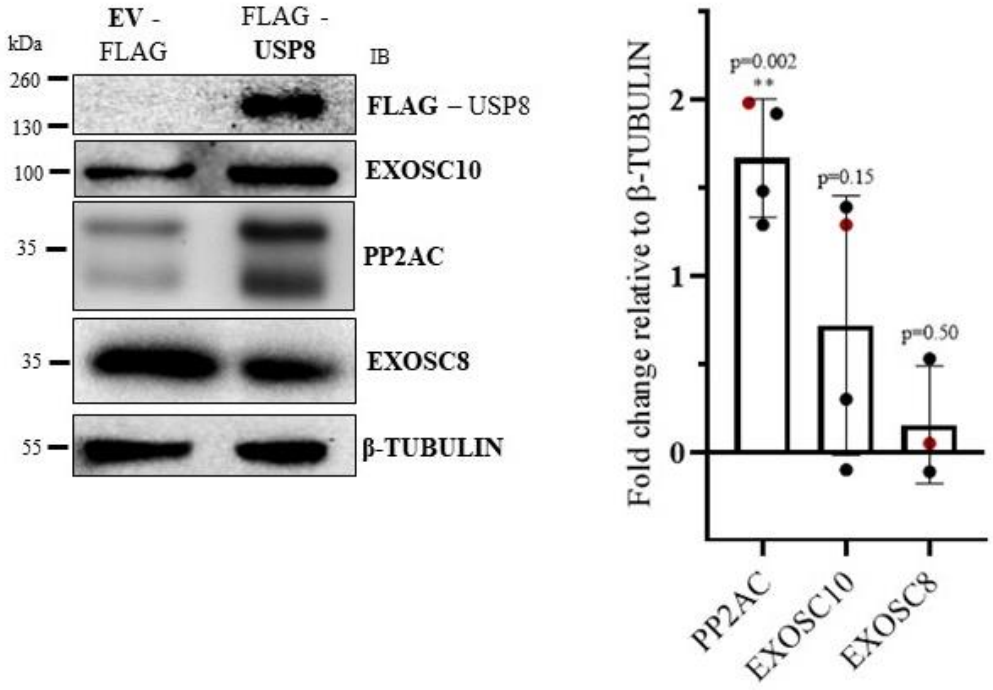

Figure 26. USP8 overexpression increases PP2AC levels. HeLa cells were transfected with 2.5µg FLAG-USP8 for 72 hours or with the Empty Vector (EV) as a control. Representative Western Blot (WB) of PP2AC upon USP8 overexpression is shown. Quantification of at least three assays for each condition (n=3) using densitometry analysis with the Image Lab software. Expression is shown as the ratio between PP2AC, and β-TUBULIN referenced to the EV. The graph is presented as mean ± standard deviation and the PP2AC level of the representative WB is highlighted in red. PP2AC (M=1.67; SD=0.34), EXOSC10 (M=0.72; SD=0.74), and EXOSC8 (M=0.16; SD=0.33). For statistical analysis a One sample T-test was performed setting 1 as the reference value, **p≤0.01. Antibodies: β-TUBULIN (55 kDa) from Sigma (1:2500); EXOSC8 (35 kDa) from Proteintech (1:2000); EXOSC10 (100kDa) from Bethyl (1:5000); FLAG (200 kDa) from Sigma (1:2000); PP2AC (35 kDa) from Cell Signaling (1:1000); USP8 (130kDa) from Proteintech (1:2000).

Overall, we can say that USP8 can modulate the PP2AC protein amount. We conclude that USP8/MID1 complex can operate on a shared substrate (PP2AC), resulting in the regulation of the substrate degradation likely through a switch-like antagonism (see section 1.5.1 DUBs and TRIMs pairs).

4.4 USP8 as candidate deubiquitinase of PP2AC and partner of MID1

USP8 represents a structurally unique (Komander et al., 2009), functionally promiscuous (Iphöfer et al., 2012; McGouran et al., 2013), and essential DUB (Clague et al., 2019). The crystal structure of the USP8 catalytic domain shows unique features. It is composed of two loops, namely, blocking loops 1 and 2 (BL1 and BL2), which are used for Ub recognition and are positioned in a closed conformation. There is also a finger subdomain that is tightened inwardly, making the Ub-binding pocket too narrow to capture Ub (Avvakumov et al., 2006; Kakihara et al., 2021). Despite these unfavorable features, the USP domain effectively catalyzes the deubiquitinating reaction, implying the occurrence of substrate-induced conformational changes (Avvakumov et al., 2006; Kakihara et al., 2021). The enzyme activity of USP8 is inhibited by binding to the 14-3-3-binding motif (14-3-3-BM) (**Figure 27)**. Mutations in USP8 have been associated with Cushing's disease, which is a tumor in the pituitary gland due to an excess of the hormone cortisol. Not surprisingly, ~50% of the mutations on USP8 related to Cushing's disease are present on the 14-3-3-BM (Z. Y. Ma et al., 2015; Reincke et al., 2015).

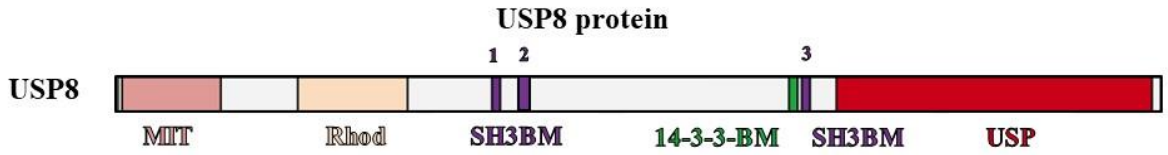

Figure 27. USP8 protein domain structure. Microtubule-interacting and trafficking domain (MIT) (aa 34 to aa 109) that is required for efficient abscission at the end of cytokinesis, together with components of the ESCRT-III complex. Rhodanese-like domain (Rhod) (aa 185 to aa 310).SH3-binding motif (SBM) (1: aa 405 to aa 413; 2: aa 440 to aa 448; 3: aa 738 to aa 746). 14-3-3-binding motif (14-3-3-BM) (aa 708 to aa 733). Vertebrate USP8 protein sequences have a well-conserved 14-3-3 BM. Ubiquitin-specific protease (USP) (aa 778 to aa 1088) is the catalytic domain that removes the conjugated ubiquitin molecules from the target proteins. Abbreviation: 14-3-3-BM: 14-3-3-binding motif; ESCRT: endosomal sorting complexes required for transport; MIT: Microtubule-interacting and trafficking domain; Rhod: Rhodanese-like domain; SH3BM: SH3-binding motif; USP: Ubiquitin specific protease. Adapted from Dufner & Knobeloch, 2019.

USP8 contains an N-terminal microtubule interacting and transport (MIT) domain (**Figure 27**) which has been associated with charged multivesicular body protein (CHMP) family (Dufner & Knobeloch, 2019). USP8 interacts with components of the endosomal sorting complexes required for transport (ESCRT) III (Row et al., 2007), and consequently, it has been highly

associated with the regulation of endosomal lysosomal trafficking, and/or stability of many other transmembrane proteins (Durcan et al., 2014; Durcan & Fon, 2015). The localization of USP8 is not cytosolic exclusive: it is also present in the nucleus, it interacts with the E2/E3 BIR (baculovirus inhibitor of apoptosis repeat) containing ubiquitin-conjugating enzyme (BRUCE), and regulates the double-strand break (DSB) repair (Ge et al., 2015). Interestingly, NRDP1, a RING E3 ligase is involved in the BRUCE degradation. is stabilized by USP8 (Wu et al., 2004).

Moreover, USP8 can directly link spermatid microtubules, being associated with acrosome biogenesis (Berruti et al., 2010). Recently, two papers have reported that USP8 participates in the control of ciliogenesis (Kasahara et al., 2018; Troilo et al., 2014). Primary cilia are microtubule-based organelles that act as sensors involved in developmental signaling pathways (Malicki & Johnson, 2017). Our group (Mascaro, et al, unpublished data; Mascaro, 2020) showed the influence of MID1 in ciliogenesis, possibly a shared pathway between MID1 and USP8. Not surprisingly, another common pathway for MID1 and USP8 is hedgehog (HH) signaling, which is dependent on the presence of primary cilia. It has been indeed reported that USP8 can antagonize the degradation of Smoothened (Smo/SMO), a member of the HH family (S. Li et al., 2012; G. Ma et al., 2016; Xia et al., 2012).

Thus, the cellular localization and pathways in which it is involved make USP8 a very promising candidate to functionally interact with MID1 protein and its substrates.

4.4.1 Effect of USP8 on mTOR pathway

Since USP8 is modulating PP2AC levels, we can conjecture that it can also affect the pathways regulated by PP2A. Section 1.3.4.3 MID1/PP2Ac and mTORC1 signaling, describes the role of PP2A in the mTOR pathway. PP2A dephosphorylates 4E-BP1 and thereby downregulates the translation of several mRNAs. Robust evidence point out that PP2A can reverse the phosphorylation state of 4E-BP1, although direct interaction between 4E-BP1 and PP2A has yet to be demonstrated (Kolupaeva, 2019). Moreover, PP2AC directly affects mTORC1 complex formation with an effect on its targets, among which is 4E-BP1 (E. Liu et al., 2011). Since USP8 can regulate the PP2AC level, herein we investigated if USP8 can also interfere with the phosphorylation levels of 4E-BP1.

Hence, HeLa cells were transfected with 2.5µg of FLAG-USP8 plasmid in a 6-well-plate for 48 hours. WB was performed to analyze the abundance of Phospho Threonine^{46} (Thr^{46}) 4E-BP1 form, normalized with the total 4E-BP1 (antibody re-incubated on the same membrane). All conditions passed the Shapiro-Wilk test for normality, so Student's t-test two-tailed was performed comparing the EV control group levels (EV: *M*=0.37; SD=0.035) with USP8 over-expression levels (USP8: *M*=0.25; SD=0.038). **Figure 28** shows the results for PhosphoThr^{46} 4E-BP1, we observed a statistically significant decrease of PhosphoThr^{46} 4E-BP1 when USP8 is overexpressed (*t* (4) =4.01; *p*=0.016; *d*=3.27). As a result of USP8 upregulation, 4E-BP1 total protein levels decrease as well, though this effect is not statistically significant and is less pronounced than the decrease in PhosphoThr^{46} 4E-BP1, which can be evaluated in future studies.

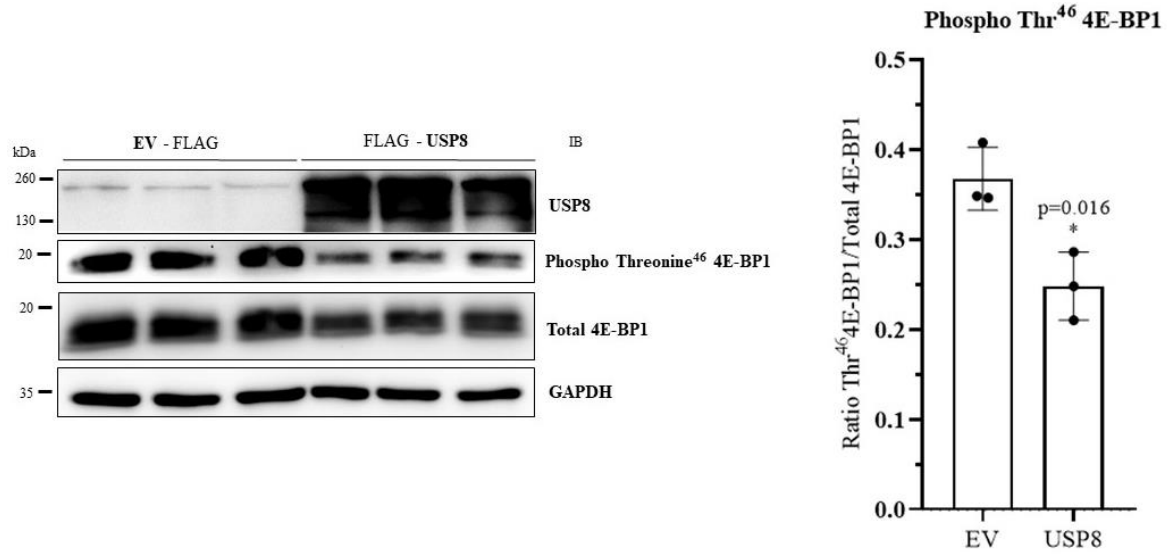

Figure 28. USP8 overexpression decreases Phospho Threonine^{46} 4E-BP1. HeLa cells were transfected with FLAG-USP8 or with the Empty Vector (EV) -FLAG for 48 hours. Western Blot (WB) of three assays (n=3) of Total and Phospho Threonine^{46} (Thr^{46}) 4E-BP1 upon USP8 overexpression is shown. The three assays for each condition (n=3) were running in parallel in the same SDS-PAGE gen and quantified using densitometry analysis with the Image Lab software. Expression is shown as the ratio between PhosphoThr^{46}- and Total-4E-BP1. The graph is presented as mean ± standard deviation. EV: *M*=0.37; SD=0.035; USP8: *M*=0.25; SD=0.038. Statistical analysis was performed by a student's t-test two-tailed, *p≤0.05. Antibodies: GAPDH (35 kDa) from Sigma (1:2500); PhosphoThr^{46} 4E-BP1 (15 kDa) from GeneTex (1:500); 4E-BP1 (15 kDa) from GeneTex (1:500); USP8 (130kDa) from Proteintech (1:2000).

It has been well reported that an increase in PP2A levels causes a decrease in the 4E-BP1 phosphorylation status (Peterson et al., 1999). The 4E-BP1 can also be phosphorylated by mTOR in its mTORC1 complex. Liu et al, showed that MID1 loss increases the levels of

PP2AC, which, as part of a βα-containing PP2A holoenzyme, disrupts mTOR/Raptor association and consequently inhibits mTORC1 signaling (E. Liu et al., 2011). The fact that, in this thesis, we found that USP8 overexpression increases PP2AC levels is consistent with a decreased 4E-BP1 phosphorylation. Therefore, the effect of USP8, likely through PP2AC regulation, has repercussions on the mTOR pathway, specifically the 4E-BP1 member.

It had already been reported that USP8 can regulate elements of the mTOR pathway. Indeed, in the papers of Jing et al and Sun et al, it was shown that USP8 can interfere with the phosphorylation of AKT, which can also be regulated by PP2A (Jing et al., 2020; J. Sun et al., 2020). Note that these studies were conducted in a tumorigenic cellular setting, where the phosphorylation levels of different pathways, especially mTOR, are deregulated. There are strong suggestions that the regulation of 4E-BP1 may be multifactorial and tissue specific. USP8 may serve as an important element for assessing the mTOR pathway in different cellular contexts.

4.4.2 Mutual regulation of MID1 and USP8

Here, we investigated the possibility that USP8/MID1 pair may have a mutual regulation. Indeed, being MID1 an E3 ubiquitin ligase and USP a DUB, USP8 can protect MID1 from degradation, while MID1 can ubiquitinate USP8 and thereby alter its activity or promote its degradation. To test this hypothesis, HeLa cells were transfected with GFP-MID1 and FLAG-USP8, alone or in combination (2.5µg of total DNA per condition), in a 6-well-plate for 48 hours. To determine how MID1 modulates USP8 levels, we treated cells for two hours with 10µM of MG132, an inhibitor of the 26S proteasome complex, and 10µM of Chloroquine (CQ), which inhibits autophagy by altering the acidic environment of the lysosomes. We chose the concentration and time for these drugs based on a previous report that also used HeLa cells (Zanchetta et al., 2017). As a control, the vehicle of MG132, DMSO, was used. The vehicle of CQ is H_2O, which is already present on the complete cellular medium. For each group (DMSO, MG132, and CQ) results were normalized to 1 using as a reference the single transfection condition of each protein.

Regarding the USP8 single transfection shown in **Figure 29**, on the DMSO condition, we observed a decrease of 25% in USP8 protein levels when co-transfection with GFP-MID1 compared with the single transfection (DMSO/FLAG-USP8). Comparing each treatment condition, the co-transfection with the respective single transfection (MG132/FLAG-USP8 and

CQ/FLAG-USP8): USP8 is increased with MG132 (1.58) and especially with CQ (8.65). These results strongly suggest that, when MID1 is overexpressed, it decreases the USP8 levels that are recovered by both the degradative pathways, with emphasis on the autophagic pathway. Interestingly, Jacomin et al showed that downregulating USP8 in HeLa cells deregulates autophagy, increasing the number of autophagosomes and increasing autophagy flux (Jacomin et al., 2015). Indeed, the ESCRT-III complex, regulated by USP8, was identified to be crucial for the closure of the autophagosome (Takahashi et al., 2018). Probably USP8 plays a direct regulatory role in autophagy through the regulation of ESCRT-III components activity (Jacomin et al., 2015). For this reason, USP8 can be more susceptible to autophagy than to the proteasomal pathway.

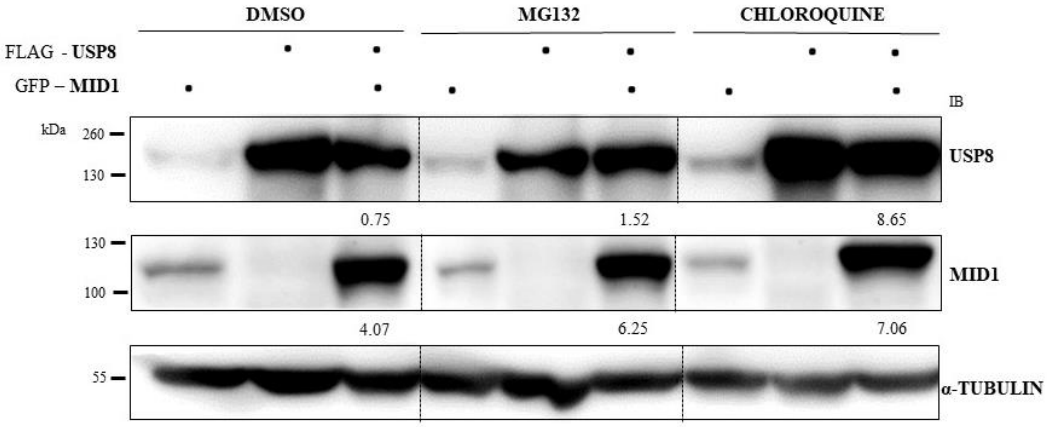

Figure 29. Mutual regulation of MID1 and USP8. HeLa cells were transfected with GFP-MID1 and/or FLAG-USP8 plasmids (2.5µg of DNA for each condition) and treated with 10µM of MG132 or Chloroquine for 2 hours. The control condition was treated with the vehicle DMSO. Quantification was performed by densitometry analysis with the Image Lab software. Expression is shown as the ratio between USP8 or MID1 and α-TUBULIN. At each group (DMSO, MG132, and CQ) results were normalized to one using as a reference the single transfection condition of each protein. Antibodies: α-TUBULIN (55 kDa) from Sigma (1:2000); MID1 (100 kDa) from GeneTex (1:2000); USP8 (200kDa) from Proteintech (1:2000).

Analyzing the MID1 protein in **Figure 29**, in the DMSO condition, it is evident that, when co-transfected with FLAG-USP8, the MID1 protein amount is significantly increased (4.07) compared with the single transfection (DMSO/GFP-MID1). The increment of MID1 in the co-transfection condition is significantly higher under treatments (MG132: 6.25 and CQ: 7.06) compared with the single transfection with the same drug (MG132/GFP-MID1, CQ/GFP-

MID1). This result strongly suggests that USP8 overexpression can increase the levels of MID1, opening the possibility that USP8 can modulate the levels of MID1.

From this assay, the MID1/USP8 pair appear to act as a rheostat-like antagonism. This means that USP8 protects MID1 from degradation probably by removing the Ub from auto-ubiquitination or other(s) E3 ligases, while MID1 can promote USP8 degradation, likely through direct or indirect ubiquitination. Considering that we cannot detect the endogenous MID1 protein due to a lack of suitable antibodies (**Figure 29** – lanes with the single FLAG-USP8 transfection), while it is possible to see the USP8 endogenous protein (**Figure 29** – lanes with the single GFP-MID1 transfection), we decided to focus the next experiments on characterizing the activity of MID1 on endogenous USP8.

4.5 USP8 as a possible substrate of MID1

4.5.1 Usp8 protein is upregulated in the *Mid1* knockout

To further confirm that the Usp8 level is controlled by Mid1, we used MEFs from family 7245 with two $Mid1^{+/Y}$ (WT) and four $Mid1^{-/Y}$ (KO) (see section 3.2.1 Mouse embryonic fibroblasts (MEFs)). The MEFs were collected at passage 2 in RIPA buffer, and WB (**Figure 30**) was performed to analyze the amount of Usp8 and Pp2ac, used as a positive control (in **Figure 19** the upregulation of Pp2ac on the *Mid1* KO was already confirmed).

For *Mid1* KO, all conditions (Pp2ac and Usp8 quantifications) passed the Shapiro-Wilk test for normality, but the WT only has two individuals (n=2), so it was not possible to verify the normality for these populations. For this reason, we performed a One sample t-test setting as the reference value of the respective WT mean (*M*) of each protein (*M*(Usp8-WT) =0.022; *M*(Pp2ac-WT) =0.014). In this way, we could measure how different the *Mid1* KO condition is with respect to the WT mean value. Usp8 protein levels (**Figure 30. A** - WT: *M*=0.022, SD=0.012; *Mid1* KO: *M*=0.12, SD=0.031) are significantly increased in the absence of *Mid1* KO compared with the WT (t (3) =6.27, p=0.008, d=3.12). Pp2ac protein levels (**Figure 30**. **B** – WT: *M*=0.014, SD=0.005; *Mid1* KO: *M*=0.034, SD=0.004) are significantly increased in the absence of *Mid1* KO compared with the WT (t (3) =8.85, p=0.003, d=4.42), as previously observed in **Figure 19** with MEFs from a different litter. From **Figure 30** it is possible to conclude that the Usp8 protein is increased in the *Mid1* KO.

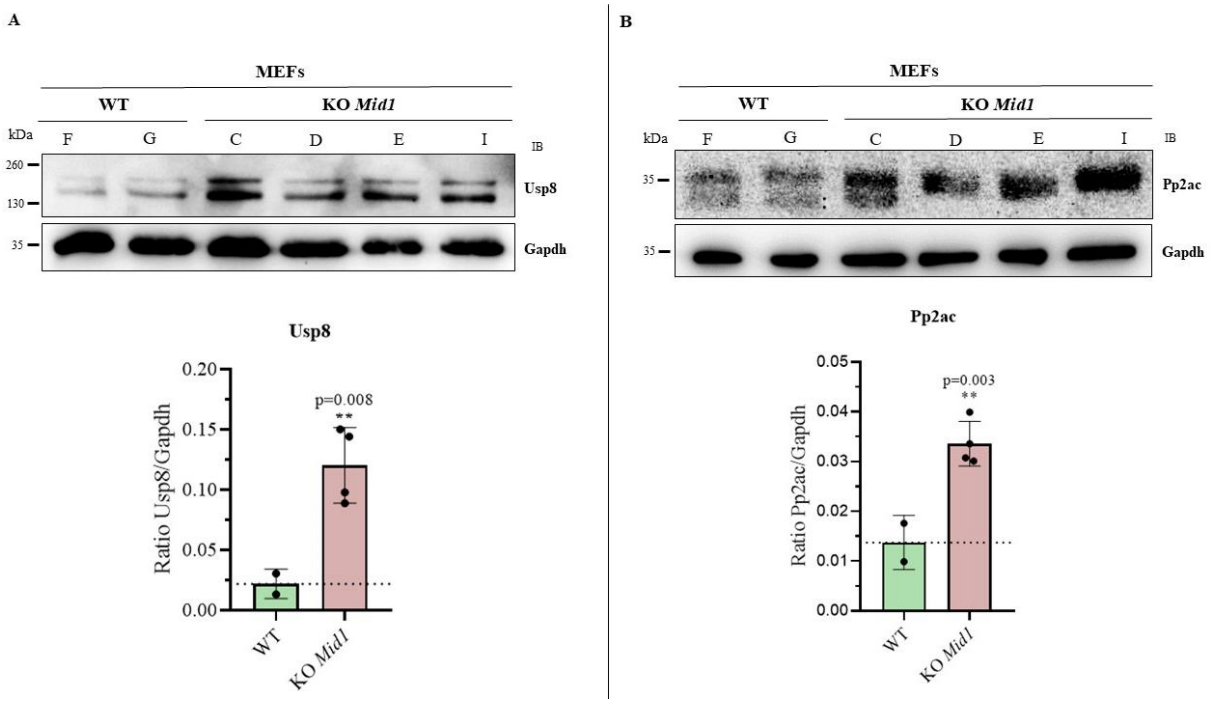

Figure 30. Usp8 is increased in *Mid1* KO. The protein levels of Usp8 (**A**) and Pp2ac (**B**) are increased in Mouse Embryonic Fibroblasts (MEFs) *Mid1* knockout (KO) compared with the wild type (WT). MEFs were from family 7245 collected at passage two in RIPA buffer. Quantification was performed by densitometry analysis with the Image Lab software. The graph is presented as mean ± standard and relative protein expression results are shown in the ratio between Usp8 or Pp2ac and Gapdh. Usp8-WT: *M*=0.022, SD=0.012; Usp8-*Mid1* KO: *M*=0.12, SD=0.031; Pp2ac-WT: *M*=0.014, SD=0.005; Pp2ac-*Mid1* KO: *M*=0.034, SD=0.004. For statistical analysis a One sample T-test was performed setting the respective WT mean as the reference value (*M*(Usp8-WT) =0.022; *M*(Pp2ac-WT) =0.014), *p≤0.05. Antibodies: Gapdh (53 kDa) from Sigma (1:2500); Pp2ac (35 kDa) from Cell Signaling (1:1000); Usp8 (200kDa) from Proteintech (1:2000).

4.5.2 MID1 promotes USP8 degradation partially through proteasome

To verify that the E3 ligase activity of MID1 is responsible for the changes in USP8 protein amount, we used ΔRING MID1, a catalytically dead form of the E3 ligase. Subsequently, to test that the effect on USP8 was due to MID1-mediated proteasomal degradation, we used the MG132 drug. HeLa cells were transfected with 2.5µg of GFP-MID1 or GFP-ΔRING-MID1 plasmid in a 6-well-plate for 24 hours. The EV-GFP plasmid was used as a transfection control. Before collecting the proteins in RIPA buffer, cells were treated for two hours with 10µM of MG132, and the vehicle, DMSO was used as a control condition. Afterward, a WB was performed to analyze the abundance of USP8, quantifying four (n=4) experiments. Protein levels were normalized with the loading control (β-TUBULIN) and the control condition (transfected with EV and treated with DMSO) set as 1. All conditions passed the Shapiro-Wilk

test for normality, so a Two-way ANOVA was performed considering two variables (transfection and treatment).

Figure 31 presents the results of the WB, upon overexpression of MID1 or ΔRING-MID1, the latter showing a reduced molecular weight since the RING domain is missing. Both MID1 forms are increased upon MG132 treatment, partially in contrast with **Figure 29**. The graph of **Figure 31** shows the quantification of USP8 levels when MID1 is overexpressed in the control condition (MID1: *M*=0.61; SD=0.041; ΔRING-MID1: *M*=1.29; SD=0.28) and upon treatment (EV: *M*=1.03; SD=0.48; MID1: *M*=0.94; SD=0.13, ΔRING-MID1: *M*=1.17; SD=0.19). The Two-way ANOVA test for transfections (EV, MID1, and ΔRING-MID1) and treatment (DMSO and MG132) as between-subjects factors revealed a main effect of transfection, F (1.782, 5.347) = 5.65, p=0.05, η_p^2=5.60, but not of treatment, F (1, 3) =0.32, p=0.061, η_p^2=0.26 (large effect when η_p^2>0.14). Regarding the interaction between transfections and treatment, there is a high effect size without significant differences, F (1.166, 3.498) = 4.692, p=0.11, η_p^2 =1.46. Post-hoc analyses using Bonferroni's test for multiple comparisons indicated that DMSO/EV is significantly different from DMSO/MID1 (t (3) =19.2; p=0.005).

These results (**Figure 31**) show that exogenous MID1 downregulates USP8 levels, an effect that cannot be observed to the same extent with the non-catalytic form of the protein, proving that the E3 ligase activity of MID1 is involved in USP8 degradation. Further, USP8 levels are recovered when treated with MG132, likely reflecting the involvement of the proteasomal pathway in the degradation of USP8 through MID1 activity. However, it is important to remember that the USP8 protein is not exclusively degraded by the proteasomal pathway. Instead, it is highly sensitive to the autophagic pathway as well, as previously observed in **Figure 29**.

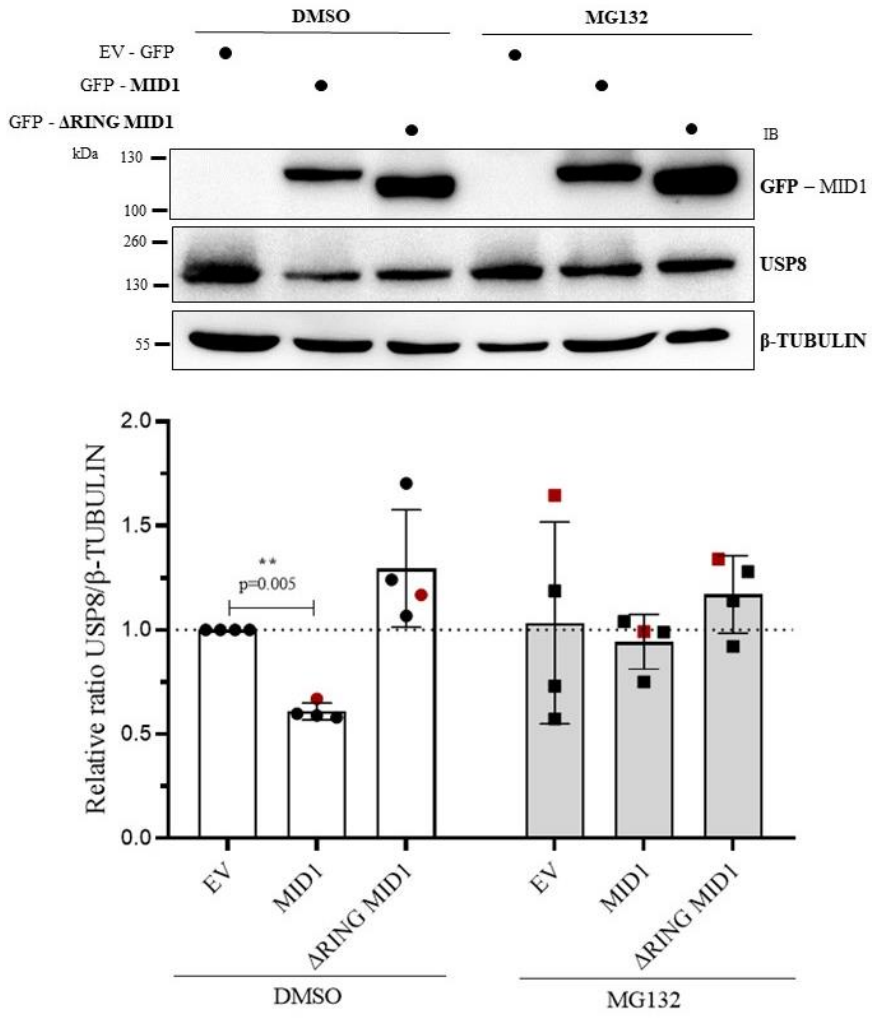

Figure 31. MID1 modulates USP8 protein levels through the proteasome. HeLa cells were transfected with GFP-MID1 or GFP-ΔRING MID1 and treated with 10μM of MG132 for 2 hours. The transfection control was with Empty Vector - GFP (EV) and the control condition to MG132 was treatment with the vehicle DMSO. Quantification of four assays for each condition (n=4) using densitometry analysis with the Image Lab software was performed. Expression is shown as the ratio between USP8, and β-TUBULIN normalized to the EV/DMSO. The graph is presented as mean ± standard deviation and the USP8 level of the representative WB is highlighted in red. DMSO/MID1: *M*=0.61; SD=0.041. DMSO/ΔRING-MID1: *M*=1.29; SD=0.28. MG132/EV: *M*=1.03; SD=0.48. MG132/MID1: *M*=0.94; SD=0.13. MG132/ΔRING-MID1: *M*=1.17; SD=0.19. For statistical analysis, a Two-way ANOVA test and Bonferroni's test were applied for multiple comparisons **p≤0.01. Antibodies: β-TUBULIN (55 kDa) from Sigma (1:2500); GFP (100 kDa) from LifeTech (1:2500); USP8 (200kDa) from Proteintech (1:2000).

4.6 Co-Localization of MID1 and USP8 in the cell

At this point, we can suggest that USP8 is a putative substrate of MID1 E3 ligase activity, however, this effect of MID1 on USP8 protein can be through direct or indirect ubiquitination. To start investigating if MID1 and USP8 are interacting, we performed immunofluorescence

(IF) to see if these proteins are co-localizing in the cell. On one hand, MID1 is dynamically associated with microtubules; when MID1 is dephosphorylated, it detaches from them and is observed in cytoplasmic bodies (J. Liu et al., 2001). **Figure 6** from the introduction is an example of the MID1 dynamic distribution in HeLa cells. On the other hand, USP8 has been reported in different cellular localizations: Golgi apparatus, microtubules, and nucleus. USP8 protein possibly also has a tissue-specific cellular localization. In this work, we decided to first analyze the cellular localization of USP8 in HeLa cells.

4.6.1 Partial co-localization of MID1 and USP8

HeLa cells were transfected with 1µg FLAG-USP8 plasmid in a 12-well-plate for 48 hours. Afterward, an IF was performed using an anti-FLAG antibody for the detection of the USP8 exogenous protein. **Figure 32** shows an epifluorescent microscope image for USP8 localization in HeLa cells. USP8 exogenous protein is widely distributed in the cell, both in the cytoplasm and nucleus, with a stronger signal in the cytoplasm. These results agree with the literature previously described. Moreover, USP8 can also form dots in the cytoplasm, which we can speculate to be endosomes, lysosomes, or other vesicles.

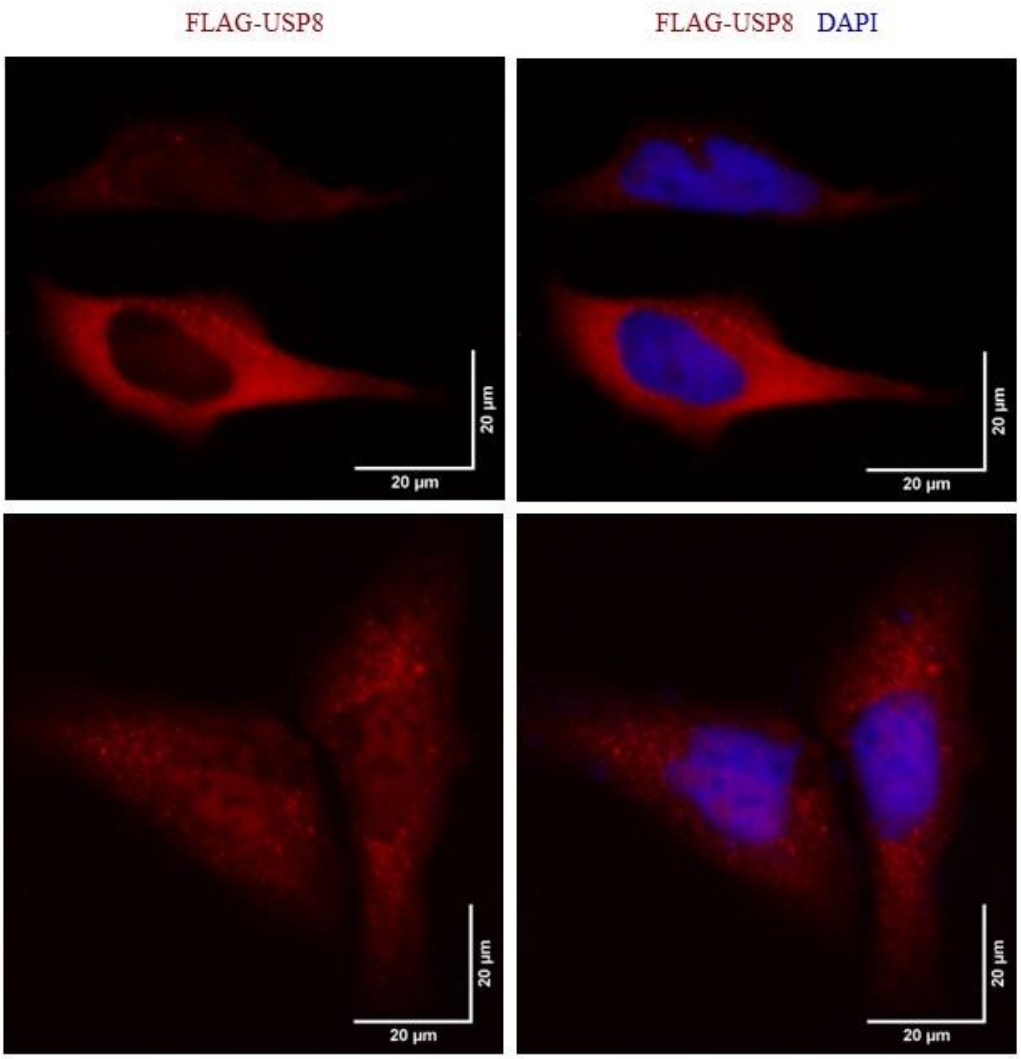

Figure 32. Localization of USP8 in HeLa cells. HeLa cells were transfected with Flag-USP8 plasmid for 48 hours. Immunofluorescence shows the distribution of USP8 (in red) mainly in the cytoplasm but also the nucleus. DAPI was used as nuclear staining. Images are taken at a 63X magnification with a scale bar of 20µm. Magnified image of the white square section (scale bar of 10µm) with USP8 dots in the cytoplasm. Antibodies: FLAG from Sigma (1:500).

Successively, we wanted to study if MID1 and USP8 are co-localizing in HeLa cells. Thus, HeLa cells were transfected with 1µg FLAG-USP8 and GFP-MID1 plasmids on a coverslip for 48 hours. Afterward, an IF was performed using an anti-FLAG antibody for the detection of the USP8 exogenous protein, whereas MID1 could be detected as a GFP signal. **Figure 33** shows the IF images from an epifluorescent microscope. GFP-MID1 and FLAG-USP8 both display a predominantly cytoplasmic distribution, with MID1 adopting its classical microtubular localization. When merged (FLAG-USP8 with GFP-MID1 and DAPI), the two proteins do

not show a strong co-localization. To evaluate if co-localization does exist, these samples were also analyzed under a confocal microscope.

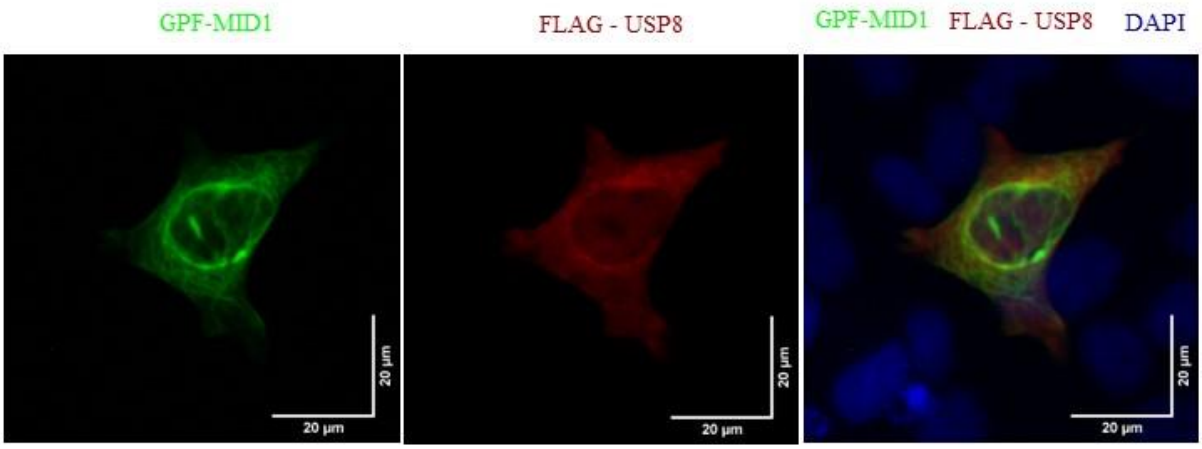

Figure 33. Subcellular localization of USP8 and MID1 in HeLa cells. HeLa cells were transfected with Flag-USP8 and GFP-MID1 plasmids (1µg of DNA in total) for 48 hours. Immunofluorescence shows the distribution of USP8 (in red) and MID1 (in green) in the cell. DAPI was used as nuclear staining. Images were captured in an epifluorescent microscope with 63X magnification (scale bar of 20µm). Antibodies: FLAG from Sigma (1:500).

Figure 34 shows a confocal image of USP8 and MID1 localization in HeLa cells. The dotted USP8 distribution and microtubular MID1 are more evident. In the magnified image from the merge of GFP-MID1, FLAG-USP8, and DAPI, some yellow spots identifying partial co-localization are observed. Therefore, we can conclude that USP8 and MID1 co-localize just partially. We can hypothesize that USP8 interacts with MID1 only when the latter is detached from microtubules and forms cytoplasmic bodies, or that interaction can occur along the microtubules but not throughout them. To complete the study of MID1 and USP8 co-localization, the IFs experiments would need to include more conditions and the use of specific markers for sub-cellular compartments. Besides, both proteins are observed upon overexpression, and it would be interesting to observe the localization of the endogenous proteins once specific antibodies working in immunofluorescence are available.

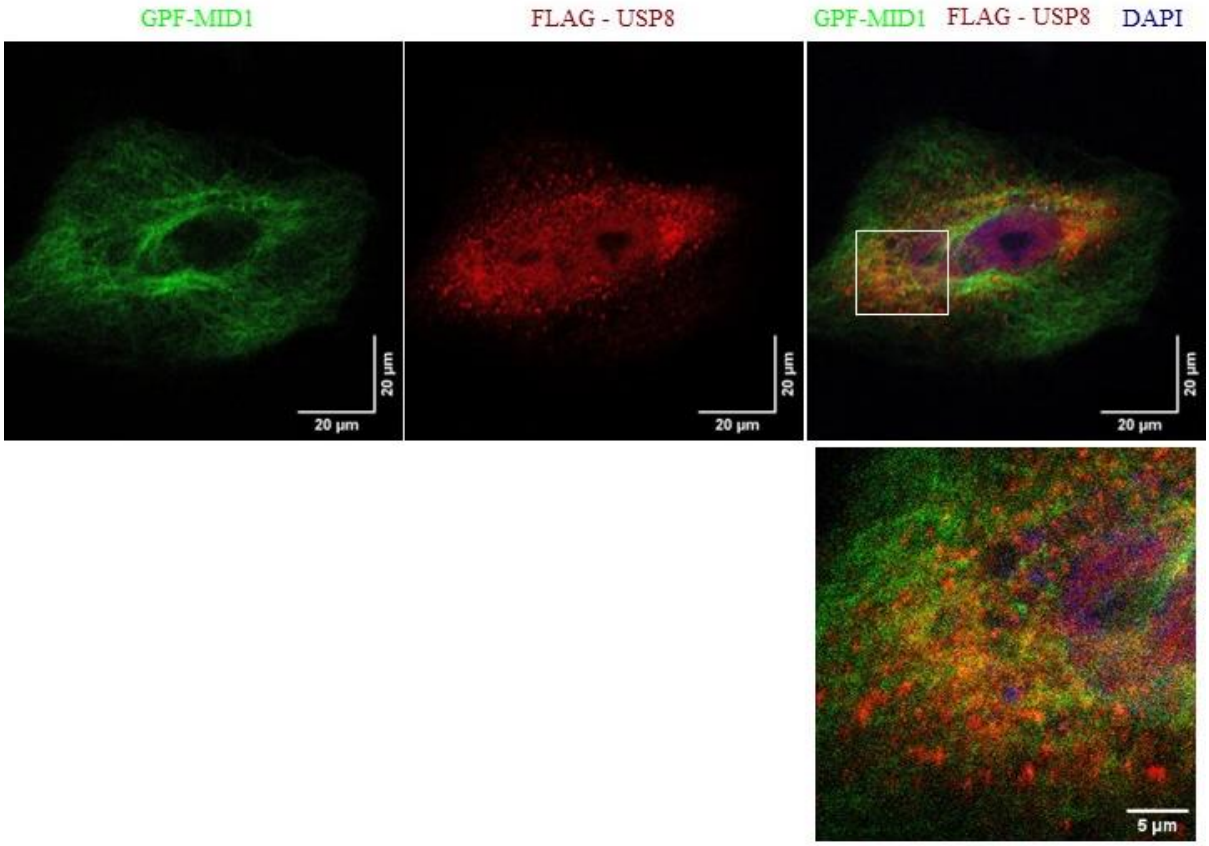

Figure 34. Subcellular co-localization of USP8 and MID1 in HeLa cells. HeLa cells were transfected with Flag-USP8 and GFP-MID1 plasmids (1µg of DNA in total) for 48 hours. Immunofluorescence shows the distribution of USP8 (in red) and MID1 (in green) in the cell. DAPI was used as nuclear staining. Images were captured in a confocal microscope with 60X magnification (1024x1024 Pixels; scale bar of 20µm). Magnified image of the white square section (scale bar of 5µm). Antibodies: FLAG from Sigma (1:500).

4.7 Sub-cellular localization of the MID1/USP8/PP2AC proteins upon cellular fractionation

The cellular localization of the possible MID1/USP8/PP2AC complex is a paradox that deserves further investigation. Both USP8 and PP2AC proteins are widely distributed in the nucleus and cytoplasm, but MID1 is restricted to microtubules. This raises the question of where MID1 modulates USP8 levels. We investigated this issue by performing protein fractionation (cytoplasm and nucleus), to determine where the reciprocal effects on protein levels of the MID1/USP8/PP2AC complex can be observed.

4.7.1 Cellular Localization of MID1-mediated USP8 regulation

Firstly, we studied which cellular compartment MID1 is modulating USP8 protein levels. HeLa cells were transfected with 2.5µg of GFP-MID1 or GFP-ΔRING MID1 in a 6-well-plate for 24 hours, and the control condition was transfection with Empty Vector - GFP (EV). Cell extracts were fractionated in the following compartments: whole cell lysates (WCL), cytoplasm (CYT), and nuclei (NUC). Afterward, WB was performed to analyze the protein abundance of USP8, quantifying at least three (n=3) assays per condition. Proteins levels were normalized with the respective loading: β-TUBULIN for the WLC and CYT fractions, and P84 for the WLC and NUC fractions. Each transfection condition was normalized to the relative EV, in which 1 is the reference value.

Figure 35 presents the results of the WB and the graph for the quantification of the USP8 level. Each group, WLC, CYT, and NUC, had different loading controls so we considered four independent data sets: WLC-USP8/β-TUBULIN (MID1: *M*=0.55; SD=0.33; ΔRING-MID1: *M*=1.22; SD=0.69), CYT-USP8/β-TUBULIN (MID1: *M*=0.61; SD=0.17; ΔRING-MID1: *M*=0.77; SD=0.16), WLC-USP8/P84 (MID1: *M*=0.79; SD=0.49; ΔRING-MID1: *M*=0.97; SD=0.54), and NUC-USP8/P84 (MID1: *M*=0.64; SD=0.085; ΔRING-MID1: *M*=1.06; SD=.25). In each set one variable was evaluated: the transfection effect (EV-GFP, MID1, and ΔRING MID1) on the USP8 levels. All conditions passed the Shapiro-Wilk test for normality, so a One-way ANOVA test was applied to each of the data sets evaluating the transfection effect. For WLC-β-TUBULIN a strong tendency (large effect size when η_p^2>0.14) to reduce USP8 levels upon MID1 overexpression was observed, F (2, 6) = 1.80, *p*=0.24, η_p^2=0.37. This result is in line with the data previously presented (**Figure 31**). For CYT-β-TUBULIN we observed a significant effect of transfection, F (2, 8) = 9.09, *p*=0.009, η_p^2=0.69. Post-hoc analyses using Tukey's test for multiple comparisons indicated that USP8 levels are significantly lower when MID1 is overexpressed compared to the EV (t (8) =4.25; *p*=0.009). For WLC-P84 a significant effect of the transfection was not observed, F (2, 6) =0.21, *p*=0.81, η_p^2=0.076. However, NUC-P84 revealed a significant effect of transfection, F (2, 8) = 9.71, *p*=0.007, η_p^2=0.71. Post-hoc analyses with Tukey's test indicated that USP8 levels are downregulated upon MID1 overexpression in comparison with EV (t (8) =3.62; *p*=0.020). Also, Tukey's test showed that USP8 levels are decreased upon MID1 transfection compared to ΔRING MID1 transfection (t (8) =3.90; *p*=0.014). Accordingly, with this posthoc analysis, MID1 E3 activity is highly critical for the downregulation of USP8 resulting from MID1 overexpression mainly in the nucleus.

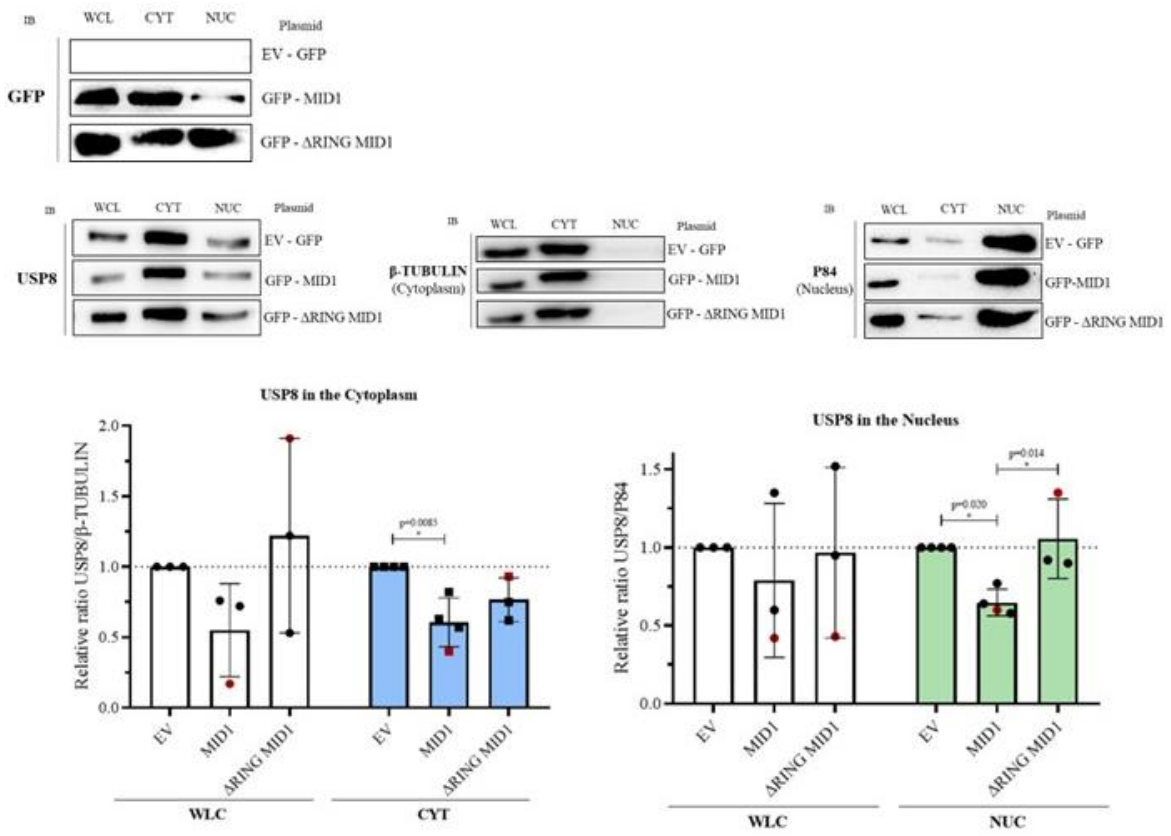

Figure 35. USP8 distribution in subcellular compartments upon MID1 overexpression. HeLa cells were transfected with 2.5µg of GFP-MID1 or GFP-ΔRING MID1 for 24 hours, the control condition was transfected with Empty Vector - GFP (EV). Cells were fractionated in subcellular compartments: whole cell lysates (WCL), cytoplasm (CYT), and nuclei (NUC). For loading control, β-TUBULIN was used for the CYT fraction and P84 for the NUC fraction. Quantification of at least three assays to each condition (n=3) using densitometry analysis with the Image Lab software. Expression is shown as the ratio between USP8 and β-TUBULIN for the WLC and CYT fractions and P84 for the WLC and NUC fractions, each one normalized to the respective EV. The graph is presented as mean ± standard deviation and the USP8 level of the representative WB is highlighted in red. For statistical analysis, a One-way ANOVA and Tukey's tests were applied for multiple comparisons among EV-GFP, MID1, and ΔRING MID1 at each condition (WLC-USP8/β-TUBULIN; CYT-USP8/β-TUBULIN; WLC-USP8/P84; NUC-USP8/P84). WLC-USP8/β-TUBULIN (MID1: *M*=0.55; SD=0.33; ΔRING-MID1: *M*=1.22; SD=0.69), CYT-USP8/β-TUBULIN (MID1: *M*=0.61; SD=0.17; ΔRING-MID1: *M*=0.77; SD=0.16), WLC-USP8/P84 (MID1: *M*=0.79; SD=0.49; ΔRING-MID1: *M*=0.97; SD=0.54), and NUC-USP8/P84 (MID1*: M*=0.64; SD=0.085; ΔRING-MID1: *M*=1.06; SD=0.25). *p≤0.05. Antibodies: β-TUBULIN (55 kDa) from Sigma (1:2500); GFP (100 kDa) from LifeTech (1:2500); USP8 (200kDa) from Proteintech (1:2000); P84 (80kDa) from Abcam (1:5000).

Thus, we observed that overexpression of MID1 leads to a reduction in cytoplasmic and nuclear USP8 levels. In addition, the downregulation of USP8 in both compartments depends on the E3 ligase activity of MID1 because the USP8 decrease is not observed when the ΔRING form of MID1 is used.

4.7.2 Cellular Localization of USP8 effect on PP2AC

Given the results above, the study of the cellular compartment where the PP2AC levels are changed by the MID1/USP8 pair is described in this chapter. Hence, HeLa cells were transfected with 2.5µg of GFP-MID1 or FLAG-USP8 in a 6-well-plate for 48 hours, where the control condition was transfected with Empty Vector (EV). Cells were fractionated as above in the following subcellular compartments: WCL, CYT, and NUC. Afterward, WB was performed to analyze the abundance of PP2AC, quantifying at least three (n=3) experiments. Proteins levels were normalized with the respective loading control: β-TUBULIN for the WLC and CYT fractions, and P84 for the WLC and NUC fractions. Each transfection condition was normalized to the EV, in which 1 is the reference value.

Figure 36 presents the results of the WB and the graph for the quantification of the PP2AC level. We considered four independent data sets: WLC-PP2AC/β-TUBULIN (MID1: *M*=0.79; SD=0.44; USP8: *M*=2.58; SD=2.15), CYT- PP2AC/β-TUBULIN (MID1: *M*=1.24; SD=0.53; USP8: *M*=2.20; SD=2.58), WLC- PP2AC/P84 (MID1: *M*=0.63; SD=0.59; USP8: *M*=3.54; SD=1.49), and NUC- PP2AC/P84 (MID1: *M*=0.53; SD=0.27; USP8: *M*=1.99; SD=1.36). In each set, one variable was evaluated: the transfection effect (EV, MID1, and USP8) on the PP2AC levels. All conditions passed the Shapiro-Wilk test for normality, so a One-way ANOVA test was applied. For WLC-β-TUBULIN, $F(2, 12) = 2.97$, $p=0.33$, $\eta_p^2=0.37$, the main effect of transfection on PP2AC levels was not statistically robust, but a strong tendency was observed (large effect size when $\eta_p^2>.14$). For CYT-β-TUBULIN, $F(2, 12) =.87$, $p=.44$, $\eta_p^2=.13$, a significant effect of transfection on PP2AC levels was not shown, but only a medium tendency (medium effect size when $0.06<\eta_p^2<0.14$). For WLC-P84 a significant effect of the transfection was observed, $F(2, 6) =8.75$, $p=.017$, $\eta_p^2=0.74$. Post-hoc analyses with Tukey's test indicated that PP2AC levels are significantly increased by USP8 expression compared to EV ($t(6) =3.36$; $p=0.046$) and MID1 ($t(6) =3.84$; $p=0.026$). However, for NUC-P84, $F(2, 6) = 2.61$, $p=0.15$, $\eta_p^2=0.47$, a significant effect of transfection on PP2AC levels was not shown, but a strong tendency was observed (large effect size when $\eta_p^2>0.14$).

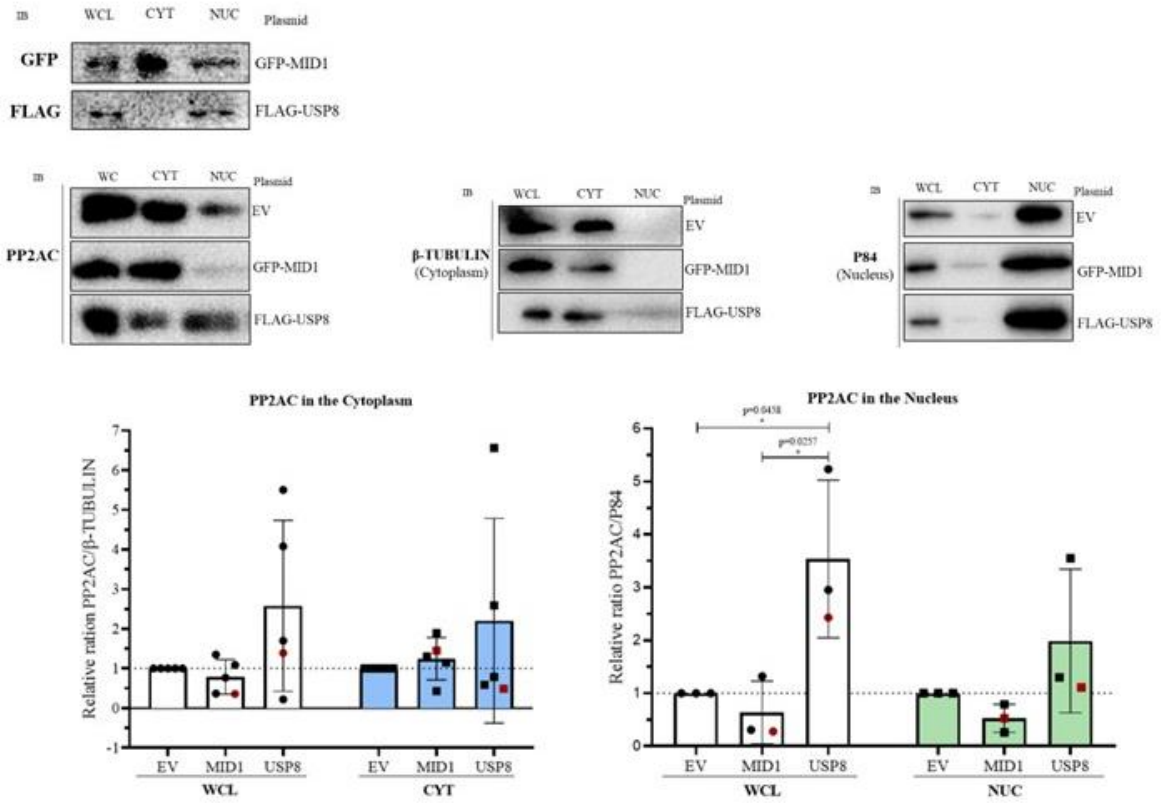

Figure 36. PP2AC distribution in subcellular compartments. HeLa cells were transfected with GFP-MID1 or FLAG-USP8 for 48 hours, the control condition was transfected with an Empty Vector (EV). Cells were fractionated in subcellular compartments: whole cell lysates (WCL), cytoplasm (CYT), and nuclei (NUC). For loading control, β-TUBULIN was used for the CYT fraction and P84 for the NUC fraction. Quantification of at least three assays to each condition (n=3) using densitometry analysis with the Image Lab software. Expression is shown as the ratio between PP2AC and β-TUBULIN for the WLC and CYT fractions and P84 for the WLC and NUC fractions, each one normalized to the respective EV. The graph is presented as mean ± standard deviation and the PP2AC level of the representative WB is highlighted in red. For statistical analysis, a One-way ANOVA and Tukey's tests were applied for multiple comparisons among EV, MID1, and USP8 at each condition (WLC-PP2AC/β-TUBULIN; CYT-PP2AC/β-TUBULIN; WLC-PP2AC/P84; NUC-PP2AC/P84). WLC-PP2AC/β-TUBULIN (MID1: *M*=0.79; SD=0.44; USP8: *M*=2.58; SD=2.15), CYT- PP2AC/β-TUBULIN (MID1: *M*=1.24; SD=0.53; USP8: *M*=2.20; SD=2.58), WLC- PP2AC/P84 (MID1: *M*=0.63; SD=0.59; USP8: *M*=3.54; SD=1.49), and NUC- PP2AC/P84 (MID1: *M*=0.53; SD=0.27; USP8: *M*=1.99; SD=1.36). *p≤0.05. Antibodies: β-TUBULIN (55 kDa) from Sigma (1:2500); FLAG (200kDa) from Sigma (1:2000); GFP (100 kDa) from LifeTech (1:2500); P84 (80kDa) from Abcam (1:5000); PP2AC (35 kDa) from Cell Signaling (1:1000).

In this experiment (**Figure 36**) the downregulation of PP2AC levels when MID1 is overexpressed is not clear. It has been reported in the literature that MID1 modulates the PP2AC microtubular pool (Trockenbacher et al., 2001). Interestingly, we observed that MID1 overexpression tends to decrease PP2AC levels in the nuclear fraction, the same compartment that previously was shown where MID1 overexpression can significantly decrease USP8 protein (**Figure 35).** It is also possible that MID1 causes a decrease in the nuclear PP2AC protein by

downregulating USP8, which in turn downregulates PP2AC. This hypothesis is corroborated by the fact that USP8 overexpression causes a general tendency to increase PP2AC levels in all compartments, but it is in the nucleus (WLC-P84 in specific) that this effect is more evident (**Figure 36**).

In the literature, it was not proven that MID1 can directly ubiquitinate PP2AC, and indeed some reports demonstrated that MID1 controls PP2AC levels by ubiquitinating α4 (Han et al., 2011; J. Liu et al., 2001; Watkins et al., 2012). This thesis opens a new perspective namely that MID1 has a second pathway to control PP2AC levels through the modulation of the USP8 protein amount. Nonetheless, it seems that the effect of MID1 on USP8 is not through direct ubiquitination, since MID1 is not present in the nuclear compartment. To understand if MID1, USP8, and PP2AC form a complex, we next investigated their putative interaction.

4.8 Investigating the interaction of MID1, USP8, and PP2AC

Our results demonstrated that PP2AC is a mutual substrate of MID1 and USP8, and in parallel that USP8 and MID1 regulate each other. To understand if MID1, USP8, and PP2AC form a complex we investigated their interaction through co-Immunoprecipitation (co-IP) assays.

4.8.1 MID1 is not interacting with USP8 or PP2AC

Firstly, we started to evaluate if PP2AC or USP8 is immunoprecipitated together with MID1. Regarding PP2AC, there is consistent evidence that MID1 is regulating its protein levels, while less consistent is the direct interaction of these two proteins (Han et al., 2011; Trockenbacher et al., 2001; Watkins et al., 2012). To clarify this aspect, HEK293T cells were transfected with GFP-MID1 using the calcium phosphate method for 24 hours. As a control, we used the EV-GFP and GFP-TRIM32 plasmids. TRIM32 was used as a further negative control because it belongs to the same family as MID1. Afterward, cells were lysed in non-denaturing conditions to preserve protein interactions, and the anti-GFP antibody was incubated for three hours at 4°C, followed by incubation with protein G beads for two hours at 4°C. The endogenous PP2AC protein was analyzed through immunoblot.

Figure 37 represents the IP assay results. Both MID1 and TRIM32 were immunoprecipitated, despite TRIM32 not being detected in the input lane. All GFP proteins were efficiently

precipitated (see Unbound lanes). PP2AC, however, was not precipitated together with MID1 (and neither with TRIM32). Previous studies were able to show an interaction of PP2AC with MID1 using the microtubular protein pool (Trockenbacher et al., 2001). This indicates that MID1-PP2AC interaction could be cellularly localized and probably not detectable when using the total extracts. It would be of interest to isolate the microtubular protein fraction to further perform an IP.

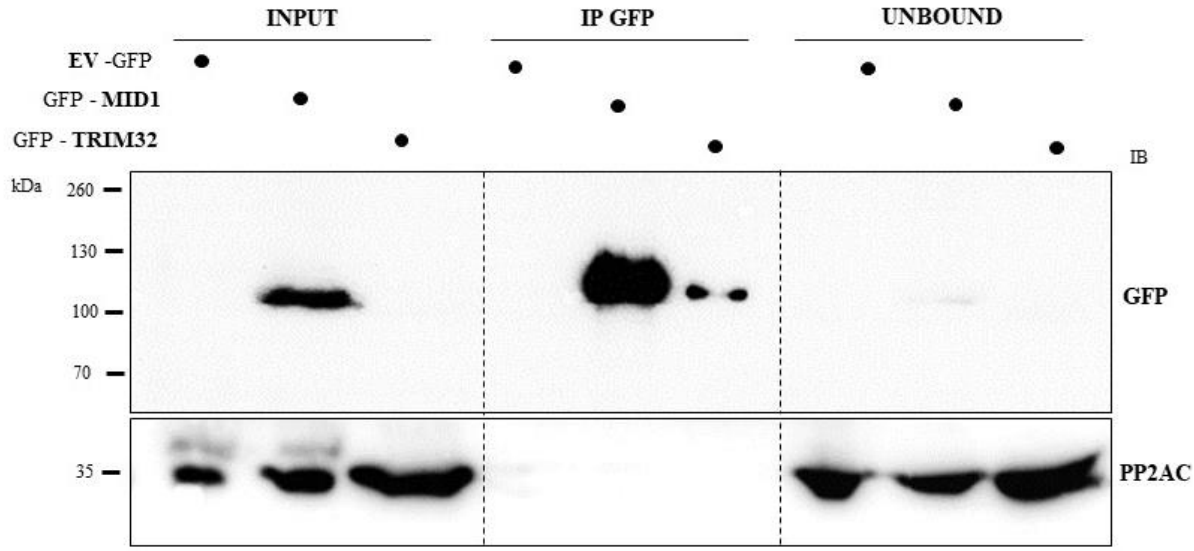

Figure 37. PP2AC is not immunoprecipitated with MID1. HEK293T cells were transfected with GFP-MID1 and GFP-TRIM32 for 24 hours, the control condition was transfected with Empty Vector - GFP (EV-GFP). MID1 and TRIM32 were immunoprecipitated using 1µg of GFP antibody. Total cell lysate (INPUT), immunoprecipitated proteins (IP), unbound proteins (Unbound). In the IP lanes, PP2AC was not co-immunoprecipitated either with MID1 or TRIM32 and consistently the proteins are completely found in the unbound fraction. EV-GFP and GFP-TRIM32 were used as a negative control. Antibodies: GFP from Sigma (1:2500); PP2AC (35 kDa) from Cell Signaling (1:1000).

A similar experiment was performed to test if USP8 and MID1 are interacting. HEK293T cells were transfected with X-tremeGENE HP DNA reagent and GFP-MID1 plasmid for 24 hours. As a control, we used the EV-GFP and GFP-TRIM32 plasmids. Cells were lysed in non-denaturing conditions and the anti-GFP antibody was incubated overnight at 4°C with extracts, followed by incubation with protein G beads for two hours at 4°C. The endogenous USP8 protein was analyzed through immunoblot analysis.

Figure 38 represents the IP assay. In the IP lanes, we can observe that both MID1 and TRIM32 proteins were immunoprecipitated. Next, the USP8 protein was not precipitated together with MID1 (nor TRIM32). The reason for the lack of co-precipitation of USP8 together with MID1 could be due to the same issue as for PP2AC protein, being confined to the microtubular protein fraction, not visible when using the total protein amount. This hypothesis is supported by the IF results, which showed a limited co-localization of USP8 with MID1.

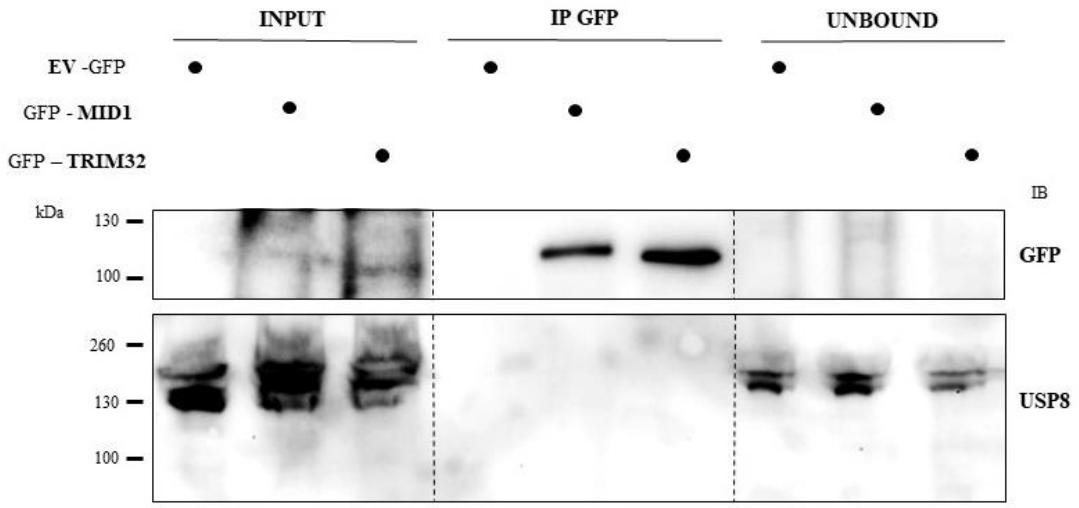

Figure 38. USP8 is not immunoprecipitated with MID1. HEK293T cells were transfected with GFP-MID1 and GFP-TRIM32 for 24 hours, the control condition was transfected with Empty Vector - GFP (EV-GFP). MID1 and TRIM32 were immunoprecipitated using 1µg of GFP antibody. Total cell lysate (INPUT), immunoprecipitated proteins (IP), unbound proteins (Unbound). In the IP lanes, USP8 was not co-immunoprecipitated either with MID1 or TRIM32 and consistently the proteins are completely found in the unbound fraction. EV-GFP and GFP-TRIM32 were used as a negative control. Antibodies: GFP from Sigma (1:2500); USP8 (200kDa) from Proteintech (1:2000).

4.8.2 The nuclear protein fraction of PP2AC and USP8 co-precipitate

We also wanted to test the possible interaction between PP2AC and USP8. Since PP2AC and USP8 proteins are widely distributed in the cell, the IP was performed in the extracts of the different cellular compartments. Hence HEK293T cells were fractionated in the following compartments: whole cell lysates (WCL), cytoplasm (CYT), and nuclei (NUC). We used the anti-USP8 antibody or the rabbit IgG antibody as a control in the co-immunoprecipitation assay. The antibody was incubated overnight at 4°C, followed by incubation with protein A

agarose beads for three hours at 4°C. Both endogenous USP8 and PP2AC proteins were analyzed through immunoblot.

Figure 39 represents the IP assay. In the Input lanes, we can appreciate the endogenous levels of USP8 and PP2AC on WLC, CYT, and NUC extracts. USP8 protein was efficiently precipitated on CYT and NUC extracts, specifically when the relative antibody was used and not with the control IgG. The PP2AC protein was precipitated together with USP8 on the nuclear extract. It was not possible to check for MID1 presence since there are no specific antibodies for this protein. Berruti et al showed in spermatogenic cell lines that Usp8 precipitates with Tubulin (Berruti et al., 2010). In our experiments we tried to use TUBULIN as a positive control; however, TUBULIN is not precipitating with USP8 in HEK293T cells (data not shown).

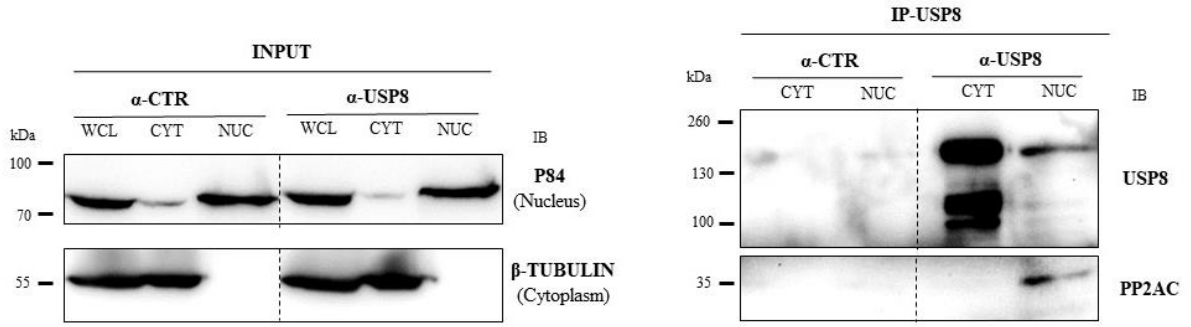

Figure 39. PP2AC is immunoprecipitated with the nuclear protein of USP8. HEK293T cells were fractionated in subcellular compartments: whole cell lysates (WCL), cytoplasm (CYT), and nuclei (NUC). Total cell lysate (INPUT), immunoprecipitated proteins (IP). In the INPUT, as a control, we used β-TUBULIN for the CYT fraction and P84 for the NUC fraction. The control condition (CTR) was performed with normal rabbit IgG antibody and USP8 protein was immunoprecipitated using 1µg of USP8 antibody. In the IP lanes, the PP2AC band is co-immunoprecipitated with USP8 on the nuclear fraction. Antibodies: β-TUBULIN (55 kDa) from Sigma (1:2500); P84 (80kDa) from Abcam (1:5000); USP8 (200kDa) from Proteintech (1:2000); PP2AC (35 kDa) from Cell Signaling (1:1000).

The IP shows a co-precipitation of USP8 with PP2AC on the nuclear protein extraction, which is in concordance with the previous results that showed a prevalence of the USP8 effect on the nuclear PP2AC protein (**Figure 36**).

5. Conclusions

In this project, we focused on MID1, which when mutated causes the X-linked form of Opitz G/BBB Syndrome (XLOS). MID1 controls the ubiquitin-mediated proteasomal degradation of the catalytic subunit of PP2A (PP2AC), one of the major phosphatases in the cell. Although MID1 mutations lead to an increase in PP2AC levels, the exact mechanism remains unclear. The main objective of this project is to find DUBs that work in conjunction with MID1 rescuing the increase of PP2AC level observed upon its mutations.

We found for the very first time that the deubiquitinating enzyme USP8 can regulate PP2AC levels. When USP8 is overexpressed, it increases PP2AC and consistently decreases it when USP8 is silenced. Moreover, the effect of USP8, likely through PP2AC regulation, has repercussions on the mTOR pathway, specifically on the phosphorylation of 4E-BP1. The first conclusion is that USP8/MID1 is a functional pair that controls the degradative fate of PP2AC, and consequently the phosphorylation levels of 4E-BP1. USP8 might be an important element to understand the complex pathway of mTOR in different cellular contexts.

The second achievement was the discovery of the USP8/MID1 as mutual regulatory pair. In MEFs from *Mid1* KO, the Usp8 protein levels were upregulated. We also found that USP8 levels were decreased in both the cytoplasmic and nuclear fractions when MID1 was overexpressed. We discovered for the very first time that MID1 regulates a DUB protein level, which in turn regulates a common substrate.

Focusing on the proposed MID1/USP8/PP2AC complex, we discovered that PP2AC in the nuclear fraction was decreased when MID1 was overexpressed and increased when USP8 was overexpressed. Overall, MID1 controls the levels of USP8 in the cytoplasm and nucleus, and both MID1/USP8 control the levels of PP2AC, a mutual substrate, in the nuclear fraction. We hypothesize that MID1 is causing the decrease of nuclear PP2AC by downregulating USP8 protein in the nucleus and thus USP8 downregulates PP2AC. This thesis presents an alternative perspective, namely that MID1 controls PP2AC levels through the modulation of USP8 protein.

Although MID1, USP8, and PP2AC establish a functional relationship, they do not necessarily physically interact, since MID1 is on the microtubules and the main effects on USP8 and PP2AC are observed in the nucleus. The modulation of the different protein levels may occur through a direct (de)ubiquitination of the USP8/MID1 pair. Indeed, we did not find a

significant physical interaction of MID1 with USP8. Likely the regulation of MID1 on USP8 levels does not involve direct ubiquitination of USP8, but rather an intermediary enzyme between USP8 and MID1, which for example can affect the transport and/or degradation of USP8. Even the interaction of USP8 with PP2AC was restricted to the nuclear fraction, which is the compartment with the main effects of USP8 activity on PP2AC levels.

To conclude, we discovered a new DUB/TRIM pair that works in a coordinated manner. MID1 controls the levels of USP8 in the cytoplasm and nuclear, and both MID1/USP8 control the levels of PP2AC, a mutual substrate, in the nucleus fraction. Considering that MID1/USP8 pair is controlling PP2AC mainly in the nucleus, this pair is also probably affecting prevalently the phosphorylation of the nuclear 4E-BP1 (**Figure 40**). Indeed, 30% of the 4E-BP1 expressed in cells is located in the nucleus, where it regulates the availability of EIF4E for the cytoplasmic translational machinery, by retaining EIF4E in the nucleus (Qin et al., 2016).

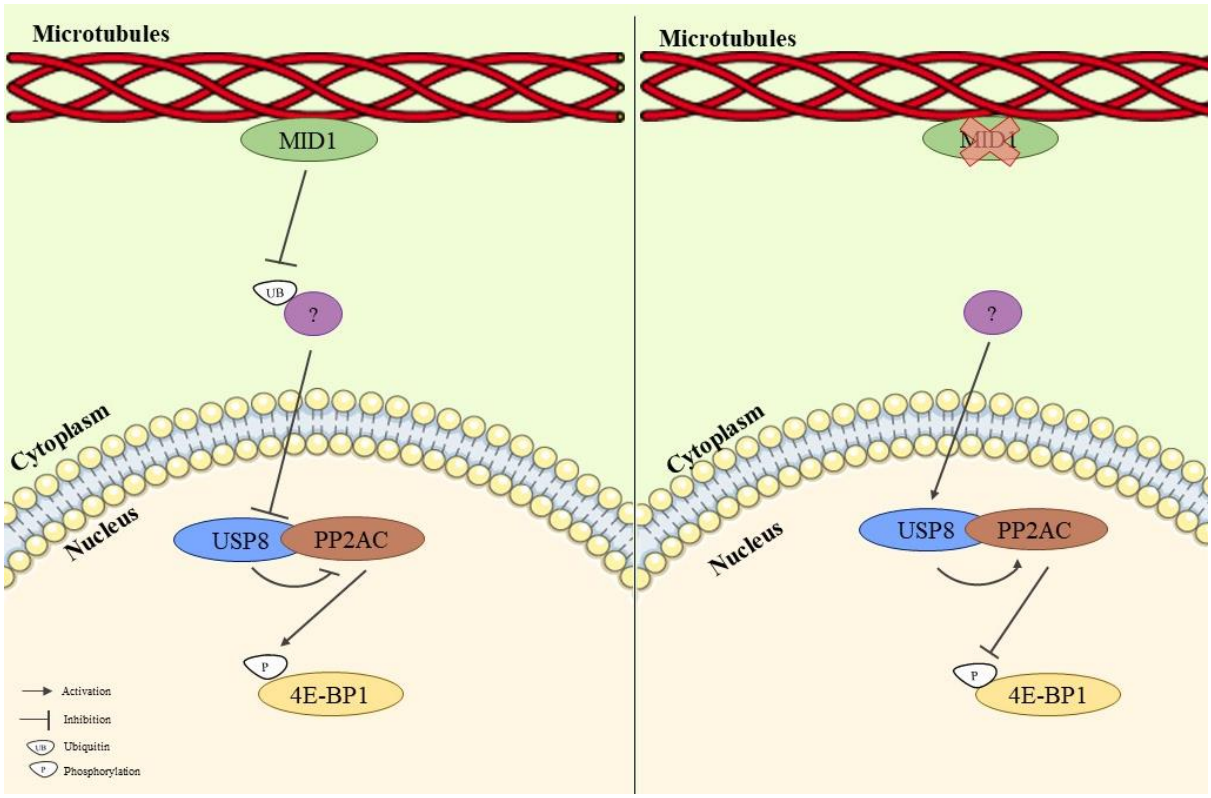

Figure 40. **Model of MID1, USP8, and PP2AC as a complex**. MID1 can interfere with the proteasomal degradation of USP8 through an indirect pathway (the intermediary is still unknown), in the cytoplasm and nucleus. For instance, USP8 can regulate PP2AC in the nucleus, which has repercussions on the mTOR pathway. The hypothesis is that the lack of MID1 would lead to the increase of USP8 in the nucleus, which in turn upregulates PP2AC and consequently represses the phosphorylation of 4E-BP1, which leads to the downregulation of several mRNAs. Abbreviations: MID1: Midline1; Ub: Ubiquitin; PP2AC: catalytic subunit of the protein phosphatase 2A.

Figure 40 shows a proposed model of the MID1/USP8/PP2AC complex dynamics. Overall, the lack of MID1 would lead to an increase of USP8 in the nucleus, which in turn increases PP2AC and consequently represses the phosphorylation of 4E-BP1, leading to the downregulation of several mRNAs. In this hypothesis, the well-studied effects of MID1 on the PP2AC and mTOR pathway are achieved thanks to a new intermediary, the USP8.

It is important to bear in mind that this pathway was mainly observed in HeLa cells, an adult and tumorigenic cell type. However, the main role of MID1 is in embryonic development where specific pathways are activated. So, it would be interesting to explore this MID1/USP8/PP2AC complex in embryonic cells and disease models (MEFs with *Mid1* KO), especially as USP8 is a potential druggable target.

6. Acknowledgements

This work has received funding from the European Union's Horizon 2020 research and Innovation Program under the Marie Sklodowska-Curie grant agreement 813599. Thanks to all the TRIM-NET consortium members for the fruitful meetings.

Thanks to all the members of Germana Meroni Lab for the support in the laboratory and the constructive discussions.

Thanks to all the members of Pascual Sanz Lab to collaborate with our group and receive me for the secondment in CSIC, Institute of Biomedicine, Valencia, Spain.

Thanks to Michael Clague, Claudio Brancolini, Giovanna Mantovani, and Pascual Sanz for kindly providing the DUB plasmids.

7. References

Abraham, D., Podar, K., Pacher, M., Kubicek, M., Welzel, N., Hemmings, B. A., Dilworth, S. M., Mischak, H., Kolch, W., & Baccarini, M. (2000). Raf-1-associated protein phosphatase 2A as a positive regulator of kinase activation. *Journal of Biological Chemistry*, *275*(29). https://doi.org/10.1074/jbc.M003259200

Akhavantabasi, S., Akman, H. B., Sapmaz, A., Keller, J., Petty, E. M., & Erson, A. E. (2010). USP32 is an active, membrane-bound ubiquitin protease overexpressed in breast cancers. *Mammalian Genome*, *21*(7–8). https://doi.org/10.1007/s00335-010-9268-4

Alexander, M., Selman, G., Seetharaman, A., Chan, K. K. M., D'Souza, S. A., Byrne, A. B., Roy, P. J., Ming Chan, K. K., D'Souza, S. A., Byrne, A. B., & Roy, P. J. (2010). MADD-2, a homolog of the Opitz syndrome protein MID1, regulates guidance to the midline through UNC-40 in Caenorhabditis elegans. *Developmental Cell*, *18*(6), 961–972. https://doi.org/10.1016/j.devcel.2010.05.016

Amerik, A. Y., & Hochstrasser, M. (2004). Mechanism and function of deubiquitinating enzymes. In *Biochimica et Biophysica Acta - Molecular Cell Research* (Vol. 1695, Issues 1–3). https://doi.org/10.1016/j.bbamcr.2004.10.003

Amerik, A. Y., Li, S. J., & Hochstrasser, M. (2000). Analysis of the deubiquitinating enzymes of the yeast Saccharomyces cerevisiae. *Biological Chemistry*, *381*(9–10). https://doi.org/10.1515/BC.2000.121

Andjelković, N., Zolnierowicz, S., Hoof, C. Van, Goris, J., & A.hammings, B. (1996). The catalytic subunit of protein phosphatase 2A associates with the translation termination factor eRF1. *EMBO Journal*, *15*(24). https://doi.org/10.1002/j.1460-2075.1996.tb01107.x

Aranda-Orgillés, B., Aigner, J., Kunath, M., Lurz, R., Schneider, R., & Schweiger, S. (2008). Active Transport of the Ubiquitin Ligase MID1 along the Microtubules Is Regulated by Protein Phosphatase 2A. *PLoS ONE*, *3*(10), e3507. https://doi.org/10.1371/journal.pone.0003507

Aranda-Orgillés, B., Trockenbacher, A., Winter, J., Aigner, J., Köhler, A., Jastrzebska, E., Stahl, J., Müller, E.-C. C., Otto, A., Wanker, E. E., Schneider, R., & Schweiger, S. (2008). The Opitz syndrome gene product MID1 assembles a microtubule-associated ribonucleoprotein complex. *Human Genetics*, *123*(2), 163–176.

https://doi.org/10.1007/s00439-007-0456-6

Avvakumov, G. V, Walker, J. R., Xue, S., Finerty, P. J., Mackenzie, F., Newman, E. M., & Dhe-Paganon, S. (2006). Amino-terminal dimerization, NRDP1-rhodanese interaction, and inhibited catalytic domain conformation of the ubiquitin-specific protease 8 (USP8). *Journal of Biological Chemistry*, *281*(49). https://doi.org/10.1074/jbc.M606704200

Baldini, R. (2018). *Understanding The Molecular Mechanisms Underlying The Pathogenesis Of Opitz G / Bbb Syndrome Exploiting The Mid1 Knock-Out Mouse* [University of Trieste]. https://arts.units.it/handle/11368/2952507

Baldini, R., Mascaro, M., & Meroni, G. (2020). The MID1 gene product in physiology and disease. *Gene*, *747*(February). https://doi.org/10.1016/j.gene.2020.144655

Berndsen, C. E., & Wolberger, C. (2014). New insights into ubiquitin E3 ligase mechanism. *Nature Structural & Molecular Biology*, *21*(4), 301–307. https://doi.org/10.1038/nsmb.2780

Berruti, G., Ripolone, M., & Ceriani, M. (2010). USP8, a regulator of endosomal sorting, is involved in mouse acrosome biogenesis through interaction with the spermatid ESCRT-0 complex and microtubules. *Biology of Reproduction*, *82*(5). https://doi.org/10.1095/biolreprod.109.081679

Bingol, B., Tea, J. S., Phu, L., Reichelt, M., Bakalarski, C. E., Song, Q., Foreman, O., Kirkpatrick, D. S., & Sheng, M. (2014). The mitochondrial deubiquitinase USP30 opposes parkin-mediated mitophagy. *Nature*, *510*(7505). https://doi.org/10.1038/nature13418

Blount, J. R., Burr, A. A., Denuc, A., Marfany, G., & Todi, S. V. (2012). Ubiquitin-specific Protease 25 functions in Endoplasmic Reticulum-associated degradation. *PLoS ONE*, *7*(5). https://doi.org/10.1371/journal.pone.0036542

Bosanac, I., Phu, L., Pan, B., Zilberleyb, I., Maurer, B., Dixit, V. M., Hymowitz, S. G., & Kirkpatrick, D. S. (2011). Modulation of K11-linkage formation by variable loop residues within UbcH5A. *Journal of Molecular Biology*, *408*(3). https://doi.org/10.1016/j.jmb.2011.03.011

Boudreau, R. T. M., Garduno, R., & Lin, T. J. (2002). Protein phosphatase 2A and protein kinase Cα are physically associated and are involved in Pseudomonas aeruginosa-induced interleukin 6 production by mast cells. *Journal of Biological Chemistry*, *277*(7).

https://doi.org/10.1074/jbc.M108623200

Budhidarmo, R., Nakatani, Y., & Day, C. L. (2012). RINGs hold the key to ubiquitin transfer. In *Trends in Biochemical Sciences* (Vol. 37, Issue 2). https://doi.org/10.1016/j.tibs.2011.11.001

Burroughs, A. M., Jaffee, M., Iyer, L. M., & Aravind, L. (2008). Anatomy of the E2 ligase fold: Implications for enzymology and evolution of ubiquitin/Ub-like protein conjugation. *Journal of Structural Biology*, *162*(2). https://doi.org/10.1016/j.jsb.2007.12.006

Cai, C., Tang, Y.-D., Zhai, J., & Zheng, C. (2022). The RING finger protein family in health and disease. *Signal Transduction and Targeted Therapy*, *7*(1), 300. https://doi.org/10.1038/s41392-022-01152-2

Cai, J., Chen, H., Peng, S., Meng, J., Wang, Y., Zhou, Y., & Qian, X. (2018). USP7 – TRIM27 axis negatively modulates antiviral type I IFN signaling. *The FASEB Journal*, *32*(10), 5238–5249. https://doi.org/10.1096/fj.201700473RR

Cainarca, S., Messali, S., Ballabio, A., & Meroni, G. (1999). Functional characterization of the Opitz syndrome gene product (midin): Evidence for homodimerization and association with microtubules throughout the cell cycle. *Human Molecular Genetics*, *8*(8). https://doi.org/10.1093/hmg/8.8.1387

Carracedo, A., Baselga, J., & Pandolfi, P. P. (2008). Deconstructing feedback-signaling networks to improve anticancer therapy with mTORC1 inhibitors. In *Cell Cycle* (Vol. 7, Issue 24). https://doi.org/10.4161/cc.7.24.7244

Chan, S. F., & Sucher, N. J. (2001). An NMDA receptor signaling complex with protein phosphatase 2A. *Journal of Neuroscience*, *21*(20). https://doi.org/10.1523/jneurosci.21-20-07985.2001

Chen, J., Martin, B. L., & Brautigan, D. L. (1992). Regulation of protein serine-threonine phosphatase type-2A by tyrosine phosphorylation. *Science*, *257*(5074). https://doi.org/10.1126/science.1325671

Chen, J., Peterson, R. T., & Schreiber, S. L. (1998). α4 Associates with protein phosphatases 2A, 4, and 6. *Biochemical and Biophysical Research Communications*, *247*(3). https://doi.org/10.1006/bbrc.1998.8792

Chen, L., Zhu, G., Johns, E. M., & Yang, X. (2018). TRIM11 activates the proteasome and promotes overall protein degradation by regulating USP14. *Nature Communications*, *9*(1), 1–14. https://doi.org/10.1038/s41467-018-03499-z

Christianson, J. C., & Ye, Y. (2014). Cleaning up in the endoplasmic reticulum: Ubiquitin in charge. In *Nature Structural and Molecular Biology* (Vol. 21, Issue 4). https://doi.org/10.1038/nsmb.2793

Ciechanover, A., Heller, H., Elias, S., Haas, A. L., & Hershko, A. (1980). ATP-dependent conjugation of reticulocyte proteins with the polypeptide required for protein degradation. *Proceedings of the National Academy of Sciences of the United States of America*, *77*(3). https://doi.org/10.1073/pnas.77.3.1365

Clague, M. J., Barsukov, I., Coulson, J. M., Liu, H., Rigden, D. J., & Urbé, S. (2013). Deubiquitylases from genes to organism. *Physiological Reviews*, *93*(3). https://doi.org/10.1152/physrev.00002.2013

Clague, M. J., Heride, C., & Urbé, S. (2015). The demographics of the ubiquitin system. In *Trends in Cell Biology* (Vol. 25, Issue 7). https://doi.org/10.1016/j.tcb.2015.03.002

Clague, M. J., & Urbé, S. (2010). Ubiquitin: Same molecule, different degradation pathways. In *Cell* (Vol. 143, Issue 5). https://doi.org/10.1016/j.cell.2010.11.012

Clague, M. J., Urbé, S., & Komander, D. (2019). Breaking the chains: deubiquitylating enzyme specificity begets function 1 2. *Nature Reviews Molecular Cell Biology*, *20*, 338–352. https://doi.org/10.1038/s41580-019-0099-1

Collison, A. M., Hatchwell, L., Verrills, N., Wark, P. A. B., De Siqueira, A. P., Tooze, M., Carpenter, H., Don, A. S., Morris, J. C., Zimmermann, N., Bartlett, N. W., Rothenberg, M. E., Johnston, S. L., Foster, P. S., & Mattes, J. (2013). The E3 ubiquitin ligase midline 1 promotes allergen and rhinovirus-induced asthma by inhibiting protein phosphatase 2A activity. *Nature Medicine*, *19*(2). https://doi.org/10.1038/nm.3049

Collison, A. M., Li, J., Siqueira, A. P. De, Lv, X., Toop, H. D., Morris, J. C., Starkey, M. R., Hansbro, P. M., Zhang, J., & Mattes, J. (2019). TRAIL signals through the ubiquitin ligase MID1 to promote pulmonary fibrosis. *BMC Pulmonary Medicine*, *19*(1). https://doi.org/10.1186/s12890-019-0786-x

Collison, A. M., Sokulsky, L. A., Sherrill, J. D., Nightingale, S., Hatchwell, L., Talley, N. J.,

Walker, M. M., Rothenberg, M. E., & Mattes, J. (2015). TNF-related apoptosis-inducing ligand (TRAIL) regulates midline-1, thymic stromal lymphopoietin, inflammation, and remodeling in experimental eosinophilic esophagitis. *Journal of Allergy and Clinical Immunology*, *136*(4). https://doi.org/10.1016/j.jaci.2015.03.031

Cooper, E. M., Cutcliffe, C., Kristiansen, T. Z., Pandey, A., Pickart, C. M., & Cohen, R. E. (2009). K63-specific deubiquitination by two JAMM/MPN+ complexes: BRISC-associated Brcc36 and proteasomal Poh1. *EMBO Journal*, *28*(6). https://doi.org/10.1038/emboj.2009.27

Cornelissen, T., Haddad, D., Wauters, F., Humbeeck, C. Van, Mandemakers, W., Koentjoro, B., Sue, C., Gevaert, K., Strooper, B. De, Verstreken, P., & Vandenberghe, W. (2014). The deubiquitinase USP15 antagonizes Parkin-mediated mitochondrial ubiquitination and mitophagy. *Human Molecular Genetics*, *23*(19). https://doi.org/10.1093/hmg/ddu244

Cox, T. C., Allen, L. R., Cox, L. L., Hopwood, B., Goodwin, B., Haan, E., & Suthers, G. K. (2000). New mutations in MID1 provide support for loss of function as the cause of X-linked Opitz syndrome. *Human Molecular Genetics*, *9*(17). https://doi.org/10.1093/hmg/9.17.2553

Crawford, L. J., Johnston, C. K., & Irvine, A. E. (2018). TRIM proteins in blood cancers. In *Journal of Cell Communication and Signaling* (Vol. 12, Issue 1). https://doi.org/10.1007/s12079-017-0423-5

Cuervo, A. M., Palmer, A., Rivett, A. J., & Knecht, E. (1995). Degradation of Proteasomes by Lysosomes in Rat Liver. *European Journal of Biochemistry*, *227*(3). https://doi.org/10.1111/j.1432-1033.1995.0792p.x

Curcio-Morelli, C., Zavacki, A. M., Christofollete, M., Gereben, B., Freitas, B. C. G. De, Harney, J. W., Li, Z., Wu, G., & Bianco, A. C. (2003). Deubiquitination of type 2 iodothyronine deiodinase by von Hippel-Lindau protein-interacting deubiquitinating enzymes regulates thyroid hormone activation. *Journal of Clinical Investigation*, *112*(2). https://doi.org/10.1172/JCI18348

Dal Zotto, L., Quaderi, N. A., Elliott, R., Lingerfelter, P. A., Carrel, L., Valsecchi, V., Montini, E., Yen, C. H., Chapman, V., Kalcheva, I., Arrigo, G., Zuffardi, O., Thomas, S., Willard, H. F., Ballabio, A., Disteche, C. M., & Rugarli, E. I. (1998). The mouse Mid1 gene: Implications for the pathogenesis of Opitz syndrome and the evolution of the mammalian

pseudoautosomal region. *Human Molecular Genetics*, *7*(3). https://doi.org/10.1093/hmg/7.3.489

Damgaard, R. B., Walker, J. A., Marco-Casanova, P., Morgan, N. V, Titheradge, H. L., Elliott, P. R., McHale, D., Maher, E. R., McKenzie, A. N. J., & Komander, D. (2016). The Deubiquitinase OTULIN Is an Essential Negative Regulator of Inflammation and Autoimmunity. *Cell*, *166*(5). https://doi.org/10.1016/j.cell.2016.07.019

Das, A., Qian, J., & Tsang, W. Y. (2017). USP9X counteracts differential ubiquitination of NPHP5 by MARCH7 and BBS11 to regulate ciliogenesis. *PLoS Genetics*, *13*(5), 1–24. https://doi.org/10.1371/journal.pgen.1006791

de Poot, S. A. H., Tian, G., & Finley, D. (2017). Meddling with Fate: The Proteasomal Deubiquitinating Enzymes. In *Journal of Molecular Biology* (Vol. 429, Issue 22). https://doi.org/10.1016/j.jmb.2017.09.015

Demir, U., Koehler, A., Schneider, R., Schweiger, S., & Klocker, H. (2014). Metformin anti-tumor effect via disruption of the MID1 translational regulator complex and AR downregulation in prostate cancer cells. *BMC Cancer*, *14*(1). https://doi.org/10.1186/1471-2407-14-52

Deshaies, R. J., & Joazeiro, C. A. P. (2009). RING Domain E3 Ubiquitin Ligases. *Annual Review of Biochemistry*, *78*(1), 399–434. https://doi.org/10.1146/annurev.biochem.78.101807.093809

Dierssen, M., Fedrizzi, L., Gomez-Villafuertes, R., de Lagran, M. M., Gutierrez-Adan, A., Sahún, I., Pintado, B., Oliveros, J. C., Dopazo, X. M., Gonzalez, P., Brini, M., Mellström, B., Carafoli, E., & Naranjo, J. R. (2012). Reduced Mid1 expression and delayed neuromotor development in daDREAM transgenic mice. *Frontiers in Molecular Neuroscience, MAY 2012*. https://doi.org/10.3389/fnmol.2012.00058

Dikic, I., Wakatsuki, S., & Walters, K. J. (2009). Ubiquitin-binding domains from structures to functions. In *Nature Reviews Molecular Cell Biology* (Vol. 10, Issue 10). https://doi.org/10.1038/nrm2767

Dirac, A. M. G., & Bernards, R. (2010). The deubiquitinating enzyme USP26 is a regulator of androgen receptor signaling. *Molecular Cancer Research*, *8*(6). https://doi.org/10.1158/1541-7786.MCR-09-0424

Dou, H., Buetow, L., Sibbet, G. J., Cameron, K., & Huang, D. T. (2012). BIRC7-E2 ubiquitin conjugate structure reveals the mechanism of ubiquitin transfer by a RING dimer. *Nature Structural and Molecular Biology*, *19*(9). https://doi.org/10.1038/nsmb.2379

Du, H., Huang, Y., Zaghlula, M., Walters, E., Cox, T. C., & Massiah, M. A. (2013). The MID1 E3 ligase catalyzes the polyubiquitination of alpha4 (α4), a regulatory subunit of protein phosphatase 2A (PP2A): Novel insights into MID1-mediated regulation of PP2A. *Journal of Biological Chemistry*, *288*(29). https://doi.org/10.1074/jbc.M113.481093

Dufner, A., & Knobeloch, K. P. (2019). Ubiquitin-specific protease 8 (USP8/UBPy): A prototypic multidomain deubiquitinating enzyme with pleiotropic functions. In *Biochemical Society Transactions* (Vol. 47, Issue 6). https://doi.org/10.1042/BST20190527

Dupont, S., Mamidi, A., Cordenonsi, M., Montagner, M., Zacchigna, L., Adorno, M., Martello, G., Stinchfield, M. J., Soligo, S., Morsut, L., Inui, M., Moro, S., Modena, N., Argenton, F., Newfeld, S. J., & Piccolo, S. (2009). FAM / USP9x , a Deubiquitinating Enzyme Essential for TGF b Signaling , Controls Smad4 Monoubiquitination. *Cell*, *136*(1), 123–135. https://doi.org/10.1016/j.cell.2008.10.051

Durcan, T. M., & Fon, E. A. (2015). The three 'P's of mitophagy: PARKIN, PINK1, and post-translational modifications. In *Genes and Development* (Vol. 29, Issue 10). https://doi.org/10.1101/gad.262758.115

Durcan, T. M., Tang, M. Y., Pérusse, J. R., Dashti, E. A., Aguileta, M. A., McLelland, G., Gros, P., Shaler, T. A., Faubert, D., Coulombe, B., & Fon, E. A. (2014). USP 8 regulates mitophagy by removing K 6-linked ubiquitin conjugates from parkin. *The EMBO Journal*, *33*(21). https://doi.org/10.15252/embj.201489729

Eichhorn, P. J. A., Creyghton, M. P., & Bernards, R. (2009). Protein phosphatase 2A regulatory subunits and cancer. In *Biochimica et Biophysica Acta - Reviews on Cancer* (Vol. 1795, Issue 1). https://doi.org/10.1016/j.bbcan.2008.05.005

Eletr, Z. M., Huang, D. T., Duda, D. M., Schulman, B. A., & Kuhlman, B. (2005). E2 conjugating enzymes must disengage from their E1 enzymes before E3-dependent ubiquitin and ubiquitin-like transfer. *Nature Structural and Molecular Biology*, *12*(10). https://doi.org/10.1038/nsmb984

Eletr, Z. M., & Wilkinson, K. D. (2013). Regulation of proteolysis by human deubiquitinating enzymes. *BBA - Molecular Cell Research*, *1843*, 114–118. https://doi.org/10.1016/j.bbamcr.2013.06.027

Faesen, A. C., Luna-Vargas, M. P. A., Geurink, P. P., Clerici, M., Merkx, R., Dijk, W. J. Van, Hameed, D. S., Oualid, F. El, Ovaa, H., & Sixma, T. K. (2011). The differential modulation of USP activity by internal regulatory domains, interactors and eight ubiquitin chain types. *Chemistry and Biology*, *18*(12). https://doi.org/10.1016/j.chembiol.2011.10.017

Fan, Y., Mao, R., Yu, Y., Liu, S., Shi, Z., Cheng, J., Zhang, H., An, L., Zhao, Y., Xu, X., Chen, Z., Kogiso, M., Zhang, D., Zhang, H., Zhang, P., Jung, J. U., Li, X., Xu, G., & Yang, J. (2014). USP21 negatively regulates antiviral response by acting as a RIG-I deubiquitinase. *Journal of Experimental Medicine*, *211*(2), 313–328. https://doi.org/10.1084/jem.20122844

Feng, L., Wang, J., & Chen, J. (2010). The Lys63-specific deubiquitinating enzyme BRCC36 is regulated by two scaffold proteins localizing in different subcellular compartments. *Journal of Biological Chemistry*, *285*(40). https://doi.org/10.1074/jbc.M110.135392

Finley, D. (2009). Recognition and processing of ubiquitin-protein conjugates by the proteasome. In *Annual Review of Biochemistry* (Vol. 78). https://doi.org/10.1146/annurev.biochem.78.081507.101607

Finley, D., Sadis, S., Monia, B. P., Boucher, P., Ecker, D. J., Crooke, S. T., & Chau, V. (1994). Inhibition of proteolysis and cell cycle progression in a multiubiquitination-deficient yeast mutant. *Molecular and Cellular Biology*, *14*(8). https://doi.org/10.1128/mcb.14.8.5501-5509.1994

Fiorentini, F., Esposito, D., & Rittinger, K. (2020). Does it take two to tango? RING domain self-association and activity in TRIM E3 ubiquitin ligases. In *Biochemical Society Transactions* (Vol. 48, Issue 6). https://doi.org/10.1042/BST20200383

Fontanella, B., Russolillo, G., & Meroni, G. (2008). MID1 mutations in patients with X-linked Opitz G/BBB syndrome. *Human Mutation*, *29*(5), 584–594. https://doi.org/10.1002/humu.20706

Ford, C. L., Randal-Whitis, L., & Ellis, S. R. (1999). Yeast proteins related to the p40/laminin

receptor precursor are required for 20S ribosomal RNA processing and the maturation of 40S ribosomal subunits. *Cancer Research*, *59*(3).

Foster, P. S., Maltby, S., Rosenberg, H. F., Tay, H. L., Hogan, S. P., Collison, A. M., Yang, M., Kaiko, G. E., Hansbro, P. M., Kumar, R. K., & Mattes, J. (2017). Modeling TH2 responses and airway inflammation to understand fundamental mechanisms regulating the pathogenesis of asthma. In *Immunological Reviews* (Vol. 278, Issue 1). https://doi.org/10.1111/imr.12549

Freemont, P. S. (1993). The RING Finger: A Novel Protein Sequence Motif Related to the Zinc Finger. *Annals of the New York Academy of Sciences*, *684*(1). https://doi.org/10.1111/j.1749-6632.1993.tb32280.x

Fuhrer, D. K., & Yang, Y. C. (1996). Complex formation of JAK2 with PP2A, P13K, and Yes in response to the hematopoietic cytokine interleukin-11. *Biochemical and Biophysical Research Communications*, *224*(2). https://doi.org/10.1006/bbrc.1996.1023

García-Santisteban, I., Bañuelos, S., & Rodríguez, J. A. (2012). A global survey of CRM1-dependent nuclear export sequences in the human deubiquitinase family. *Biochemical Journal*, *441*(1). https://doi.org/10.1042/BJ20111300

Ge, C., Che, L., Ren, J., Pandita, R. K., Lu, J., Li, K., Pandita, T. K., & Du, C. (2015). BRUCE regulates DNA double-strand break response by promoting USP8 deubiquitination of BRIT1. *Proceedings of the National Academy of Sciences of the United States of America*, *112*(11). https://doi.org/10.1073/pnas.1418335112

Gholkar, A. A., Senese, S., Lo, Y., Vides, E., Contreras, E., Hodara, E., Capri, J., Whitelegge, J. P., & Torres, J. Z. (2016). *The Mid2 X-linked Intellectual Disability Ubiquitin Ligase Associates with Astrin and Regulates Astrin Levels to Promote Cell Division*. *14*(2), 180–188. https://doi.org/10.1016/j.celrep.2015.12.035.The

Gómez-Díaz, C., & Ikeda, F. (2019). Roles of ubiquitin in autophagy and cell death. In *Seminars in Cell and Developmental Biology* (Vol. 93). https://doi.org/10.1016/j.semcdb.2018.09.004

Götz, J., Probst, A., Ehler, E., Hemmings, B., & Kues, W. (1998). Delayed embryonic lethality in mice lacking protein phosphatase 2A catalytic subunit Cα. *Proceedings of the National Academy of Sciences of the United States of America*, *95*(21).

https://doi.org/10.1073/pnas.95.21.12370

Govek, E. E., Newey, S. E., & Aelst, L. Van. (2005). The role of the Rho GTPases in neuronal development. In *Genes and Development* (Vol. 19, Issue 1). https://doi.org/10.1101/gad.1256405

Grabbe, C., & Dikic, I. (2009). Functional roles of ubiquitin-like domain (ULD) and ubiquitin-binding domain (UBD) containing proteins. In *Chemical Reviews* (Vol. 109, Issue 4). https://doi.org/10.1021/cr800413p

Graham, F. L., & van der Eb, A. J. (1973). A new technique for the assay of infectivity of human adenovirus 5 DNA. *Virology*, *52*(2). https://doi.org/10.1016/0042-6822(73)90341-3

Granata, A., & Quaderi, N. A. (2003). The Opitz syndrome gene MID1 is essential for establishing asymmetric gene expression in Hensen's node. *Developmental Biology*, *258*(2). https://doi.org/10.1016/S0012-1606(03)00131-3

Haesen, D., Sents, W., Lemaire, K., Hoorne, Y., & Janssens, V. (2014). The basic biology of PP2A in hematologic cells and malignancies. In *Frontiers in Oncology* (Vol. 4, Issue NOV). https://doi.org/10.3389/fonc.2014.00347

Han, X., Du, H., & Massiah, M. A. (2011). Detection and characterization of the in vitro E3 ligase activity of the human MID1 protein. *Journal of Molecular Biology*, *407*(4). https://doi.org/10.1016/j.jmb.2011.01.048

Hao, Y. H., Fountain, M. D., Fon Tacer, K., Xia, F., Bi, W., Kang, S. H. L., Patel, A., Rosenfeld, J. A., Le Caignec, C., Isidor, B., Krantz, I. D., Noon, S. E., Pfotenhauer, J. P., Morgan, T. M., Moran, R., Pedersen, R. C., Saenz, M. S., Schaaf, C. P., & Potts, P. R. (2015). USP7 Acts as a Molecular Rheostat to Promote WASH-Dependent Endosomal Protein Recycling and Is Mutated in a Human Neurodevelopmental Disorder. *Molecular Cell*, *59*(6), 956–969. https://doi.org/10.1016/j.molcel.2015.07.033

Hasenpusch-Theil, K., Magnani, D., Amaniti, E. M., Han, L., Armstrong, D., & Theil, T. (2012). Transcriptional analysis of Gli3 mutants identifies Wnt target genes in the developing hippocampus. *Cerebral Cortex*, *22*(12). https://doi.org/10.1093/cercor/bhr365

Hassink, G. C., Zhao, B., Sompallae, R., Altun, M., Gastaldello, S., Zinin, N. V, Masucci, M. G., & Lindsten, K. (2009). The ER-resident ubiquitin-specific protease 19 participates in

the UPR and rescues ERAD substrates. *EMBO Reports*, *10*(7). https://doi.org/10.1038/embor.2009.69

Heijman, J., Dewenter, M., El-Armouche, A., & Dobrev, D. (2013). Function and regulation of serine/threonine phosphatases in the healthy and diseased heart. In *Journal of Molecular and Cellular Cardiology* (Vol. 64). https://doi.org/10.1016/j.yjmcc.2013.09.006

Heinz, A., Schilling, J., van Roon-Mom, W., & Krauß, S. (2021). The MID1 Protein: A Promising Therapeutic Target in Huntington's Disease. *Frontiers in Genetics*, *12*(October), 1–7. https://doi.org/10.3389/fgene.2021.761714

Heride, C., Rigden, D. J., Bertsoulaki, E., Cucchi, D., Smaele, E. De, Clague, M. J., & Urbé, S. (2016). The centrosomal deubiquitylase USP21 regulates Gli1 transcriptional activity and stability. *Journal of Cell Science*, *129*(21). https://doi.org/10.1242/jcs.188516

Hettich, M. M., Matthes, F., Ryan, D. P., Griesche, N., Schröder, S., Dorn, S., Krauß, S., & Ehninger, D. (2014). The anti-diabetic drug metformin reduces BACE1 protein level by interfering with the MID1 complex. *PLoS ONE*, *9*(7). https://doi.org/10.1371/journal.pone.0102420

Huang, K., & Fingar, D. C. (2014). Growing knowledge of the mTOR signaling network. In *Seminars in Cell and Developmental Biology* (Vol. 36). https://doi.org/10.1016/j.semcdb.2014.09.011

Huibregtse, J. M., Scheffner, M., Beaudenon, S., & Howley, P. M. (1995). A family of proteins structurally and functionally related to the E6-AP ubiquitin-protein ligase. *Proceedings of the National Academy of Sciences of the United States of America*, *92*(7). https://doi.org/10.1073/pnas.92.7.2563

Ingham, P. W., & McMahon, A. P. (2001). Hedgehog signaling in animal development: Paradigms and principles. In *Genes and Development* (Vol. 15, Issue 23). https://doi.org/10.1101/gad.938601

Iphöfer, A., Kummer, A., Nimtz, M., Ritter, A., Arnold, T., Frank, R., van den Heuvel, J., Kessler, B. M., Jänsch, L., & Franke, R. (2012). Profiling Ubiquitin Linkage Specificities of Deubiquitinating Enzymes with Branched Ubiquitin Isopeptide Probes. *ChemBioChem*, *13*(10). https://doi.org/10.1002/cbic.201200261

Jacomin, A. C., Bescond, A., Soleilhac, E., Gallet, B., Schoehn, G., Fauvarque, M. O., & Taillebourg, E. (2015). The deubiquitinating enzyme UBPY is required for lysosomal biogenesis and productive autophagy in drosophila. *PLoS ONE*, *10*(11). https://doi.org/10.1371/journal.pone.0143078

Janssens, V., & Goris, J. (2001). Protein phosphatase 2A: A highly regulated family of serine/threonine phosphatases implicated in cell growth and signalling. In *Biochemical Journal* (Vol. 353, Issue 3). https://doi.org/10.1042/0264-6021:3530417

Jhanwar-Uniyal, M., Wainwright, J. V, Mohan, A. L., Tobias, M. E., Murali, R., Gandhi, C. D., & Schmidt, M. H. (2019). Diverse signaling mechanisms of mTOR complexes: mTORC1 and mTORC2 in forming a formidable relationship. In *Advances in Biological Regulation* (Vol. 72). https://doi.org/10.1016/j.jbior.2019.03.003

Ji, Y. X., Huang, Z., Yang, X., Wang, X., Zhao, L. P., Wang, P. X., Zhang, X. J., Alves-Bezerra, M., Cai, L., Zhang, P., Lu, Y. X., Bai, L., Gao, M. M., Zhao, H., Tian, S., Wang, Y., Huang, Z. X., Zhu, X. Y., Zhang, Y., … Li, H. (2018). The deubiquitinating enzyme cylindromatosis mitigates nonalcoholic steatohepatitis. *Nature Medicine*, *24*(2), 213–223. https://doi.org/10.1038/nm.4461

Jiang, L., Stanevich, V., Satyshur, K. A., Kong, M., Watkins, G. R., Wadzinski, B. E., Sengupta, R., & Xing, Y. (2013). Structural basis of protein phosphatase 2A stable latency. *Nature Communications*, *4*(1699), 1–11. https://doi.org/10.1038/ncomms2663

Jing, X., Chen, Y., Chen, Y., Shi, G., Lv, S., Cheng, N., Feng, C., Xin, Z., Zhang, L., & Wu, J. (2020). Down-regulation of usp8 inhibits cholangiocarcinoma cell proliferation and invasion. *Cancer Management and Research*, *12*. https://doi.org/10.2147/CMAR.S234586

Joo, H. Y., Zhai, L., Yang, C., Nie, S., Erdjument-Bromage, H., Tempst, P., Chang, C., & Wang, H. (2007). Regulation of cell cycle progression and gene expression by H2A deubiquitination. *Nature*, *449*(7165). https://doi.org/10.1038/nature06256

Junttila, M. R., Puustinen, P., Niemelä, M., Ahola, R., Arnold, H., Böttzauw, T., Ala-aho, R., Nielsen, C., Ivaska, J., Taya, Y., Lu, S. L., Lin, S., Chan, E. K. L., Wang, X. J., Grènman, R., Kast, J., Kallunki, T., Sears, R., Kähäri, V. M., & Westermarck, J. (2007). CIP2A Inhibits PP2A in Human Malignancies. *Cell*, *130*(1). https://doi.org/10.1016/j.cell.2007.04.044

Kakihara, K., Asamizu, K., Moritsugu, K., Kubo, M., Kitaguchi, T., Endo, A., Kidera, A., Ikeguchi, M., Kato, A., Komada, M., & Fukushima, T. (2021). Molecular basis of ubiquitin-specific protease 8 autoinhibition by the WW-like domain. *Communications Biology*, *4*(1). https://doi.org/10.1038/s42003-021-02802-x

Kalluri, R., & LeBleu, V. S. (2020). The biology, function, and biomedical applications of exosomes. In *Science* (Vol. 367, Issue 6478). https://doi.org/10.1126/science.aau6977

Kasahara, K., Aoki, H., Kiyono, T., Wang, S., Kagiwada, H., Yuge, M., Tanaka, T., Nishimura, Y., Mizoguchi, A., Goshima, N., & Inagaki, M. (2018). EGF receptor kinase suppresses ciliogenesis through activation of USP8 deubiquitinase. *Nature Communications*, *9*(1). https://doi.org/10.1038/s41467-018-03117-y

Kato, M., Miyazawa, K., & Kitamura, N. (2000). A deubiquitinating enzyme UBPY interacts with the Src homology 3 domain of Hrs-binding protein via a novel binding motif PX(V/I)(D/N)RXXKP. *Journal of Biological Chemistry*, *275*(48). https://doi.org/10.1074/jbc.M007251200

Kliza, K., & Husnjak, K. (2020). Resolving the Complexity of Ubiquitin Networks. *Frontiers in Molecular Biosciences*, *7*(February), 1–19. https://doi.org/10.3389/fmolb.2020.00021

Kloeker, S., Reed, R., McConnell, J. L., Chang, D., Tran, K., Westphal, R. S., Law, B. K., Colbran, R. J., Kamoun, M., Campbell, K. S., & Wadzinski, B. E. (2003). Parallel purification of three catalytic subunits of the protein serine/threonine phosphatase 2A family (PP2AC, PP4C, and PP6C) and analysis of the interaction of PP2AC with alpha4 protein. *Protein Expression and Purification*, *31*(1). https://doi.org/10.1016/S1046-5928(03)00141-4

Kolupaeva, V. (2019). Serine-threonine protein phosphatases: Lost in translation. In *Biochimica et Biophysica Acta - Molecular Cell Research* (Vol. 1866, Issue 1). https://doi.org/10.1016/j.bbamcr.2018.08.006

Komander, D., & Barford, D. (2008). Structure of the A20 OTU domain and mechanistic insights into deubiquitination. *Biochemical Journal*, *409*(1). https://doi.org/10.1042/BJ20071399

Komander, D., Clague, M. J., & Urbé, S. (2009). Breaking the chains: Structure and function of the deubiquitinases. *Nature Reviews Molecular Cell Biology*, *10*(8), 550–563.

https://doi.org/10.1038/nrm2731

Komander, D., & Rape, M. (2012). The ubiquitin code. *Annual Review of Biochemistry*, *81*. https://doi.org/10.1146/annurev-biochem-060310-170328

Kong, M., Ditsworth, D., Lindsten, T., & Thompson, C. B. (2009). α4 Is an Essential Regulator of PP2A Phosphatase Activity. *Molecular Cell*, *36*(1). https://doi.org/10.1016/j.molcel.2009.09.025

Kotlo, K., Johnson, K. R., Grillon, J. M., Geenen, D. L., deTombe, P., & Danziger, R. S. (2012). Phosphoprotein abundance changes in hypertensive cardiac remodeling. *Journal of Proteomics*, *77*. https://doi.org/10.1016/j.jprot.2012.05.041

Krauß, S., Foerster, J., Schneider, R., & Schweiger, S. (2008). Protein phosphatase 2A and rapamycin regulate the nuclear localization and activity of the transcription factor GLI3. *Cancer Research*, *68*(12). https://doi.org/10.1158/0008-5472.CAN-07-6174

Krauß, S., Griesche, N., Jastrzebska, E., Chen, C., Rutschow, D., Achmuller, C., Dorn, S., Boesch, S. M., Lalowski, M., Wanker, E., Schneider, R., & Schweiger, S. (2013). Translation of HTT mRNA with expanded CAG repeats is regulated by the MID1-PP2A protein complex. *Nature Communications*, *4*. https://doi.org/10.1038/ncomms2514

Kristariyanto, Y. A., Rehman, S. A. A., Weidlich, S., Knebel, A., & Kulathu, Y. (2017). A single MIU motif of MINDY -1 recognizes K48-linked polyubiquitin chains. *EMBO Reports*, *18*(3). https://doi.org/10.15252/embr.201643205

Kruszka, P., Li, D., Harr, M. H., Wilson, N. R., Swarr, D., McCormick, E. M., Chiavacci, R. M., Li, M., Martinez, A. F., Hart, R. A., McDonald-McGinn, D. M., Deardorff, M. A., Falk, M. J., Allanson, J. E., Hudson, C., Johnson, J. P., Saadi, I., Hakonarson, H., Muenke, M., & Zackai, E. H. (2015). Mutations in SPECC1L, encoding sperm antigen with calponin homology and coiled-coil domains 1-like, are found in some cases of autosomal dominant Opitz G/BBB syndrome. *Journal of Medical Genetics*, *52*(2). https://doi.org/10.1136/jmedgenet-2014-102677

Kulathu, Y., & Komander, D. (2012). Atypical ubiquitylation-the unexplored world of polyubiquitin beyond Lys48 and Lys63 linkages. In *Nature Reviews Molecular Cell Biology* (Vol. 13, Issue 8). https://doi.org/10.1038/nrm3394

Kwasna, D., Rehman, S. A. A., Natarajan, J., Matthews, S., Madden, R., Cesare, V. De,

Weidlich, S., Virdee, S., Ahel, I., Gibbs-Seymour, I., & Kulathu, Y. (2018). Discovery and Characterization of ZUFSP/ZUP1, a Distinct Deubiquitinase Class Important for Genome Stability. *Molecular Cell*, *70*(1). https://doi.org/10.1016/j.molcel.2018.02.023

Lam, Y. A., Xu, W., DeMartino, G. N., & Cohen, R. E. (1997). Editing of ubiquitin conjugates by an isopeptidase in the 26S proteasome. *Nature*, *385*(6618). https://doi.org/10.1038/385737a0

Lancioni, A., Pizzo, M., Fontanella, B., Ferrentino, R., Napolitano, L. M. R., De Leonibus, E., & Meroni, G. (2010). Lack of Mid1, the mouse ortholog of the opitz syndrome gene, causes abnormal development of the anterior cerebellar vermis. *Journal of Neuroscience*, *30*(8), 2880–2887. https://doi.org/10.1523/JNEUROSCI.4196-09.2010

Lechward, K., Awotunde, O. S., Świątek, W., & Muszyńska, G. (2001). Protein phosphatase 2A: Variety of forms and diversity of functions. *Acta Biochimica Polonica*, *48*(4). https://doi.org/10.18388/abp.2001_3858

LeNoue-Newton, M., Watkins, G. R., Zou, P., Germane, K. L., McCorvey, L. R., Wadzinski, B. E., & Spiller, B. W. (2011). The E3 ubiquitin ligase- and protein phosphatase 2A (PP2A)-binding domains of the Alpha4 protein are both required for Alpha4 to inhibit PP2A degradation. *Journal of Biological Chemistry*, *286*(20). https://doi.org/10.1074/jbc.M111.222414

Leznicki, P., Natarajan, J., Bader, G., Spevak, W., Schlattl, A., Rehman, S. A. A., Pathak, D., Weidlich, S., Zoephel, A., Bordone, M. C., Barbosa-Morais, N. L., Boehmelt, G., & Kulathu, Y. (2018). Expansion of DUB functionality generated by alternative isoforms - USP35, a case study. *Journal of Cell Science*, *131*(10). https://doi.org/10.1242/jcs.212753

Li, J., D'Angiolella, V., Seeley, E. S., Kim, S., Kobayashi, T., Fu, W., Campos, E. I., Pagano, M., & Dynlacht, B. D. (2013). USP33 regulates centrosome biogenesis via deubiquitination of the centriolar protein CP110. *Nature*, *495*(7440). https://doi.org/10.1038/nature11941

Li, S., Chen, Y., Shi, Q., Yue, T., Wang, B., & Jiang, J. (2012). Hedgehog-regulated ubiquitination controls smoothened trafficking and cell surface expression in Drosophila. *PLoS Biology*, *10*(1). https://doi.org/10.1371/journal.pbio.1001239

Li, W., Tu, D., Brunger, A. T., & Ye, Y. (2007). A ubiquitin ligase transfers preformed

polyubiquitin chains from a conjugating enzyme to a substrate. *Nature*, *446*(7133). https://doi.org/10.1038/nature05542

Li, X., Song, N., Liu, L., Liu, X., Ding, X., Song, X., Yang, S., Shan, L., Zhou, X., Su, D., Wang, Y., Zhang, Q., Cao, C., Ma, S., Yu, N., Yang, F., Wang, Y., Yao, Z., Shang, Y., & Shi, L. (2017). USP9X regulates centrosome duplication and promotes breast carcinogenesis. *Nature Communications*, *8*. https://doi.org/10.1038/ncomms14866

Li, Y., Wu, H., Wu, W., Zhuo, W., Liu, W., Zhang, Y., Cheng, M., Chen, Y. G., Gao, N., Yu, H., Wang, L., Li, W., & Yang, M. (2014). Structural insights into the TRIM family of ubiquitin E3 ligases. In *Cell Research* (Vol. 24, Issue 6). https://doi.org/10.1038/cr.2014.46

Lima, C. D., & Schulman, B. A. (2012). Structural biology: A protein engagement RING. In *Nature* (Vol. 489, Issue 7414). https://doi.org/10.1038/489043a

Liu, E., Knutzen, C. A., Krauss, S., Schweiger, S., & Chiang, G. G. (2011). Control of mTORC1 signaling by the Opitz syndrome protein MID1. *Proceedings of the National Academy of Sciences of the United States of America*, *108*(21). https://doi.org/10.1073/pnas.1100131108

Liu, J., Prickett, T. D., Elliott, E., Meroni, G., & Brautigan, D. L. (2001). Phosphorylation and microtubule association of the Opitz syndrome protein mid-1 is regulated by protein phosphatase 2A via binding to the regulatory subunit α4. *Proceedings of the National Academy of Sciences of the United States of America*, *98*(12). https://doi.org/10.1073/pnas.111154698

Liu, Z., Meray, R. K., Grammatopoulos, T. N., Fredenburg, R. A., Cookson, M. R., Liu, Y., Logan, T., & Lansbury, P. T. (2009). Membrane-associated farnesylated UCH-L1 promotes α-synuclein neurotoxicity and is a therapeutic target for Parkinson's disease. *Proceedings of the National Academy of Sciences of the United States of America*, *106*(12). https://doi.org/10.1073/pnas.0806474106

Lu, T., Chen, R., Cox, T. C., Moldrich, R. X., Kurniawan, N., Tan, G., Perry, J. K., Ashworth, A., Bartlett, P. F., Xu, L., Zhang, J., Lu, B., Wu, M., Shen, Q., Liu, Y., Richards, L. J., & Xiong, Z. (2013). X-linked microtubule-associated protein, Mid1, regulates axon development. *Proceedings of the National Academy of Sciences of the United States of America*, *110*(47). https://doi.org/10.1073/pnas.1303687110

Luo, Q., Wu, X., Nan, Y., Chang, W., Zhao, P., Zhang, Y., Su, D., & Liu, Z. (2020). TRIM32/USP11 Balances ARID1A Stability and the Oncogenic/Tumor-Suppressive Status of Squamous Cell Carcinoma. *Cell Reports*, *30*(1), 98-111.e5. https://doi.org/10.1016/j.celrep.2019.12.017

Ma, G., Li, S., Han, Y., Li, S., Yue, T., Wang, B., & Jiang, J. (2016). Regulation of Smoothened Trafficking and Hedgehog Signaling by the SUMO Pathway. *Developmental Cell*, *39*(4). https://doi.org/10.1016/j.devcel.2016.09.014

Ma, Z. Y., Song, Z. J., Chen, J. H., Wang, Y. F., Li, S. Q., Zhou, L. F., Mao, Y., Li, Y. M., Hu, R. G., Zhang, Z. Y., Ye, H. Y., Shen, M., Shou, X. F., Li, Z. Q., Peng, H., Wang, Q. Z., Zhou, D. Z., Qin, X. L., Ji, J., … Zhao, Y. (2015). Recurrent gain-of-function USP8 mutations in Cushing's disease. *Cell Research*, *25*(3). https://doi.org/10.1038/cr.2015.20

Makarova, O. V, Makarov, E. M., & Lührmann, R. (2001). The 65 and 110 kDA SR-related proteins of the U4/U6·U5 tri-snRNP are essential for the assembly of mature spliceosomes. *EMBO Journal*, *20*(10). https://doi.org/10.1093/emboj/20.10.2553

Malicki, J. J., & Johnson, C. A. (2017). The Cilium: Cellular Antenna and Central Processing Unit. In *Trends in Cell Biology* (Vol. 27, Issue 2). https://doi.org/10.1016/j.tcb.2016.08.002

Marcassa, E., Kallinos, A., Jardine, J., Rusilowicz-Jones, E. V, Martinez, A., Kuehl, S., Islinger, M., Clague, M. J., & Urbé, S. (2018). Dual role of USP 30 in controlling basal pexophagy and mitophagy. *EMBO Reports*, *19*(7). https://doi.org/10.15252/embr.201745595

Martin, L., Latypova, X., Wilson, C. M., Magnaudeix, A., Perrin, M. L., & Terro, F. (2013). Tau protein phosphatases in Alzheimer's disease: The leading role of PP2A. In *Ageing Research Reviews* (Vol. 12, Issue 1). https://doi.org/10.1016/j.arr.2012.06.008

Mascaro, M. (2020). *Role of TRIM18, the Opitz Syndrome gene product, in the control of ciliogenesis through autophagy* [University of Trieste]. https://arts.units.it/handle/11368/2996095

Mashtalir, N., Daou, S., Barbour, H., Sen, N. N., Gagnon, J., Hammond-Martel, I., Dar, H. H., Therrien, M., & Affar, E. B. (2014). Autodeubiquitination protects the tumor suppressor BAP1 from cytoplasmic sequestration mediated by the atypical ubiquitin ligase UBE2O.

Molecular Cell, *54*(3). https://doi.org/10.1016/j.molcel.2014.03.002

Matthes, F., Hettich, M. M., Schilling, J., Flores-Dominguez, D., Blank, N., Wiglenda, T., Buntru, A., Wolf, H., Weber, S., Vorberg, I., Dagane, A., Dittmar, G., Wanker, E., Ehninger, D., & Krauss, S. (2018). Inhibition of the MID1 protein complex: a novel approach targeting APP protein synthesis. *Cell Death Discovery*, *4*(1). https://doi.org/10.1038/s41420-017-0003-8

McConnell, J. L., Watkins, G. R., Soss, S. E., Franz, H. S., McCorvey, L. R., Spiller, B. W., Chazin, W. J., & Wadzinski, B. E. (2010). Alpha4 is a ubiquitin-binding protein that regulates protein serine/threonine phosphatase 2A ubiquitination. *Biochemistry*, *49*(8). https://doi.org/10.1021/bi901837h

McCullough, J., Row, P. E., Lorenzo, Ó., Doherty, M., Beynon, R., Clague, M. J., & Urbé, S. (2006). Activation of the endosome-associated ubiquitin isopeptidase AMSH by STAM, a component of the multivesicular body-sorting machinery. *Current Biology*, *16*(2). https://doi.org/10.1016/j.cub.2005.11.073

McGouran, J. F., Gaertner, S. R., Altun, M., Kramer, H. B., & Kessler, B. M. (2013). Deubiquitinating enzyme specificity for ubiquitin chain topology profiled by di-ubiquitin activity probes. *Chemistry and Biology*, *20*(12). https://doi.org/10.1016/j.chembiol.2013.10.012

Meroni, G., & Diez-Roux, G. (2005). TRIM/RBCC, a novel class of "single protein RING finger" E3 ubiquitin ligases. *BioEssays*, *27*(11), 1147–1157. https://doi.org/10.1002/bies.20304

Mevissen, T. E. T., Hospenthal, M. K., Geurink, P. P., Elliott, P. R., Akutsu, M., Arnaudo, N., Ekkebus, R., Kulathu, Y., Wauer, T., Oualid, F. El, Freund, S. M. V, Ovaa, H., & Komander, D. (2013). XOTU deubiquitinases reveal mechanisms of linkage specificity and enable ubiquitin chain restriction analysis. *Cell*, *154*(1). https://doi.org/10.1016/j.cell.2013.05.046

Mevissen, T. E. T., & Komander, D. (2017). Mechanisms of Deubiquitinase Specificity and Regulation. *Annual Review of Biochemistry*, *86*(May), 1–33. https://doi.org/https://doi.org/10.1146/annurev-biochem-061516-044916

Migliore, C., Athanasakis, E., Dahoun, S., Wonkam, A., Lees, M., Calabrese, O., Connell, F.,

Lynch, S. A., Izzi, C., Pompilii, E., Thakur, S., van Maarle, M., Wilson, L. C., & Meroni, G. (2013). Complex rearrangement of the exon 6 genomic region among Opitz G/BBB Syndrome MID1 alterations. *European Journal of Medical Genetics*, *56*(8). https://doi.org/10.1016/j.ejmg.2013.05.009

Migliore, C., Vendramin, A., McKee, S., Prontera, P., Faravelli, F., Sachdev, R., Dias, P., Mascaro, M., Licastro, D., & Meroni, G. (2022). SPECC1L Mutations Are Not Common in Sporadic Cases of Opitz G/BBB Syndrome. *Genes*, *13*(2). https://doi.org/10.3390/genes13020252

Murata, K., Wu, J., & Brautigan, D. L. (1997). B cell receptor-associated protein α4 displays rapamycin-sensitive binding directly to the catalytic subunit of protein phosphatase 2A. *Proceedings of the National Academy of Sciences of the United States of America*, *94*(20). https://doi.org/10.1073/pnas.94.20.10624

Nakamura, N., & Hirose, S. (2008). Regulation of mitochondrial morphology by USP30, a deubiquitinating enzyme present in the mitochondrial outer membrane. *Molecular Biology of the Cell*, *19*(5). https://doi.org/10.1091/mbc.E07-11-1103

Nakamura, T., Ueyama, T., Ninoyu, Y., Sakaguchi, H., Choijookhuu, N., Hishikawa, Y., Kiyonari, H., Kohta, M., Sakahara, M., de Curtis, I., Kohmura, E., Hisa, Y., Aiba, A., & Saito, N. (2017). Novel role of Rac-Mid1 signaling in medial cerebellar development. *Development (Cambridge)*, *144*(10). https://doi.org/10.1242/dev.147900

Nakashima, A., Tanimura-Ito, K., Oshiro, N., Eguchi, S., Miyamoto, T., Momonami, A., Kamada, S., Yonezawa, K., & Kikkawa, U. (2013). A positive role of mammalian Tip41-like protein, TIPRL, in the amino-acid dependent mTORC1-signaling pathway through interaction with PP2A. *FEBS Letters*, *587*(18). https://doi.org/10.1016/j.febslet.2013.07.027

Nanahoshi, M., Tsujishita, Y., Tokunaga, C., Inui, S., Sakaguchi, N., Hara, K., & Yonezawa, K. (1999). Alpha4 protein as a common regulator of type 2A-related serine/threonine protein phosphatases. *FEBS Letters*, *446*(1). https://doi.org/10.1016/S0014-5793(99)00189-1

Napolitano, L. M., Jaffray, E. G., Hay, R. T., & Meroni, G. (2011). Functional interactions between ubiquitin E2 enzymes and TRIM proteins. *Biochemical Journal*, *434*(2), 309–319. https://doi.org/10.1042/BJ20101487

Napolitano, L. M., & Meroni, G. (2012). TRIM family: Pleiotropy and diversification through homomultimer and heteromultimer formation. *IUBMB Life*, *64*(1), 64–71. https://doi.org/10.1002/iub.580

Nematullah, M., Hoda, M. N., & Khan, F. (2018). Protein Phosphatase 2A: a Double-Faced Phosphatase of Cellular System and Its Role in Neurodegenerative Disorders. In *Molecular Neurobiology* (Vol. 55, Issue 2). https://doi.org/10.1007/s12035-017-0444-3

Nicassio, F., Corrado, N., Vissers, J. H. A., Areces, L. B., Bergink, S., Marteijn, J. A., Geverts, B., Houtsmuller, A. B., Vermeulen, W., Fiore, P. P. Di, & Citterio, E. (2007). Human USP3 Is a Chromatin Modifier Required for S Phase Progression and Genome Stability. *Current Biology*, *17*(22). https://doi.org/10.1016/j.cub.2007.10.034

Nicklas, S., Hillje, A. L., Okawa, S., Rudolph, I. M., Collmann, F. M., van Wuellen, T., del Sol, A., & Schwamborn, J. C. (2019). A complex of the ubiquitin ligase TRIM32 and the deubiquitinase USP7 balances the level of c-Myc ubiquitination and thereby determines neural stem cell fate specification. *Cell Death and Differentiation*, *26*(4), 728–740. https://doi.org/10.1038/s41418-018-0144-1

Nielsen, C. P., & MacGurn, J. A. (2020). Coupling Conjugation and Deconjugation Activities to Achieve Cellular Ubiquitin Dynamics. *Trends in Biochemical Sciences*, *45*(5), 427–439. https://doi.org/10.1016/j.tibs.2020.01.008

Nijman, S. M. B., Huang, T. T., Dirac, A. M. G., Brummelkamp, T. R., Kerkhoven, R. M., D'Andrea, A. D., & Bernards, R. (2005). The deubiquitinating enzyme USP1 regulates the fanconi anemia pathway. *Molecular Cell*, *17*(3). https://doi.org/10.1016/j.molcel.2005.01.008

Nilsson, J., Sengupta, J., Frank, J., & Nissen, P. (2004). Regulation of eukaryotic translation by the RACK1 protein: A platform for signalling molecules on the ribosome. In *EMBO Reports* (Vol. 5, Issue 12). https://doi.org/10.1038/sj.embor.7400291

Oshiumi, H., Matsumoto, M., & Seya, T. (2012). Ubiquitin-mediated modulation of the cytoplasmic viral RNA sensor RIG-I. *Journal of Biochemistry*, *151*(1), 5–11. https://doi.org/10.1093/jb/mvr111

Özkaynak, E., Finley, D., & Varshavsky, A. (1984). The yeast ubiquitin gene: Head-to-tail repeats encoding a polyubiquitin precursor protein. *Nature*, *312*(5995).

https://doi.org/10.1038/312663a0

Park, J. M., Yang, S. W., Yu, K. R., Ka, S. H., Lee, S. W., & Seol, J. H. (2014). Modification of PCNA by ISG15 Playsa Crucial Role in Termination ofError-Prone Translesion DNA Synthesis. *Molecular Cell*, *54*, 1–13. https://doi.org/10.1016/j.molcel.2014.03.031

Pauli, E.-K., Chan, Y. K. C., Davis, M. E. D., Gableske, S., Wang, M. K., Feister, K., & Gack, M. U. (2011). The Ubiquitin-Specific Protease USP15 Promotes RIG-I– Mediated Antiviral Signaling by Deubiquitylating TRIM25 Eva-Katharina. *Science Signalling*, *46*(4), 564–574. https://doi.org/10.1016/j.cortex.2009.08.003.Predictive

Peterson, R. T., Desai, B. N., Hardwick, J. S., & Schreiber, S. L. (1999). Protein phosphatase 2A interacts with the 70-kDa S6 kinase and is activated by inhibition of FKBP12-rapamycin-associated protein. *Proceedings of the National Academy of Sciences of the United States of America*, *96*(8). https://doi.org/10.1073/pnas.96.8.4438

Pfirrmann, T., Jandt, E., Ranft, S., Lokapally, A., Neuhaus, H., Perron, M., & Hollemann, T. (2016). Hedgehog-dependent E3-ligase Midline1 regulates ubiquitin-mediated proteasomal degradation of Pax6 during visual system development. *Proceedings of the National Academy of Sciences of the United States of America*, *113*(36). https://doi.org/10.1073/pnas.1600770113

Pickart, C. M., & Eddins, M. J. (2004). Ubiquitin: Structures, functions, mechanisms. In *Biochimica et Biophysica Acta - Molecular Cell Research* (Vol. 1695, Issues 1–3). https://doi.org/10.1016/j.bbamcr.2004.09.019

Pinson, L., Augé, J., Audollent, S., Mattéi, G., Etchevers, H., Gigarel, N., Razavi, F., Lacombe, D., Odent, S., Le Merrer, M., Amiel, J., Munnich, A., Meroni, G., Lyonnet, S., Vekemans, M., & Attié-Bitach, T. (2004). Embryonic expression of the human MID1 gene and its mutations in Opitz syndrome. *Journal of Medical Genetics*, *41*(5). https://doi.org/10.1136/jmg.2003.014829

Popov, N., Wanzel, M., Madiredjo, M., Zhang, D., Beijersbergen, R., Bernards, R., Moll, R., Elledge, S. J., & Eilers, M. (2007). The ubiquitin-specific protease USP28 is required for MYC stability. *Nature Cell Biology*, *9*(7). https://doi.org/10.1038/ncb1601

Pruneda, J. N., & Komander, D. (2019). Evaluating enzyme activities and structures of DUBs. In *Methods in Enzymology* (1st ed., Vol. 618). Elsevier Inc.

https://doi.org/10.1016/bs.mie.2019.01.001

Qin, X., Jiang, B., & Zhang, Y. (2016). 4E-BP1, a multifactor regulated multifunctional protein. In *Cell Cycle* (Vol. 15, Issue 6). https://doi.org/10.1080/15384101.2016.1151581

Quaderi, N. A., Schweiger, S., Gaudenz, K., Franco, B., Rugarli, E. I., Berger, W., Feldman, G. J., Volta, M., Andolfi, G., Gilgenkrantz, S., Marion, R. W., Hennekam, R. C. M., Opitz, J. M., Muenke, M., Ropers, H. H., & Ballabio, A. (1997). Opitz G/BBB syndrome, a defect of midline development, is due to mutations in a new RING finger gene on Xp22. *Nature Genetics*, *17*(3). https://doi.org/10.1038/ng1197-285

Rehman, S. A. A., Kristariyanto, Y. A., Choi, S. Y., Nkosi, P. J., Weidlich, S., Labib, K., Hofmann, K., & Kulathu, Y. (2016). MINDY-1 Is a Member of an Evolutionarily Conserved and Structurally Distinct New Family of Deubiquitinating Enzymes. *Molecular Cell*, *63*(1). https://doi.org/10.1016/j.molcel.2016.05.009

Reincke, M., Sbiera, S., Hayakawa, A., Theodoropoulou, M., Osswald, A., Beuschlein, F., Meitinger, T., Mizuno-Yamasaki, E., Kawaguchi, K., Saeki, Y., Tanaka, K., Wieland, T., Graf, E., Saeger, W., Ronchi, C. L., Allolio, B., Buchfelder, M., Strom, T. M., Fassnacht, M., & Komada, M. (2015). Mutations in the deubiquitinase gene usp8 cause cushing's disease. *Nature Genetics*, *47*(1). https://doi.org/10.1038/ng.3166

Reymond, A., Meroni, G., Fantozzi, A., Merla, G., Cairo, S., Luzi, L., Riganelli, D., Zanaria, E., Messali, S., Cainarca, S., Guffanti, A., Minucci, S., Pelicci, P. G., & Ballabio, A. (2001). The tripartite motif family identifies cell compartments. *EMBO Journal*, *20*(9), 2140–2151. https://doi.org/10.1093/emboj/20.9.2140

Richman, J. M., Fu, K. K., Cox, L. L., Sibbons, J. P., & Cox, T. C. (2002). Isolation and characterisation of the chick orthologue of the Opitz syndrome gene, Mid1, supports a conserved role in vertebrate development. *International Journal of Developmental Biology*, *46*(4 SPEC.).

Ritorto, M. S., Ewan, R., Perez-Oliva, A. B., Knebel, A., Buhrlage, S. J., Wightman, M., Kelly, S. M., Wood, N. T., Virdee, S., Gray, N. S., Morrice, N. A., Alessi, D. R., & Trost, M. (2014). Screening of DUB activity and specificity by MALDI-TOF mass spectrometry. *Nature Communications*, *5*. https://doi.org/10.1038/ncomms5763

Robin, N. H., Feldman, G. J., Aronson, A. L., Mitchell, H. F., Weksberg, R., Leonard, C. O.,

Burton, B. K., Josephson, K. D., Laxová, R., Aleck, K. A., Allanson, J. E., Guion-Almeida, M. L., Martin, R. A., Leichtman, L. G., Arlen Price, R., Opitz, J. M., & Muenke, M. (1995). Opitz syndrome is genetically heterogeneous, with one locus on Xp22, and a second locus on 22q11.2. *Nature Genetics*, *11*(4). https://doi.org/10.1038/ng1295-459

Robin, N. H., Opitz, J. M., & Muenke, M. (1996). Opitz G/BBB syndrome: Clinical comparisons of families linked to Xp22 and 22q, and a review of the literature. In *American Journal of Medical Genetics* (Vol. 62, Issue 3). https://doi.org/10.1002/(SICI)1096-8628(19960329)62:3<305::AID-AJMG20>3.0.CO;2-N

Row, P. E., Liu, H., Hayes, S., Welchman, R., Charalabous, P., Hofmann, K., Clague, M. J., Sanderson, C. M., & Urbé, S. (2007). The MIT domain of UBPY constitutes a CHMP binding and endosomal localization signal required for efficient epidermal growth factor receptor degradation. *Journal of Biological Chemistry*, *282*(42). https://doi.org/10.1074/jbc.M704009200

Ruediger, R., Hood, J. E. V. W., Mumby, M., & Walter, G. (1991). Constant expression and activity of protein phosphatase 2A in synchronized cells. *Molecular and Cellular Biology*, *11*(8). https://doi.org/10.1128/mcb.11.8.4282-4285.1991

Sahtoe, D. D., & Sixma, T. K. (2015). Layers of DUB regulation. *Trends in Biochemical Sciences*, *40*(8), 456–467. https://doi.org/10.1016/j.tibs.2015.05.002

Sanchez, J. G., Okreglicka, K., Chandrasekaran, V., Welker, J. M., Sundquist, W. I., & Pornillos, O. (2014). The tripartite motif coiled-coil is an elongated antiparallel hairpin dimer. *Proceedings of the National Academy of Sciences of the United States of America*, *111*(7). https://doi.org/10.1073/pnas.1318962111

Sardiello, M., Cairo, S., Fontanella, B., Ballabio, A., & Meroni, G. (2008). Genomic analysis of the TRIM family reveals two groups of genes with distinct evolutionary properties. *BMC Evolutionary Biology*, *8*(1), 1–22. https://doi.org/10.1186/1471-2148-8-225

Sasai, N., Toriyama, M., & Kondo, T. (2019). Hedgehog Signal and Genetic Disorders. In *Frontiers in Genetics* (Vol. 10). https://doi.org/10.3389/fgene.2019.01103

Schweiger, S., Dorn, S., Fuchs, M., Köhler, A., Matthes, F., Müller, E. C., Wanker, E., Schneider, R., & Krauß, S. (2014). The E3 ubiquitin ligase MID1 catalyzes ubiquitination

and cleavage of Fu. *Journal of Biological Chemistry*, *289*(46). https://doi.org/10.1074/jbc.M113.541219

Schweiger, S., Foerster, J., Lehmann, T., Suckow, V., Muller, Y. A., Walter, G., Davies, T., Porter, H., Van Bokhoven, H., Lunt, P. W., Traub, P., & Ropers, H. H. (1999). The Opitz syndrome gene product, MID1, associates with microtubules. *Proceedings of the National Academy of Sciences of the United States of America*, *96*(6). https://doi.org/10.1073/pnas.96.6.2794

Schweiger, S., Matthes, F., Posey, K., Kickstein, E., Weber, S., Hettich, M. M., Pfurtscheller, S., Ehninger, D., Schneider, R., & Krauß, S. (2017). Resveratrol induces dephosphorylation of Tau by interfering with the MID1-PP2A complex. *Scientific Reports*, *7*(1). https://doi.org/10.1038/s41598-017-12974-4

Sengupta, S., Peterson, T. R., & Sabatini, D. M. (2010). Regulation of the mTOR Complex 1 Pathway by Nutrients, Growth Factors, and Stress. In *Molecular Cell* (Vol. 40, Issue 2). https://doi.org/10.1016/j.molcel.2010.09.026

Shaham, O., Menuchin, Y., Farhy, C., & Ashery-Padan, R. (2012). Pax6: A multi-level regulator of ocular development. In *Progress in Retinal and Eye Research* (Vol. 31, Issue 5). https://doi.org/10.1016/j.preteyeres.2012.04.002

Shi, Y. (2009). Serine/Threonine Phosphatases: Mechanism through Structure. In *Cell* (Vol. 139, Issue 3). https://doi.org/10.1016/j.cell.2009.10.006

Short, K. M., & Cox, T. C. (2006). Subclassification of the RBCC/TRIM superfamily reveals a novel motif necessary for microtubule binding. *Journal of Biological Chemistry*, *281*(13), 8970–8980. https://doi.org/10.1074/jbc.M512755200

Short, K. M., Hopwood, B., Yi, Z., & Cox, T. C. (2002). MID1 and MID2 homo- and heterodimerise to tether the rapamycin-sensitive PP2A regulatory subunit, Alpha 4, to microtubules: Implications for the clinical variability of X-linked Opitz GBBB syndrome and other developmental disorders. *BMC Cell Biology*, *3*. https://doi.org/10.1186/1471-2121-3-1

Sobol, A., Askonas, C., Alani, S., Weber, M. J., Ananthanarayanan, V., Osipo, C., & Bocchetta, M. (2017). Deubiquitinase OTUD6B isoforms are important regulators of growth and proliferation. *Molecular Cancer Research*, *15*(2). https://doi.org/10.1158/1541-

7786.MCR-16-0281-T

Song, E. J., Werner, S. L., Neubauer, J., Stegmeier, F., Aspden, J., Rio, D., Harper, J. W., Elledge, S. J., Kirschner, M. W., & Rape, M. (2010). The Prp19 complex and the Usp4Sart3 deubiquitinating enzyme control reversible ubiquitination at the spliceosome. *Genes and Development*, *24*(13). https://doi.org/10.1101/gad.1925010

Stelzmann, R. A., Schnitzlein, H. N., & Murtagh, F. R. (1995). An english translation of alzheimer's 1907 paper, "über eine eigenartige erkankung der hirnrinde." *Clinical Anatomy*, *8*(6). https://doi.org/10.1002/ca.980080612

Sun, J., Shen, D., Zheng, Y., Ren, H., Liu, H., Chen, X., & Gao, Y. (2020). USP8 inhibitor suppresses HER-2 positive gastric cancer cell proliferation and metastasis via the PI3K/AKT signaling pathway. *OncoTargets and Therapy*, *13*. https://doi.org/10.2147/OTT.S271496

Sun, X. X., He, X., Yin, L., Komada, M., Sears, R. C., & Dai, M. S. (2015). The nucleolar ubiquitin-specific protease USP36 deubiquitinates and stabilizes c-Myc. *Proceedings of the National Academy of Sciences of the United States of America*, *112*(12). https://doi.org/10.1073/pnas.1411713112

Suresh, B., Ramakrishna, S., Lee, H., Choi, J., Kim, J., Ahn, W., & Baek, K. (2010). K48- and K63-linked polyubiquitination of deubiquitinating enzyme USP44. *Cell Biology International*, *34*(8). https://doi.org/10.1042/cbi20090144

Suzuki, M., Hara, Y., Takagi, C., Yamamoto, T. S., & Ueno, N. (2010). MID1 and MID2 are required for Xenopus neural tube closure through the regulation of microtubule organization. *Development*, *137*(14). https://doi.org/10.1242/dev.048769

Tacer, K. F., & Potts, P. R. (2017). Cellular and disease functions of the Prader-Willi Syndrome gene MAGEL2. *Biochemical Journal*, *474*(13), 139–148. https://doi.org/10.1016/j.physbeh.2017.03.040

Tait, D., Riccio, M., Sittler, A., Scherzinger, E., Santi, S., Ognibene, A., Maraldi, N. M., Lehrach, H., & Wanker, E. E. (1998). Ataxin-3 is transported into the nucleus and associates with the nuclear matrix. *Human Molecular Genetics*, *7*(6). https://doi.org/10.1093/hmg/7.6.991

Takahashi, Y., He, H., Tang, Z., Hattori, T., Liu, Y., Young, M. M., Serfass, J. M., Chen, L.,

Gebru, M., Chen, C., Wills, C. A., Atkinson, J. M., Chen, H., Abraham, T., & Wang, H. G. (2018). An autophagy assay reveals the ESCRT-III component CHMP2A as a regulator of phagophore closure. *Nature Communications*, *9*(1). https://doi.org/10.1038/s41467-018-05254-w

Tanaka, N., Kaneko, K., Asao, H., Kasai, H., Endo, Y., Fujita, T., Takeshita, T., & Sugamura, K. (1999). Possible involvement of a novel STAM-associated molecule "AMSH" in intracellular signal transduction mediated by cytokines. *Journal of Biological Chemistry*, *274*(27). https://doi.org/10.1074/jbc.274.27.19129

Tao, H., Simmons, B. N., Singireddy, S., Jakkidi, M., Short, K. M., Cox, T. C., & Massiah, M. A. (2008). Structure of the MID1 tandem B-boxes reveals an interaction reminiscent of intermolecular ring heterodimers. *Biochemistry*, *47*(8), 2450–2457. https://doi.org/10.1021/bi7018496

Teyra, J., Singer, A. U., Schmitges, F. W., Jaynes, P., Kit Leng Lui, S., Polyak, M. J., Fodil, N., Krieger, J. R., Tong, J., Schwerdtfeger, C., Brasher, B. B., Ceccarelli, D. F. J., Moffat, J., Sicheri, F., Moran, M. F., Gros, P., Eichhorn, P. J. A., Lenter, M., Boehmelt, G., & Sidhu, S. S. (2019). Structural and Functional Characterization of Ubiquitin Variant Inhibitors of USP15. *Structure*, *27*(4), 590-605.e5. https://doi.org/10.1016/j.str.2019.01.002

Thorne, C., Eccles, R. L., Coulson, J. M., Urbé, S., & Clague, M. J. (2011). Isoform-specific localization of the deubiquitinase USP33 to the golgi apparatus. *Traffic*, *12*(11). https://doi.org/10.1111/j.1600-0854.2011.01261.x

Tokgöz, Z., Siepmann, T. J., Streich, F., Kumars, B., Kleins, J. M., & Haass, A. L. (2012). E1-E2 interactions in ubiquitin and Nedd8 ligation pathways. *Journal of Biological Chemistry*, *287*(1). https://doi.org/10.1074/jbc.M111.294975

Torre, S., Polyak, M. J., Langlais, D., Fodil, N., Kennedy, J. M., Radovanovic, I., Berghout, J., Leiva-Torres, G. A., Krawczyk, C. M., Ilangumaran, S., Mossman, K., Liang, C., Knobeloch, K. P., Healy, L. M., Antel, J., Arbour, N., Prat, A., Majewski, J., Athrop, M., … Gros, P. (2017). USP15 regulates type i interferon response and is required for pathogenesis of neuroinflammation. *Nature Immunology*, *18*(1), 54–63. https://doi.org/10.1038/ni.3581

Trockenbacher, A., Suckow, V., Foerster, J., Winter, J., Krauß, S., Ropers, H. H., Schneider,

R., & Schweiger, S. (2001). MID1, mutated in Opitz syndrome, encodes an ubiquitin ligase that targets phosphatase 2A for degradation. *Nature Genetics*, *29*(3). https://doi.org/10.1038/ng762

Troilo, A., Alexander, I., Muehl, S., Jaramillo, D., Knobeloch, K. P., & Krek, W. (2014). HIF1α deubiquitination by USP8 is essential for ciliogenesis in normoxia. *EMBO Reports*, *15*(1). https://doi.org/10.1002/embr.201337688

Turner, G. C., & Varshavsky, A. (2000). Detecting and measuring cotranslational protein degradation in vivo. *Science*, *289*(5487). https://doi.org/10.1126/science.289.5487.2117

Unterbruner, K., Matthes, F., Schilling, J., Nalavade, R., Weber, S., Winter, J., & Krauß, S. (2018). MicroRNAs miR-19, miR-340, miR-374 and miR-542 regulate MID1 protein expression. *PLoS ONE*, *13*(1). https://doi.org/10.1371/journal.pone.0190437

Urbé, S., Liu, H., Hayes, S. D., Heride, C., Rigden, D. J., & Clague, M. J. (2012). Systematic survey of deubiquitinase localization identifies USP21 as a regulator of centrosome-and microtubule-associated functions. *Molecular Biology of the Cell*, *23*(6). https://doi.org/10.1091/mbc.E11-08-0668

vanLoosdregt, J., Fleskens, V., Fu, J., Brenkman, A. B., Bekker, C. P. J., Pals, C. E. G. M., Meerding, J., Berkers, C. R., Barbi, J., Gröne, A., Sijts, A. J. A. M., Maurice, M. M., Kalkhoven, E., Prakken, B. J., Ovaa, H., Pan, F., Zaiss, D. M. W., & Coffer, P. J. (2013). Stabilization of the transcription factor Foxp3 by the deubiquitinase USP7 increases treg-cell-suppressive capacity. *Immunity*, *39*(2). https://doi.org/10.1016/j.immuni.2013.05.018

Walczak, H., Iwai, K., & Dikic, I. (2012). Generation and physiological roles of linear ubiquitin chains. In *BMC Biology* (Vol. 10). https://doi.org/10.1186/1741-7007-10-23

Walden, M., Masandi, S. K., Pawłowski, K., & Zeqiraj, E. (2018). Pseudo-DUBs as allosteric activators and molecular scaffolds of protein complexes. In *Biochemical Society Transactions* (Vol. 46, Issue 2). https://doi.org/10.1042/BST20160268

Wang, S., Kollipara, R. K., Humphries, C. G., Ma, S. H., Hutchinson, R., Li, R., Siddiqui, J., Tomlins, S. A., Raj, G. V., & Kittler, R. (2016). The ubiquitin ligase TRIM25 targets ERG for degradation in prostate cancer. *Oncotarget*, *7*(40), 64921–64931. https://doi.org/10.18632/oncotarget.11915

Watanabe, M., & Hatakeyama, S. (2017). TRIM proteins and diseases. *Journal of*

Biochemistry, *161*(2), 135–144. https://doi.org/10.1093/jb/mvw087

Watkins, G. R., Wang, N., Mazalouskas, M. D., Gomez, R. J., Guthrie, C. R., Kraemer, B. C., Schweiger, S., Spiller, B. W., & Wadzinski, B. E. (2012). Monoubiquitination promotes calpain cleavage of the protein phosphatase 2A (PP2A) regulatory subunit α4, altering PP2A stability and microtubule-associated protein phosphorylation. *Journal of Biological Chemistry*, *287*(29). https://doi.org/10.1074/jbc.M112.368613

Weissman, A. M., Shabek, N., & Ciechanover, A. (2011). The predator becomes the prey: Regulating the ubiquitin system by ubiquitylation and degradation. In *Nature Reviews Molecular Cell Biology* (Vol. 12, Issue 9). https://doi.org/10.1038/nrm3173

Wenzel, D. M., Lissounov, A., Brzovic, P. S., & Klevit, R. E. (2011). UBCH7 reactivity profile reveals parkin and HHARI to be RING/HECT hybrids. *Nature*, *474*(7349). https://doi.org/10.1038/nature09966

Wijk, S. J. L., & Timmers, H. T. M. (2010). The family of ubiquitin-conjugating enzymes (E2s): deciding between life and death of proteins. *The FASEB Journal*, *24*(4). https://doi.org/10.1096/fj.09-136259

Winborn, B. J., Travis, S. M., Todi, S. V, Scaglione, K. M., Xu, P., Williams, A. J., Cohen, R. E., Peng, J., & Paulson, H. L. (2008). The deubiquitinating enzyme ataxin-3, a polyglutamine disease protein, edits Lys63 linkages in mixed linkage ubiquitin chains. *Journal of Biological Chemistry*, *283*(39). https://doi.org/10.1074/jbc.M803692200

Wing, S. S., & Coyne, E. S. (2016). The business of deubiquitination - location, location, location. In *F1000Research* (Vol. 5). https://doi.org/10.12688/f1000research.7220.1

Winter, J., Basilicata, M. F., Stemmler, M. P., & Krauss, S. (2016). The MID1 protein is a central player during development and in disease. In *Frontiers in Bioscience - Landmark* (Vol. 21, Issue 3). https://doi.org/10.2741/4413

Wlodarchak, N., & Xing, Y. (2016). PP2A as a master regulator of the cell cycle. In *Critical Reviews in Biochemistry and Molecular Biology* (Vol. 51, Issue 3). https://doi.org/10.3109/10409238.2016.1143913

Wright, K. M., Du, H., Dagnachew, M., & Massiah, M. A. (2016). Solution structure of the microtubule-targeting COS domain of MID1. *The FEBS Journal*, *283*(16), 3089–3102. https://doi.org/10.1111/febs.13795

Wu, X., Yen, L., Irwin, L., Sweeney, C., & Carraway, K. L. (2004). Stabilization of the E3 Ubiquitin Ligase Nrdp1 by the Deubiquitinating Enzyme USP8. *Molecular and Cellular Biology*, *24*(17). https://doi.org/10.1128/mcb.24.17.7748-7757.2004

Xia, R., Jia, H., Fan, J., Liu, Y., & Jia, J. (2012). USP8 promotes smoothened signaling by preventing its ubiquitination and changing its subcellular localization. *PLoS Biology*, *10*(1). https://doi.org/10.1371/journal.pbio.1001238

Xiong, J., Wang, Y., Gong, Z., Liu, J., & Li, W. (2014). Identification of a functional nuclear localization signal within the human USP22 protein. *Biochemical and Biophysical Research Communications*, *449*(1). https://doi.org/10.1016/j.bbrc.2014.04.133

Yan, Z., Fedorov, S. A., Mumby, M. C., & Williams, R. S. (2000). PR48, a Novel Regulatory Subunit of Protein Phosphatase 2A, Interacts with Cdc6 and Modulates DNA Replication in Human Cells. *Molecular and Cellular Biology*, *20*(3). https://doi.org/10.1128/mcb.20.3.1021-1029.2000

Yang, J., Roe, S. M., Prickett, T. D., Brautigan, D. L., & Barford, D. (2007). The structure of Tap42/α4 reveals a tetratricopeptide repeat-like fold and provides insights into PP2A regulation. *Biochemistry*, *46*(30). https://doi.org/10.1021/bi7007118

Yao, T., Song, L., Jin, J., Cai, Y., Takahashi, H., Swanson, S. K., Washburn, M. P., Florens, L., Conaway, R. C., Cohen, R. E., & Conaway, J. W. (2008). Distinct Modes of Regulation of the Uch37 Deubiquitinating Enzyme in the Proteasome and in the Ino80 Chromatin-Remodeling Complex. *Molecular Cell*, *31*(6). https://doi.org/10.1016/j.molcel.2008.08.027

Yau, R., & Rape, M. (2016). The increasing complexity of the ubiquitin code. *Nature Cell*, *18*(6), 579–586. https://doi.org/10.1038/ncb3358

Ye, Y., & Rape, M. (2009). Building ubiquitin chains: E2 enzymes at work. In *Nature Reviews Molecular Cell Biology* (Vol. 10, Issue 11). https://doi.org/10.1038/nrm2780

Yokoyama, N., & Miller, W. T. (2001). Inhibition of Src by direct interaction with protein phosphatase 2A. *FEBS Letters*, *505*(3). https://doi.org/10.1016/S0014-5793(01)02874-5

Yokoyama, N., Reich, N. C., & Miller, W. T. (2001). Involvement of protein phosphatase 2A in the interleukin-3-stimulated Jak2-Stat5 signaling pathway. *Journal of Interferon and Cytokine Research*, *21*(6). https://doi.org/10.1089/107999001750277844

Zanchetta, M. E. (2015). *BRAF35 as Target of MID1/TRIM18 E3 Ligase Activity*. University of Trieste.

Zanchetta, M. E., Napolitano, L. M. R., Maddalo, D., & Meroni, G. (2017). The E3 ubiquitin ligase MID1/TRIM18 promotes atypical ubiquitination of the BRCA2-associated factor 35, BRAF35. *Biochimica et Biophysica Acta - Molecular Cell Research*, *1864*(10), 1844–1854. https://doi.org/10.1016/j.bbamcr.2017.07.014

Zhang, Y. W., Thompson, R., Zhang, H., & Xu, H. (2011). APP processing in Alzheimer's disease. In *Molecular Brain* (Vol. 4, Issue 1). https://doi.org/10.1186/1756-6606-4-3

Zhao, M., Song, K., Hao, W., Wang, L., Patil, G., Li, Q. L., Xu, L., Hua, F., Fu, B., Schwamborn, J. C., Dorf, M. E., & Li, S. (2019). Non-proteolytic ubiquitination of OTULIN regulates NF-κB signaling pathway. *Journal of Molecular Cell Biology*, *12*(3), 163–175. https://doi.org/10.1093/jmcb/mjz081

Zheng, N., Schulman, B. A., Song, L., Miller, J. J., Jeffrey, P. D., Wang, P., Chu, C., Koepp, D. M., Elledge, S. J., Pagano, M., Conaway, R. C., Conaway, J. W., Harper, J. W., & Pavletich, N. P. (2002). Structure of the Cul1-Rbx1-Skp1-F boxSkp2 SCF ubiquitin ligase complex. *Nature*, *416*(6882). https://doi.org/10.1038/416703a

Zheng, N., & Shabek, N. (2017). Ubiquitin ligases: Structure, function, and regulation. In *Annual Review of Biochemistry* (Vol. 86). https://doi.org/10.1146/annurev-biochem-060815-014922

Zhou, J., Pham, H. T., Ruediger, R., & Walter, G. (2003). Characterization of the Aα and Aβ subunit isoforms of protein phosphatase 2A: Differences in expression, subunit interaction, and evolution. *Biochemical Journal*, *369*(2). https://doi.org/10.1042/BJ20021244

Zhu, P., Zhou, W., Wang, J., Puc, J., Ohgi, K. A., Erdjument-Bromage, H., Tempst, P., Glass, C. K., & Rosenfeld, M. G. (2007). A Histone H2A Deubiquitinase Complex Coordinating Histone Acetylation and H1 Dissociation in Transcriptional Regulation. *Molecular Cell*, *27*(4). https://doi.org/10.1016/j.molcel.2007.07.024

Zhu, Y., Lambert, K., Corless, C., Copeland, N. G., Gilbert, D. J., Jenkins, N. A., & D'Andrea, A. D. (1997). DUB-2 is a member of a novel family of cytokine-inducible deubiquitinating enzymes. *Journal of Biological Chemistry*, *272*(1).

https://doi.org/10.1074/jbc.272.1.51

Zong, Z., Zhang, Z., Wu, L., Zhang, L., & Zhou, F. (2021). The Functional Deubiquitinating Enzymes in Control of Innate Antiviral Immunity. In *Advanced Science* (Vol. 8, Issue 2). https://doi.org/10.1002/advs.202002484